Energy Systems Research

Volume 7 • Number 1 • 2024

Published by
Melentiev Energy Systems Institute
Siberian Branch of Russian Academy of Sciences

Available online: esrj.ru

ISSN 2618-9992

Energy Systems Research

Volume 7, Number 1, 2024

International scientific peer-reviewed journal since 2018

Available online: http://esrj.ru

Copyright © 2024 by Melentiev Energy Systems Institute of Siberian Branch of the Russian Academy of Sciences and individual contributors. All rights reserved.

About the journal

Energy Systems Research is an international peer-reviewed journal addressing all the aspects of energy systems, including their sustainable development and effective use, smart and reliable operation, control and management, integration and interaction in a complex physical, technical, economic and social environment.

Within this broad multi-disciplinary scope, topics of particular interest include strategic energy systems development at the international, regional, national and local levels; energy supply reliability and security; energy markets, regulations and policy; technological innovations with their impacts and future-oriented transformations of energy systems. The journal welcomes papers on advances in heat and electric power industries, energy efficiency and energy saving, renewable energy and clean fossil fuel generation, and other energy technologies.

Energy Systems Research is also concerned with energy systems challenges related to the applications of information and communication technologies, including intelligent control and cyber security, modern approaches of systems analysis, modeling, forecasting, numerical computations and optimization.

The journal is published by Melentiev Energy Systems Institute of Siberian Branch of Russian Academy of Sciences. The journal's ISSN is 2618-9992. There are 4 issues per year (special issues are available). All articles are available online on English as Open access articles.

From December 19, 2023, the journal is included in the list of peer-reviewed scientific publications (VAK) in which the main scientific results of dissertations should be published in scientific specialties:

1.2.2. Mathematical modeling, numerical methods and software packages (technical sciences),

2.4.3. Electrical power engineering (technical sciences),

2.4.5. Energy systems and complexes (technical sciences).

Indexed by: RSCI, CyberLeninka, Google Scholar, Crossref.

The journal is registered with Roskomnadzor. Certificate Эл № ФС77-84526 January 16, 2023

Topics

- Energy production, conversion, transport and distribution systems
- Integrated energy systems
- Energy complexes
- National, regional, international and global energy systems
- Energy system protection, control and management
- Smart energy systems, smart grids
- Energy systems reliability and energy security
- Electric, gas, oil and heat supply systems
- Energy system development and operation
- System problems of energy consumers
- Energy economics and policy
- Renewable energy and clean fossil fuel based systems
- Distributed energy systems
- Sustainable energy transitions
- System problems of power and thermal engineering
- Artificial intelligence in energy systems
- Information and communication technologies in energy systems
- Energy system analysis and modelling
- Computational methods and optimization in energy systems

Editor-in-chief
Valery Stennikov,
academician of Russian Academy of Sciences,
director of *Melentiev Energy Systems Institute SB RAS, Russia*

Editorial board
- Sereeter Batmunkh, Mongolian University of Science and Technology, Mongolia
- Vitaly Bushuev, Institute of Energy Strategy, Russia
- Elena Bycova, Institute of Power Engineering of Academy of Sciences of Moldova, Republic of Moldova
- Gary Chang, National Chung Cheng University, Taiwan
- Pang Changwei, China University of Petroleum, China
- Cheng-I Chen, National Central University, Taiwan
- Gianfranco Chicco, Politecnico di Torino, Italy
- Van Binh Doan, lnstitute of Energy Science of VAST, Vietnam
- Petr Ekel, Federal University of Minas Gerais, Pontificial Catholic University of Minas Gerais, Brasil
- Ines Hauer, Otto-von-Guericke-Universität, Magdeburg, Germany
- Marija Ilic, Massachusetts Institute of Technology, Cambridge, USA
- James Kendell,Asian Pacific Energy Research Center, Japan
- Oleg Khamisov, Melentiev Energy Systems Institute SB RAS, Russia
- Alexander Kler, Melentiev Energy Systems Institute SB RAS, Russia
- Przemyslaw Komarnicki, University of Applied Sciences Magdeburg-Stendal, Germany
- Nadejda Komendantova, International Institute for Applied Systems Analysis, Austria
- Yuri Kononov, Melentiev Energy Systems Institute SB RAS, Russia
- Marcel Lamoureux, Policy and Governance Research Institute, USA
- Yong Li, Hunan University, China
- Faa-Jeng Lin, National Central University, Taiwan
- Alexey Makarov, Energy Research Institute RAS, Russia
- Lyudmila Massel, Melentiev Energy Systems Institute SB RAS, Russia
- Alexey Mastepanov, Oil and Gas Research Institute RAS, Institute of Energy Strategy, Russia
- Alexander Mikhalevich, Institute of Energy, Belarus
- Mikhael Negnevitsky, Tasmania University, Australia
- Takato Ojimi, Asian Pacific Energy Research Center, Japan
- Sergey Philippov, Energy Research Institute RAS, Russia
- Sergey Podkovalnikov, Melentiev Energy Systems Institute SB RAS, Russia
- Waldemar Rebizant, Wroclaw University of Science and Technology, Poland
- Christian Rehtanz, Dortmund Technical University, Germany
- Boris Saneev, Melentiev Energy Systems Institute SB RAS, Russia
- Sergey Senderov, Melentiev Energy Systems Institute SB RAS, Russia
- Zbigniew Styczynski, Otto-von-Guericke University Magdeburg, Germany
- Constantine Vournas, National Technical University of Athens, Greece
- Felix Wu, Hong-Kong University, China
- Ryuichi Yokoyama, Energy and Environment Technology Research Institute, Waseda University,Tokyo, Japan
- Jae-Young Yoon, Korea Electrotechnology Research Institute, Republic of Korea
- Xiao-Ping Zhang, University of Birmingham, United Kingdom

Publishing board

Copyeditors:	Marina Ozerova, Eugenia Markova

Contacts

Scientific secretary:	Alexey Mikheev, Dr. of Eng.
E-mail:	info@esrj.ru
Tel:	+7 (9148) 950980 (English, Russian)
Fax:	+7 (3952) 426796
Address:	130, Lermontov str., Irkutsk, 664033, Russia

CONTENTS

Dissociation of Gas Hydrates in a Combustion Environment

I.G. Donskoy[1,*]

[1] Melentiev Energy Systems Institute SB RAS, Irkutsk, Russia

***Abstract* — This paper proposes mathematical models of gas hydrate decomposition in high-temperature media. These models are based on heat and mass balances with a set of assumptions about transfer mechanisms and features of chemical reactions. The calculations provide an insight into dynamics of hydrate particles in a flame environment and shed light on possible results of interaction between the combustion front and emission of gas and vapor. Several examples are provided to illustrate the potential of hydrates as a fuel and as a flame extinguishing material. The developed models enable the generation of numerical estimates, which can be employed to design technologies for beneficial uses of gas hydrates.**

***Index Terms* — gas hydrates, thermal processing, diffusion flame, dissociation kinetics.**

I. INTRODUCTION

Gas hydrates are widespread in nature and constitute a significant part of hydrocarbon reserves [1, 2]. However, gas hydrates are not viewed as a significant energy resource and, according to technological forecasts, will not become significant for decades to come [3, 4]. This is due to their physicochemical and geochemical characteristics [5–7]. There are a small number of projects aimed at extracting gas hydrates (mostly research projects), or using them as materials or energy carriers (due to their specific properties) [8–10]. Interest in hydrates is associated, among other things, with their possible role in climate change processes [11].

Hydrates of combustible gases can be considered as a low-grade fuel (the water content in the crystals usually exceeds 70–80%). Nevertheless, there are still combustion conditions that enable efficient use of combustible matter. First of all, this is the diffusion combustion of powders: as experiments show [12–14], it is possible to select the conditions under which the emitted gas burns above the layer, providing the required level of combustion temperature at which the flame-to-surface heat flow maintains hydrate decomposition sufficient for self-sustained combustion.

Hydrates of non-flammable gases can be used as extinguishing agents [10]. In addition to high water content (also in crystalline form), hydrates are characterized by a higher latent heat of decomposition (since dissociation is an endothermic process), while the decomposition itself leads to the release of non-flammable gases that dilute the reacting medium.

Most studies on the interaction of gas hydrates with flames focus on experiments. Theoretical works usually rely on rather rough assumptions about the occurrence of physicochemical processes, especially in interphase regions. The authors of [15, 16] consider the one-dimensional non-stationary problem of the dissociation front propagation and phase transitions during the diffusion combustion of released methane. In [17, 18], the hydrate layer is considered as a bundle of pipes through which the

* Corresponding author.
E-mail: donskoy.chem@mail.ru

http://dx.doi.org/10.25729/esr.2024.01.0001

Received December 27, 2023. Revised January 25, 2024. Accepted February 1, 2024. Available online April 30, 2024.

This is an open-access article under a Creative Commons Attribution-NonCommercial 4.0 International License.

© 2024 ESI SB RAS and authors. All rights reserved.

components of the combustible mixture flow. The numerical description of experimentally observed non-stationary features of surface behavior remains impossible (although it is not clear whether such details are required for plausible modelling). In the study of combustion processes, we encounter a multitude of temporal and spatial scales associated with different components of the overall process, and significant changes in their ratios during the development of the process.

Mathematical models of flat hydrate layer dissociation are proposed in the papers [19] (for the diffusive gas transfer in the continuous approximation) and [20] (for the filtration intraparticle transfer). In [21], the latter model was verified using experimental data. In this case, however, the conditions on the outer surface of the powder layer are approximate. In [22], this model is used to estimate the stability of a methane-air-steam diffusion flame (such flames are considered experimentally and theoretically in [23, 24]).

Extinguishing flames with carbon dioxide hydrate is investigated in several experimental works [25, 26], where the hydrate is used in various forms (falling powder, stationary backfill). These experiments show the greater relative efficiency of hydrate compared to ice and water. In order to conduct a more detailed analysis of flame extinction mechanisms, suitable mathematical models are needed to study the impact of various factors, such as hydrodynamics and chemical reactions. Generally, such mathematical models tend to be quite complex. As in the case of the combustion of flammable gases emitted during hydrate dissociation, they must include a full-scale description of involved physicochemical processes, including interphase interactions. The huge number of elementary chemical reactions and multiple coexisting phases practically prevent any attempts to study numerically any realistic problem. In this regard, "computable", simplified models that contain the main features, and at the same time are not overloaded with a large number of details (that do not always have a decisive influence) are of greater interest.

The purpose of this work is to construct simple mathematical models of the stability of hydrocarbon flames in the presence of gas hydrates and to conduct numerical studies based on these models to clarify the basic mechanisms of observed critical phenomena. Exclusion of a detailed chemical description of flames inevitably reduces the problem to the thermal stability problem. On the one hand, this significantly simplifies the analysis of flame thermal stability, since it has a very wide range of tools [27], but on the other hand, this reduction narrows the applicability of the results, since the analysis does not allow the other features (for example, the chain reaction development) to be explained [28].

II. Models of Gas Hydrate Granule and Pellet Dissociation

Further, the difference between a single granule of gas hydrate and an agglomerate of such granules plays a significant role. The gas hydrate properties at the granule level are described in isothermal approximation, and the dissociation kinetics depends on the granule conversion degree. Since dissociation is a heterogeneous process, the interface between the fresh hydrate phase and the porous ice (that remains after the gas escapes into the gas phase) is of primary importance. This study, similarly to the classical works on the hydrate dissociation kinetics [29] assumes that the granules can be approximately considered spherical and the shrinkage of reacting surface is related to the granule conversion degree by simple geometric relationships. Other models of heterogeneous reactions are constructed in a similar manner (for example, thermochemical conversion of solid fuels [30]). In some cases, it is possible to approximate hydrate dissociation front movement as a Stefan problem [31] (when temperature gradients are high enough).

Particle dissociation becomes possible under thermobaric conditions above the equilibrium curve. The equilibrium curve, which defines the boundaries of the hydrate phase stability, is usually given in the form of a parametric equation:

$$\ln\left(\frac{P_{eq}}{P_0}\right) = C_0 - \frac{C_1}{T}. \qquad (1)$$

Here P_{eq} is equilibrium pressure, P_0 is atmospheric pressure, T is temperature, C_0 and C_1 are empirical constant. Note that for gas mixtures, there can be corrections, which we do not consider here. The equations of the equilibrium curves for methane hydrate and carbon dioxide hydrate are given in [32].

Following the work [29], we consider the dissociation process driving force to be the difference between the equilibrium and current gas pressure above the hydrate.

Then the equation for dissociation kinetics can be approximately written as follows [33]:

$$-\frac{dX}{dt}=\frac{K_d\left(P_{eq}-P_{out}\right)}{6B\rho_H d_0}X^{2/3}\frac{Da'}{1+Da'}, \quad (2)$$

where X is a conversion degree, K_d is the apparent kinetic constant, and Da' is a coefficient taking into account the pore resistance of the hydrate particle, P_{out} is output pore pressure, B is hydrate-forming gas mass fraction, ρ_H is hydrate mass density, d_0 is an average granule diameter. In a more precise formulation, when considering quasi-stationary filtration through a particle with spherical symmetries, one can obtain the equation:

$$-\frac{dX}{dt}=\frac{K_d}{6B\rho_H d_0}X^{2/3}\times$$
$$\times\left\{P_{eq}-P_{out}\left[\sqrt{\frac{1}{4Da^2}+\frac{P_{eq}}{P_{out}}\frac{1}{Da}+1}-\frac{1}{2Da}\right]\right\}, \quad (3)$$

where Da is a ratio of dissociation and filtration rates: when Da is large, the gas hydrate granule decomposition is controlled by kinetics (these conditions favor K_d measurements); when Da is small, the decomposition is controlled by filtration. In the latter case, data on the decomposition kinetics are disturbed by the porous structure influence - from here, for example, it is possible to estimate the characteristic pore sizes and gas permeability [34]. The difference between equations (2) and (3) is determined by the assumed approximation (see Appendix).

Agglomerates of granules (we will call them pellets) are formed when granules stick together (for example, under the action of a press, or due to partial melting). Such objects consist of a large number of granules. Each of them reacts along its trajectory, yet depending on neighbor granules, since they exchange heat and/or mass. The pellet density is less than the granule density due to the porous space between the particles, through which the gas flows during dissociation. Usually, with a good degree of approximation, the hydraulic resistance of the pellet can be assumed to be lower than the hydraulic resistance of the pores in the granules, therefore, the gas pressure drop in the pore space of the pellet is considered negligible. Conditions for heat transfer, however, are opposite: whereas for an individual granule, temperature can be considered uniform, for a pellet, it is necessary to factor in temperature inhomogeneity.

Then, given the granules are motionless, we obtain heat transfer equation for the pellet:

$$c_p\,\rho\frac{\partial T}{\partial t}=\frac{1}{r^n}\frac{\partial}{\partial r}\left(r^n\lambda\frac{\partial T}{\partial r}\right)+Q\left(t,r\right), \quad (4)$$

where Q is a heat sink, concerned with dissociation and phase transition latent heat; T is the temperature; c_p is the heat capacity; ρ is the pellet density; r is a characteristic spatial coordinate (radius or depth); λ is the thermal conductivity; n is a geometric (symmetry) exponent. The location of the reaction and phase transition fronts are calculated using an option of the enthalpy scheme. The boundary conditions are as follows:

$$\frac{\partial T}{\partial r}\left(0\right)=0,$$
$$-\lambda\frac{\partial T}{\partial r}\left(R\right)=\alpha\left(T_{env}-T\right)+\varepsilon\sigma\left(T_{rad}^4-T^4\right)-Q_{ev}J_{ev}, \quad (5)$$

where α is a heat transfer coefficient, σ is the Stefan-Boltzmann constant, ε is the emissivity, Q_{ev} is the evaporation heat, J_{ev} is the evaporation rate. Depending on environment conditions, values of T_{env} and T_{rad} may coincide or differ (for example, for muffle conditions T_{rad} is a wall temperature, and T_{env} is a flame temperature).

Surface water evaporation rate is calculated using the formula:

$$J_{ev}=\beta\left(C_{eq}-C_{env}\right), \quad (6)$$

where C_{eq} is the equilibrium water vapor concentration, C_{env} is the environmental water vapor concentration (usually close to zero). Mass transfer coefficient β is calculated taking into account Stefan flow [35]. Solving equations (1)–(6) yileds the dynamics of changes in temperature and pellet mass under high-temperature conditions. In this case, as mentioned above, quite serious simplifications are made. Namely, the water flow on the pellet surface is neglected (as is shown below, water flow losses can be partially factored in by introducing the effective evaporation heat); the structure of the boundary layer is not considered (all features are contained in the integral coefficients of heat and mass transfer), the multiphase flow in the porous space is not taken into consideration. The validity of these assumptions can be proved only by comparing calculation with experimental data. Model (1)–(6) is simplified because it includes only some basic balance equations. However, it contains a large number of coefficients. As is known, by varying these coefficients, we can achieve the agreement between calculations and experiments as close as desired. Therefore, restrictions are imposed on the values of the coefficients, depending on the degree of their certainty.

The thermal conductivity coefficient of backfills and pellets is calculated using the formulas for granular structures recommended in [36]. The porosity required for calculations is usually uncertain, with its value varying from 0.3 to 0.6 (a lower porosity corresponds to a sparse backfill and a larger porosity corresponds to a dense compaction). The particle sizes of the powder are determined by the synthesis conditions, but they can also change during preparation and measurement (for example, due to sticking or fragmentation). In calculations, it is necessary to use a certain average effective granule size. Due to experimental procedures, the powder bed is rarely uniform in height, therefore, the local height is also an uncertain value (although the average height can be determined quite accurately). The thermodynamic properties of the hydrate depend on the ice saturation degree. This value depends on the synthesis method and the sample preparation. In some cases, an undersaturated sample manages to lose a significant part of the gas during preparation for the experiment. Therefore, the gas content in the hydrate can range from the theoretical limit to half of this value. Some properties (for example, thermal conductivity and kinetic coefficients) can be determined only in a narrow temperature range. Therefore, they have to be replaced by averaged values (the uncertainty is quite high).

The previous paragraph is intended to show how uncertain is the choice of the quantities that are necessary for calculations. Trying to describe the effects of interfacial interactions and detailed kinetics of chemical reactions, we encounter a multiply growing uncertainty of the input information. In this context, as mentioned above, it is more reliable to use simplified models.

The main result of solving equations (1)–(6) is the numerical estimate of the characteristic decomposition times for a gas hydrate pellet (dissociation time, melting time, evaporation time), as well as the characteristic values of the gas-vapor surface mass flows. These data are

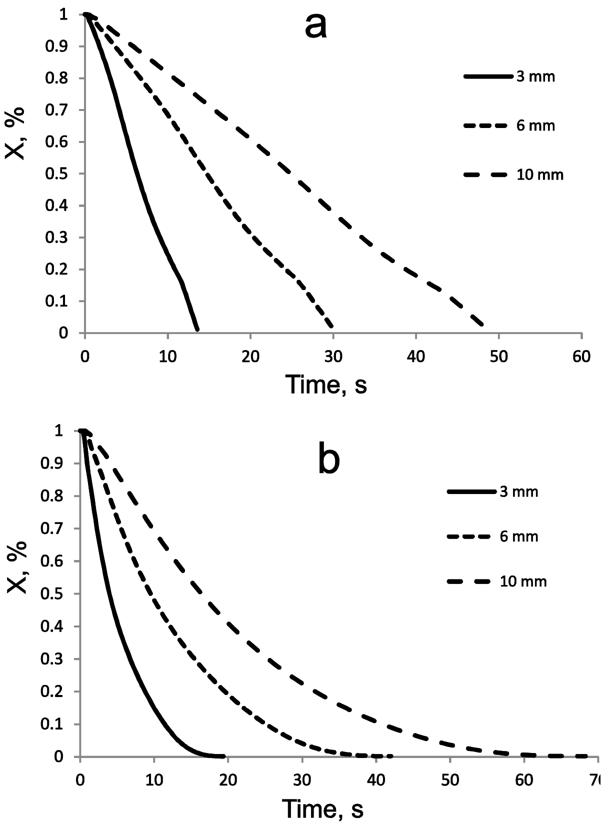

Fig. 1. Dynamics of CO_2 hydrate dissociation at 800°C: (a) – flat layer, (b) – cube.

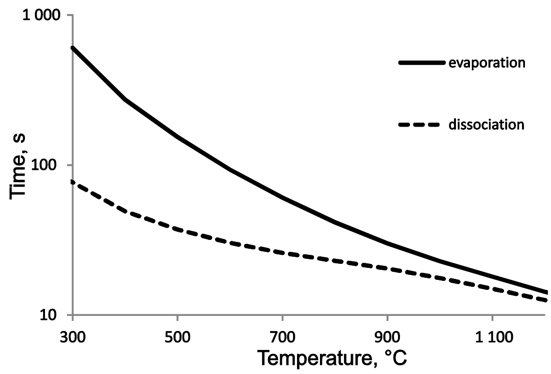

Fig. 2. Dynamics of CO_2 hydrate dissociation at 800°C: (a) – flat layer, (b) – cube.

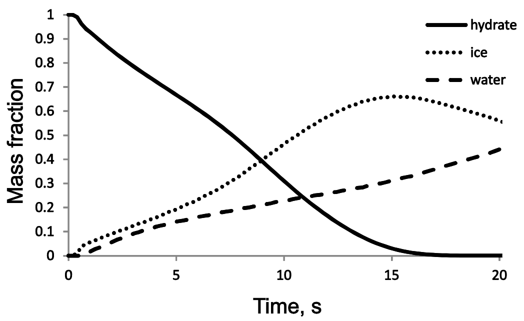

Fig. 3. Time dependence of CO_2 hydrate pellet composition (initial size – 5 cm, environment temperature – 900°C).

necessary for the next modelling stage, where the gas mixture compositions and heat flows associated with the hydrate particles conversion are needed to calculate the flame characteristics.

The numerical model was used to calculate dependencies. These dependencies make it possible to estimate the duration of decomposition stages under various temperature conditions. Figure 1 shows that geometric factor plays an important part in dissociation process. During conversion of flat layer, dissociation front surface does not change, and conversion rate is close to constant. When cubic sample is heated, dissociation front surface shrinks, leading to a decrease in conversion rate.

Figure 2 shows that evaporation time is much more sensitive to environment temperature (equilibrium vapor pressure in equation (6) exponentially depends on temperature). Dissociation forms an ice layer, which melts forming a liquid cover layer (its temperature does not exceed 100°C, but is quite close to this value most of the evaporation time). The processes of dissociation, melting, and evaporation occur simultaneously (Fig. 3). At the same time, the water can leave pellet not only by evaporation but also by flowing down. To allow for this effect, a slight modification of the model is proposed: non-evaporative water losses are simulated by lowering the evaporation heat. Figure 4 presents the results of calculations for coefficients 0.75, 0.5, and 0.25. As expected, reducing the evaporative water losses enhances dissociation kinetics and increases surface temperature. Liquid layer width for all cases is of the order of tenth mm.

Since the dissociation stage is the fastest stage of all, gas is released in a high, short-lived peak. Further, depending on the sample size, the surface temperature increases until intense evaporation begins. The evaporation is very energy-consuming, therefore, the water vapor flux is usually lower than the gas flux. Due to the high water content in the hydrate, evaporation lasts much longer. Thus, when hydrate enters the flame zone, a large injection of hydrate-forming gas occurs, and then evaporation begins. There is a short time period when the gas-vapor mixture composition is determined by the position of the dissociation front and phase transition fronts. If the hydrate releases flammable gas, the release of flammable gas should enhance the flame stability, but it is necessary to remove the condensed ice residue in order to reduce the heat sink. If the hydrate releases non-flammable gas, the

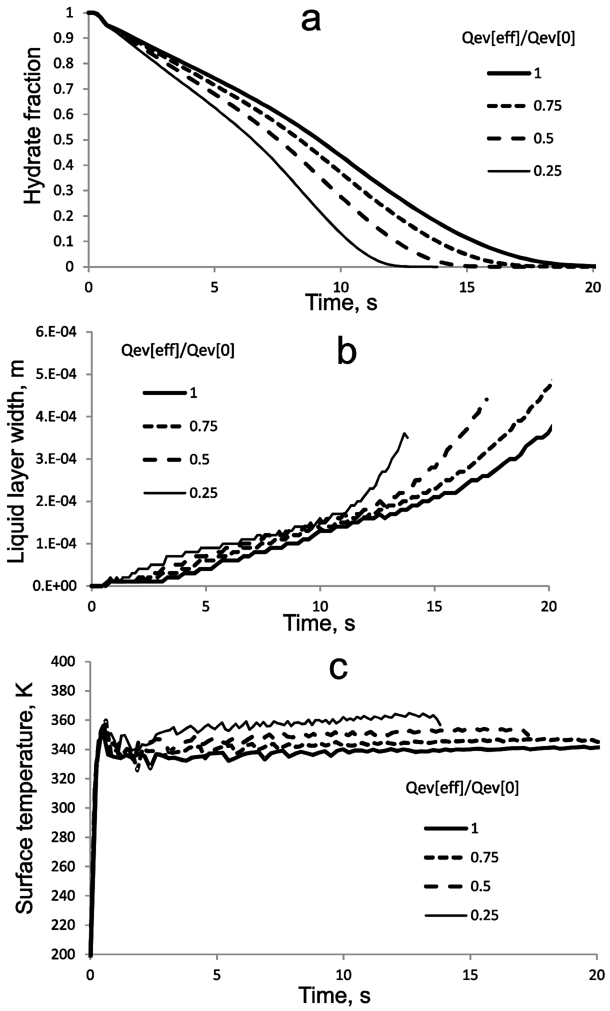

Fig. 4. CO_2 pellet decomposition for varying evaporation heat: (a) – hydrate fraction; (b) – width of surface water layer; (c) – surface temperature.

initial injection of gas leads to dilution of the reacting medium, therefore, quenching by inert diluent has higher possibility in the first period of decomposition. After this, extinction may occur due to the heat losses, and stability depends on the conditions of heat and mass transfer between ice particles and the flame zone.

III. Diffusion Flame Model

Typically, the combustion of gas during hydrate decomposition is diffusion combustion. The authors of [37, 38] propose mathematical models of flame near a single suspended hydrate particle and flame propagation in a cloud of such particles. These models are based on the

Shvab-Zeldovich approximation widely used in combustion theory [39, 40]. Gas combustion above a decomposing hydrate powder can be considered as a reaction process in the boundary layer above a permeable surface [41] (in this case, the injection velocity is, as a rule, low enough to consider its effect insignificant and to use the approximation for an impermeable surface [12, 22]). In some experimental setups, air is supplied through the hydrate layer [42, 17]. In such cases, we can assume that the mixture has already been mixed before entering the space above the layer. In this work, however, we address a diffusion flame and the limits of its stability during interaction with hydrates of flammable and non-flammable gases. The diffusion flame models are even more adequate to consider extinguishing liquid fuel flames by hydrate particles.

The basis for our calculations is the model proposed in [43]. This model relies on correspondence between the original stationary diffusion combustion problem and the simpler problem of a stoichiometric well-mixed combustion (stoichiometry condition follows from the Shvab-Zeldovich approximation). Such a replacement is possible due to the similar nature of critical phenomena in the thermal theory of flames. The mentioned work [43] examines the thermal balance of a diffusion flame, taking into account the combustion heat and heat losses (conductive, convective, and radiative). The residence time of the reagents in the flame zone is determined by the flow velocity and the characteristic spatial scale. The model allows calculating the critical conditions for flame extinction (including local extinction in turbulent flows [44]). In [22], we calculated the stability limits of combustion for methane/water vapor mixtures (using data from the experimental work [24]). In addition, it is shown that with the accurately chosen spatial scale, it is possible to reproduce the extinction conditions for methane above the methane hydrate layer.

The model is constructed by analogy with the description of a perfectly stirred flow reactor. The material balance equation can be written as follows:

$$n_j^0 - n_j = \tau \sum_i \gamma_{ij} w_i \, , \tag{7}$$

where n_j is the amount of the j-th substance, τ is a residence time, γ_{ij} is a stoichiometric coefficient, and w_i is a rate of the i-th reaction.

The simplest choice of kinetic description of a chemical reaction is to use a lumped mechanism with effective kinetic coefficients. This approach is also used in [43] (kinetics constants can be found in the paper). For hydrocarbon fuels, the lumped equation is written as follows:

$$C_n H_m + \left(n + \frac{m}{4} \right) O_2 = nCO_2 + \frac{m}{2} H_2 O \, . \tag{8}$$

Heat balance is written in the following form:

$$\sum_j h_j \left(T_0 \right) n_j^0 = \sum_j h_j \left(T \right) n_j + q_{cond} + q_{conv} + q_{rad} \, , \tag{9}$$

where h_j is the specific enthalpy of the j-th component (calculated using the database from [45]), and q is heat losses:

$$q_{cond} = \tau \frac{\lambda_g}{L^2} \left(T - T_{env} \right), \tag{10}$$

$$q_{conv} = \tau \frac{\alpha}{L} \left(T - T_{env} \right), \tag{11}$$

$$q_{rad} = \tau \frac{\kappa}{L} \left(T^4 - T_{rad}^4 \right). \tag{12}$$

Here λ_g is heat conductivity, and L is characteristic length (reaction zone width).

To obtain adequate numerical results, it is important to select appropriate scales. In the simplest configurations of diffusion flames, the linear and time scales are uniquely determined by the distance between the nozzles and the flow rate of the reagents. In the combustion of a boundary layer, the linear scale is related to its thickness; therefore, in general, it depends on the position of the flame front. Even for moving flame front, it is possible to choose an averaged length that allows calculating its stability under conditions of convective heat transfer [22]. The calculations show that the radiative term (12) cannot be neglected due to high concentration of CO_2 and H_2O [20]. The value of κ is estimated using recommendations given in [46].

For the combustion conditions of methane-vapor mixtures, it is possible to calculate the theoretical dependences of the combustion temperature on the composition and characteristic scales. For one-stage reactions, such dependences usually show the existence of regions with one solution and three solutions (in the latter case, two of them are stable). At large degrees of dilution, the stationary solutions form closed curves (isolas) [27, 47]. The separation of isola from the region of low-temperature solutions indicates the impossibility of self-ignition in such mixtures, which is consistent with the

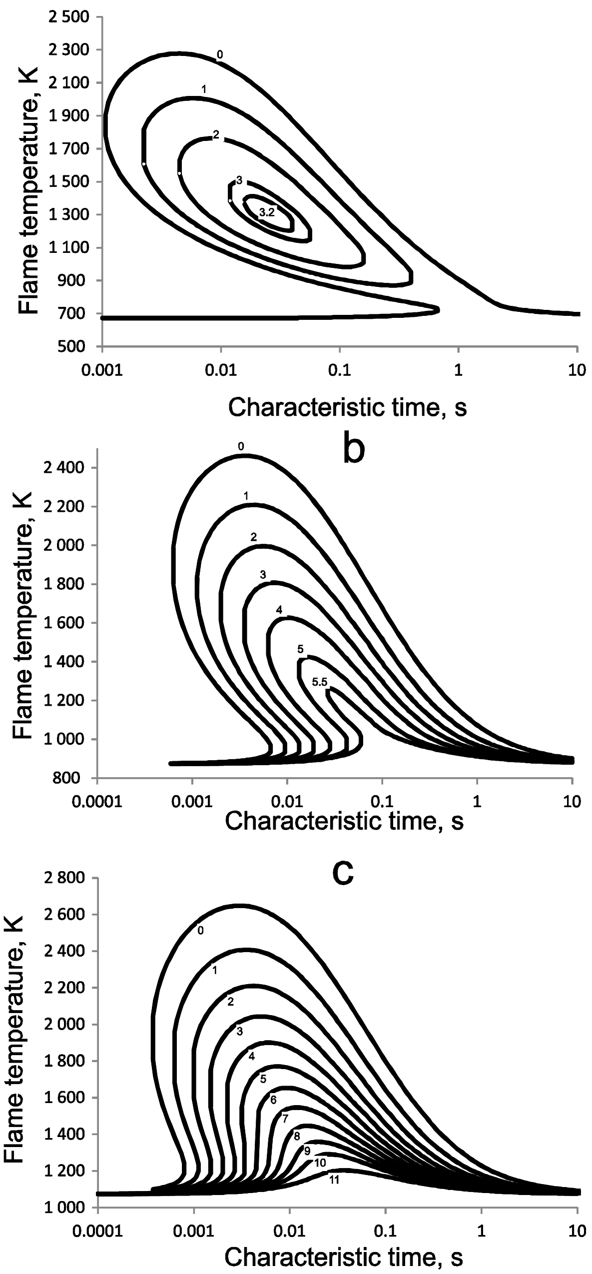

Fig. 5. Dependence of calculated flame temperature for methane-water vapor mixtures (numbers near curves are dilution ratios) on environment temperature: (a) – 400°C; (b) – 600°C; (c) – 800°C.

reality (methane hydrate flames are usually initiated by pilot heat source). The critical concentration of water vapor in a mixture with methane for the room temperature environment is of the order of 70% [22]. The higher the environment temperature, the wider the flame stability limits. Figure 5 shows calculated temperature curves for various environment conditions (400°C, 600°C, and 800°C). At the temperature of 600°C, isolas merge with the low-temperature solution branch; at the temperature of 800°C, critical points degenerate at dilution ratios larger than 5.

In the case of flame extinguishing by gas hydrate, the composition of the diluent has a significant influence on the flame stability limits [43]. Since the lumped chemical mechanism is not sensitive to the composition of the diluent (although some diluents can act as chain reaction inhibitors), specific heat capacity is the major factor. For example, carbon dioxide is more effective than water vapor, which, in turn, is more effective than nitrogen. The calculations performed using the model align with these concepts. During the hydrate decomposition, it is possible to distinguish three main stages: release of the hydrate-forming gas; release of the gas-water vapor mixture; release of the water vapor. For carbon dioxide hydrate, these stages correspond to the compositions of the diluents CO_2, CO_2/H_2O (for simplicity, we take an equimolar mixture for calculation), and H_2O. Then it is possible to find the conditions for the extinction of hydrocarbon flames when gas hydrate particles enter them.

Depending on the size of the particles and the average flame temperature (such an approximation inevitably has to be made, because of both the uncertainty of the particle trajectory and the perturbations of the flame front), the decomposition takes various amounts of time to complete. Calculated decomposition time gives the average gas and water vapor flows entering the flame region. Then, knowing the average burning rate of an undisturbed flame, we can approximately calculate the quantity of hydrate particles, which allows creating diluent mass flow sufficient for flame extinction (assuming that the particles are distributed evenly). When considering diffusion combustion, the fuel combustion rate is related to the area. Then the calculations give the critical mass of hydrate particles per unit area of flame (which is enough to extinguish the flame). For liquid fuel combustion, we consider a dispersed particle flow with an average particle diameter of 2 mm and an average decomposition rate of 0.4 mg/s. The environment temperature is 300 K.

Figure 6 shows dependences of flame temperature on mass flow for CO_2 hydrate: right termination points correspond to extinction. The stable combustion limits depend on fuel heat value (as expected, the higher the heat value, the higher the hydrate mass flow required for the

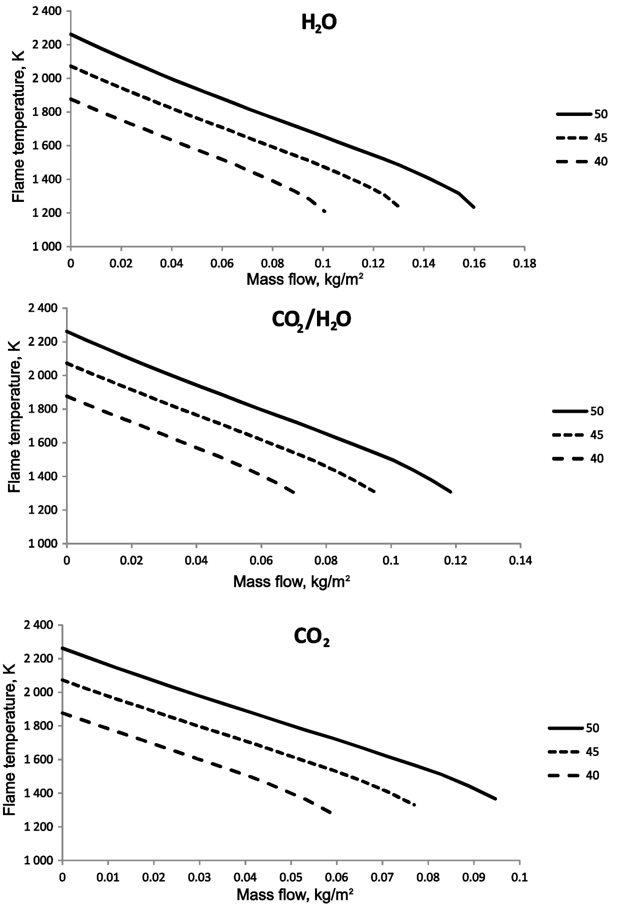

Fig. 6. Influence of diluting gas flow composition on stability limits of diffusion flame (for fuel heat value, MJ/kg).

flame extinction). CO_2 has a higher specific heat capacity, which is why, CO_2-added flame demonstrates narrower stability boundaries.

According to Fig. 7, heat values of real liquid fuels fill a narrow band between boundary values (40 and 50 MJ/kg). Given the hydrate powder particle size of 2 mm, we obtain a critical amount of powder of about 100 g/m^2, which corresponds to a heat flow ranging from 100 to 200 kW. The figure shows the dependence of calculated flame temperature and heat losses on mass flow during diffusion combustion of evaporating liquid fuels in the presence of CO_2 hydrate powder.

IV. Conclusions

Interaction of gas hydrates with high-temperature media is considered using a set of simplified mathematical models, which allow estimating individual particle (pellet) behavior and stability of hydrocarbon-air diffusion flames. The behavior of flame and hydrate particles is interdependent, and the simplest approximation splits overall process into two subsystems: one providing boundary conditions (temperature, mass flows) for the other.

The calculations show the influence of geometric, thermal, and reactivity factors on hydrate decomposition macrokinetics and flame stability. In the first scenario, dissociation and phase transitions under external heat supply determine the expected decomposition time and product gas composition. In the second scenario, saturation of the zone of flame with inert gases determines its stationary temperature.

Problems related to combustion stability are interesting from the perspective of safe storage and transport of hydrates: in the case of flammable gas emissions (for example, during unplanned heating or depression), a large amount of water does not guarantee that ignition will not occur (although it may contribute to faster extinction).

On the other hand, determining the conditions for stable combustion, especially in confined spaces, may be of crucial importance for the technologies of gas production

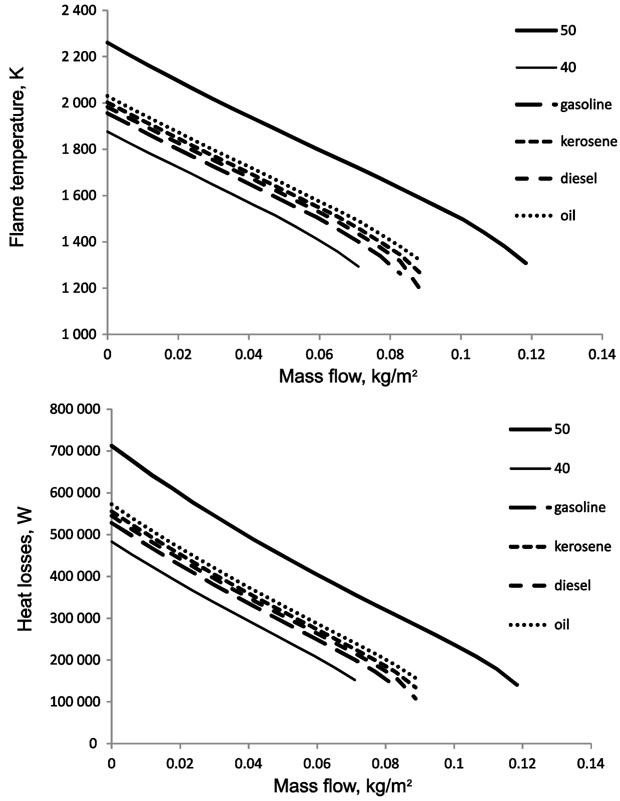

Fig. 7. Flame temperature and heat losses at different CO_2 hydrate power mass flows for various liquid fuels.

from hydrates associated with thermal stimulation of gas-saturated formations due to the heat of combustion of additional fuel or part of the gas produced [48]. The effectiveness of such methods depends significantly on the intensity of heat exchange in the area of contact between the hot medium and the rock. These problems may be a subject for the future works.

APPENDIX

The problem of gas hydrate granule dissociation is very similar to those of droplet evaporation or carbon particle combustion [35].

Let us consider a one-dimensional problem of filtration between two concentric spherical surfaces. The fluid is an ideal gas with the molecular mass M_r. The stationary Darci flow conditions give the equation:

$$\frac{d}{dr}\left(r^2 \frac{k_F}{\mu}\frac{PM_r}{R_gT}\frac{dP}{dr}\right)=0\,, \tag{A1}$$

where P is the gas pressure, μ is the viscosity, k_F is the permeability, R_g is a gas constant. Further, we use a set of approximations: the permeability is uniform; the area is isothermal; the gas composition is uniform. The internal boundary is maintained at pressure P_{in} and the outer boundary – at P_{out}. This set allows us to obtain the formula for the stationary Darci flow rate:

$$J=\frac{P_{in}^2-P_{out}^2}{1-{r}/{R}}\frac{k_FM_r}{2r\mu R_gT}\,, \tag{A2}$$

where r and R are the radii of the two spheres (if $r << R$, equation (A2) becomes the Darci flow for a thin flat layer).

Next, the internal boundary condition is changed: instead of constant pressure, we deal with the chemical reaction whose rate is proportional to kinetic coefficient K_d and pressure difference between equilibrium and boundary pressure values. Pressure P_{in} becomes a variable. Then, applying the stationary condition again, we obtain:

$$K_d\left(P_{eq}-P_{in}\right)=\frac{P_{in}^2-P_{out}^2}{1-{r}/{R}}\frac{k_FM_r}{2r\mu RT}\,. \tag{A3}$$

Equation (A3) is a quadratic equation having the only physical (non-negative) root:

$$P_{in}=P_{out}\left[\sqrt{\frac{1}{4Da^2}+\frac{P_{eq}}{P_{out}}\frac{1}{Da}+1}-\frac{1}{2Da}\right], \tag{A4}$$

where Da is the Damkohler number, which is a ratio between characteristic times of heterogeneous reaction and filtration transport:

$$Da=\frac{k_F}{2r\mu}\frac{1}{K_d}\frac{P_{out}M_r}{R_gT}\frac{1}{1-{r}/{R}}\,. \tag{A5}$$

Now, we can write the formula for reaction rate in the following way:

$$J=K_d\left\{P_{eq}-P_{out}\left[\sqrt{\frac{1}{4Da^2}+\frac{P_{eq}}{P_{out}}\frac{1}{Da}+1}-\frac{1}{2Da}\right]\right\}. \tag{A6}$$

Equation (A6) looks clumsy, but it can be reduced to a simpler form by using some approximations. Let us first show that it gives a reasonable kinetic behavior for small and large values of Da. For $Da >> 1$ we immediately obtain $P_{in} \to P_{out}$, which corresponds to kinetics-controlled heterogeneous reaction. For $Da << 1$, we need to operate more accurately. First, we consider P_{out} in (A4) as a function of $P_{eq}/P_{out} = w$. If $Da^{-1} > 1$, w becomes a small parameter, and we have the estimate (the first two terms of the Taylor series):

$$P_{in}\approx P_{out}\left\{\left[\sqrt{\frac{1}{4Da^2}+\frac{1}{Da}}-\frac{1}{2Da}\right]+\frac{w}{\sqrt{1+4Da}}\right\}. \tag{A7}$$

Now, we take the limit $Da \to 0$ and obtain $P_{in} \to P_{eq}$. This range of Da corresponds to filtration-controlled decomposition, and the flow rate J in (A6) becomes close to zero (compared to kinetic equation).

Now, let us solve an easier problem. Instead of compressed gas, we consider an equivalent fluid with the averaged density ρ, and obtain a simplified solution for the stationary Darci flow:

$$J=\frac{P_{in}-P_{out}}{1-{r}/{R}}\frac{k_F\rho}{\mu r}\,. \tag{A8}$$

Using stationary conditions and the same kinetic equation, we have the simplified formula for the boundary pressure:

$$P_{in}=\frac{P_{eq}+P_{out}Da'}{1+Da'}\,, \tag{A9}$$

where Da' is a modified Damkohler number:

$$Da'=\frac{k_F}{r\mu}\frac{\rho}{K_d}\frac{1}{1-{r}/{R}}\,. \tag{A10}$$

The difference between equations (A5) and (A10) is the choice of gas density (in [48], a suitable approximation for averaged density is proposed). Then the reaction rate can be written as follows:

$$J = K_d\left(P_{eq} - P_{out}\right)\frac{Da'}{1+Da'}. \quad \text{(A11)}$$

It can be seen that $Da' \ll 1$ leads to low flow rates (filtration-controlled decomposition) and $Da' \gg 1$ gives kinetic-controlled decomposition.

During the dissociation, reaction front moves from the outer surface towards the particle's core. It is important to note that the location of dissociation front is geometrically related to the conversion degree. Considering progress variable X (a relative amount of gas stored in a hydrate phase), we can write:

$$Da = \frac{k_F}{2R\mu}\frac{1}{K_d}\frac{P_{out}M_r}{R_g T}\frac{1}{X^{1/3} - X^{2/3}}, \quad \text{(A5a)}$$

$$Da' = \frac{k_F}{R\mu}\frac{\rho}{K_d}\frac{1}{X^{1/3} - X^{2/3}}. \quad \text{(A10a)}$$

The factors depending on X have a greater influence on dissociation kinetics in the vicinity of $X = 1$ and $X = 0$ (as shown in [33]). For the gas flow given by (A11), the decomposition time (which is finite) can be obtained in the following form:

$$\tau = \frac{B\rho_H d_0}{2K_d\left(P_{eq} - P_{out}\right)}\left(1 + \frac{6}{Da''}\right), \quad \text{(A12)}$$

where $Da'' = Da'(X^{1/3} - X^{2/3})$, B is the gas mass fraction in fresh hydrate, ρ_H is the fresh hydrate density, d_0 is an effective particle diameter [49].

Acknowledgment

This research was supported by TPU development program Priority 2030 (Priority-2030-NIP/EB-006-0000-2022), by a grant from the Ministry of Science and Higher Education of Russia, Agreement of 29 September 2020 Number 075-15-2020-806 (Contract Number 13.1902.21.0014) and by State Assignment Project (no. FWEU-2021-0005) of the Fundamental Research Program of Russian Federation 2021–2030 using the resources of the High-Temperature Circuit Multi-Access Research Center (Ministry of Science and Higher Education of the Russian Federation, project no 13.CKP.21.0038).

References

[1] Z. R. Chong, S. H. B. Yang, P. Babu, P. Linga, X.-S. Li, "Review of natural gas hydrates as an energy resource: Prospects and challenges," *Appl. Energy*, vol. 162, pp. 1633–1652, 2016. doi: 10.1016/j.apenergy.2014.12.061

[2] Z. Yin, P. Linga, "Methane hydrates: A future clean energy resource," *Chinese J. Chem. Eng.*, vol. 27, pp. 2026–2036, 2019. doi: 10.1016/j.cjche.2019.01.005

[3] *Energy technology perspectives 2020*. International Energy Agency, 2021.

[4] *Prospects for the development of global energy, taking into account the impact of technological progress*. Moscow: ERI RAS, 2020. (In Russian)

[5] X.-S. Li, C.-G. Xu, Y. Zhang, X.-K. Ruan, G. Li, Y. Wang, "Investigation into gas production from natural gas hydrate: A review," *Appl. Energy*, vol. 172, pp. 286–322, 2016. doi: 10.1016/j.apenergy.2016.03.101

[6] F. Li, Q. Yuan, T. Li, Z. Li, C. Sun, G. Chen, "A review: Enhanced recovery of natural gas hydrate reservoirs," *Chinese J. Chem. Eng.*, vol. 27, pp. 2062–2073, 2019. doi: 10.1016/j.cjche.2018.11.007

[7] N. Wu, Y. Li, Y. Wan, J. Sun, L. Huang, P. Mao, "Prospect of marine natural gas hydrate stimulation theory and technology system," *Natural Gas Industry B*, vol. 8, pp 173–187, 2021. doi: 10.1016/j.ngib.2020.08.003

[8] H. P. Veluswamy, A. Kumar, Y. Seo, J. D. Lee, P. Linga, "A review of solidified natural gas (SNG) technology for gas storage via clathrate hydrates," *Appl. Energy*, vol. 216, pp. 262–285, 2018. doi: 10.1016/j.apenergy.2018.02.059

[9] C. Cheng, F. Wang, Y. Tian, X. Wu, J. Zheng, J. Zhang, L. Li, P. Yang, J. Zhao, "Review and prospects of hydrate cold storage technology," *Renewable and Sustainable Energy Reviews*, vol. 117, p. 109492, 2020. doi: 10.1016/j.rser.2019.109492

[10] O. Gaidukova, S. Misyura, V. Morozov, P. Strizhak, "Gas Hydrates: Applications and Advantages," *Energies*, vol. 16, p. 2866, 2023. doi: 10.3390/en16062866

[11] V. Krey, J.G. Canadell, N. Nakicenovic, et al., "Gas hydrates: entrance to a methane age or climate threat?" *Environ. Res. Lett.*, vol. 4, p. 034007, 2009. doi: 10.1088/1748-9326/4/3/034007

[12] Y. Maruyama, M.J. Fuse, T. Yokomori, R. Ohmura, S. Watanabe, T. Iwasaki, W. Iwabuchi, T. Ueda, "Experimental investigation of flame spreading over pure methane hydrate in a laminar boundary layer," *Proc. Combust. Inst.*, vol. 34, pp. 2131–2138, 2013. doi: 10.1016/j.proci.2012.06.179

[13] S. Y. Misyura, "Non-stationary combustion of natural and artificial methane hydrate at heterogeneous dissociation," *Energy*, vol. 181, pp. 589–602, 2019. doi: 10.1016/j.energy.2019.05.177

[14] G. Cui, Z. Dong, K. Xie, S. Wang, T. Guo, J. Liu, X. Xing, Z. Li, "Experimental study on the effect of airflow conditions on the combustion characteristics of methane hydrate," *Fuel*, vol. 300, p. 120926, 2021. doi: 10.1016/j.fuel.2021.120926

[15] I. M. Bayanov, I. K. Gilmatdinov, M. V. Stolpovskii, "Modeling the Process of Combustion of Methane Hydrate with Allowance for Nonequilibrium Decomposition," *J. Eng. Phys. Thermophys.*, vol. 96, pp. 104–111, 2023. doi: 10.1007/s10891-023-02666-4

[16] I. K. Gilmatdinov, I. M. Bayanov, M. V. Stolpovskii, A. S. Chiglintseva, "On the Confined Combustion of a Hydrate," *J. Eng. Phys. Thermophys.*, vol. 95, pp. 591–598, 2022. doi: 10.1007/s10891-022-02515-w

[17] G. Cui, T. Guo, K. Xie, Z. Dong, D. Wu, J. Yin, Z. Li, "Combustion experiment and numerical simulation of methane hydrate sediment under different airflow environments," *Fuel*, vol. 333, p. 126560, 2023. doi: 10.1016/j.fuel.2022.126560

[18] G. Cui, D. Wu, Y. Li, S. Yao, T. Guo, J. Yin, X. Xing, J. Liu, "Effect of Lithological Parameters on Combustion Characteristics of Methane Hydrate Sediments," *Fire*, vol. 6, p. 463, 2023. doi: 10.3390/fire6120463

[19] V. A. Vlasov, "Diffusion model of gas hydrate dissociation into ice and gas that takes into account the ice microstructure," *Chem. Eng. Sci.*, vol. 215, p. 115443, 2020. doi: 10.1016/j.ces.2019.115443

[20] S. Y. Misyura, I. G. Donskoy, "Dissociation and Combustion of a Layer of Methane Hydrate Powder: Ways to Increase the Efficiency of Combustion and Degassing," *Energies*, vol. 14, p. 4855, 2021. doi: 10.3390/en14164855

[21] S. Y. Misyura, I. G. Donskoy, A. Y. Manakov, V. S. Morozov, P. A. Strizhak, S. S. Skiba, A. K. Sagidullin, "Studying the influence of key parameters on the methane hydrate dissociation in order to improve the storage efficiency," *Journal of Energy Storage*, vol. 44A, pp. 103288, 2021. doi: 10.1016/j.est.2021.103288

[22] I. G. Donskoy, S. Ya. Misyura, "Experimental and theoretical study of diffusion combustion of methane above a gas hydrate layer in a laminar air flow," *Combustion, Explosion, and Shock Waves*, vol. 58, pp. 440–449, 2022. doi: 10.1134/S0010508222040062

[23] F. H. Wu, R. E. Padilla, D. Dunn-Rankin, G. B. Chen, Y. C. Chao, "Thermal structure of methane hydrate fueled flames," *Proc. Combust. Inst.*, vol. 36, pp. 4391–4398, 2017. doi: 10.1016/j.proci.2016.06.012

[24] R. E. Padilla, D. Escofet-Martin, T. Pham, W. J. Pitz, D. Dunn-Rankin, "Structure and behavior of water-laden CH4/air counterflow diffusion flames," *Combust. Flame*, vol. 196, pp. 439–451, 2018. doi: 10.1016/j.combustflame.2018.06.037

[25] O. Gaidukova, V. Morozov, R. Volkov, P. Strizhak, "Containment and Suppression of Class A Fires Using CO_2 Hydrate," *Fire*, vol. 6, p. 82, 2023. doi: 10.3390/fire6030082

[26] O. Gaidukova, I. Donskoy, S. Misyura, V. Morozov, R. Volkov, "The Interaction between a Liquid Combustion Front and a Fire Barrier Made of CO2 Hydrate," *Fire*, vol. 6, p. 124, 2023. doi: 10.3390/fire6030124

[27] L. A. Vulis, *Thermal regimes of combustion*, NY, McGraw-Hill Book Company, Incorporated, 1961.

[28] V. V. Azatyan, "Decisive Role of the Laws of Chain Reactions in Processes of Combustion, Explosion, and Detonation of Gases," *Kinet. Catal.,* vol. 62, pp. 233–244, 2021. doi: 10.1134/S0023158421020014

[29] H. C. Kim, P. R. Bishnoi, R. A. Heidemann, S. S. H. Rizvi, "Kinetics of methane hydrate decomposition," *Chem. Eng. Sci.*, vol. 42, pp. 1645–1653, 1987. doi: 10.1016/0009-2509(87)80169-0

[30] N. M. Laurendeau, "Heterogeneous kinetics of coal char gasification and combustion," *Progress in Energy and Combustion Science*, vol. 4, pp. 221–270, 1978.

[31] D.V. Antonov, E.A. Shchepakina, V.A. Sobolev, S.Y. Misyura, I.G. Donskoy, P.A. Strizhak, S.S. Sazhin, "Dissociation of methane from a layer of methane-hydrate particles: A new simple model," *Int. J. Heat Mass Transfer*, vol. 213, p. 124225, 2023. doi: 10.1016/j.ijheatmasstransfer.2023.124225

[32] E. D. Sloan, C. A. Koh, *Clathrate hydrates of natural gases*, 3rd ed. Boca Raton, Florida, USA: CRC Press, Taylor and Francis Group, 2008.

[33] I. G. Donskoy, S. Ya. Misyura, "Non-Isothermal Kinetic Model of the Methane Hydrate Dissociation Process at Temperatures Below Ice Melting Point," *Energy Systems Research*, vol. 3, no. 1, pp. 27–42, 2020. doi: 10.38028/esr.2020.01.0003

[34] S. Y. Misyura, I. G. Donskoy, "Dissociation kinetics of methane hydrate and CO2 hydrate for different granular composition," *Fuel*, vol. 262, p. 116614, 2020. doi: 10.1016/j.fuel.2019.116614

[35] D. B. Spalding, *Combustion and mass transfer*. Oxford, UK: Pergamon Press, 1979.

[36] M. E. Aerov, O. M. Todes, D. A. Narinskii, *Stationary granular beds: hydraulics and heat transfer*. Leningrad, USSR: Chemistry Publishing, 1979. (In Russian)

[37] T. Bar-Kohany, W.A. Sirignano, "Transient combustion of a methane-hydrate sphere," *Combust. Flame*, vol. 163, pp. 284–300, 2016. doi: 10.1016/j.combustflame.2015.10.004

[38] Y. Dagan, T. Bar-Kohany, "Flame propagation through three-phase methane-hydrate particles," *Combust. Flame*, vol. 193, pp. 25–35, 2018. doi: 10.1016/j.combustflame.2018.02.026

[39] Ya. B. Zeldovich, *Selected works. Volume I: Chemical Physics and Hydrodynamics*. Princeton, New Jersey, USA: Princeton Univ. Press, 1992.

[40] A. Linan, "The asymptotic structure of counterflow diffusion flames for large activation energies," *Acta Astronautica*, vol. 1, pp. 1007–1039, 1974. doi: 10.1016/0094-5765(74)90066-6

[41] E. P. Volchkov, V. I. Terekhov, V. V. Terekhov, "Flow Structure and Heat and Mass Transfer in Boundary Layers with Injection of Chemically Reacting Substances (Review)," *Combustion, Explosion, and Shock Waves*, vol. 40, pp. 1–16, 2004. doi: 10.1023/B:CESW.0000013663.27112.ab

[42] S. Y. Misyura, "Efficiency of methane hydrate combustion for different types of oxidized flow," *Energy*, vol. 103, pp. 430–439, 2016. doi: 10.1016/j.energy.2016.03.005

[43] A. Yu. Snegirev, "Perfectly stirred reactor model to evaluate extinction of diffusion flame," *Combust. Flame*, vol. 162, pp. 3622–3631, 2015. doi: 10.1016/j.combustflame.2015.06.019

[44] A. Yu. Snegirev, A. S. Tsoy, "Treatment of local extinction in CFD fire modeling," *Proc. Combust. Inst.*, vol. 35, pp. 2519–2526, 2015. doi: 10.1016/j.proci.2014.07.051

[45] B. J. McBride, M. J. Zehe, S. Gordon, *NASA Glenn Coefficients for Calculating Thermodynamic Properties of Individual Species (NASA\TP-2002-211556)*. Cleveland, USA: Glenn Research Center, 2002.

[46] Y. Ju, H. Guo, F. Liu, K. Maruta, "Effects of the Lewis number and radiative heat loss on the bifurcation and extinction of CH4/O2-N2-He flames," *J. Fluid Mech.*, vol. 379, pp. 165–190, 1999. doi: 10.1017/S0022112098003231

[47] V. Hlavacek, P. Van Rompay, "On the birth and death of isolas," *Chem. Eng. Sci.*, vol. 36, pp. 1730–1731, 1981. doi: 10.1016/0009-2509(81)80019-X

[48] C. Cranganu, "In-situ thermal stimulation of gas hydrates," *J. Petroleum Sci. Technol.*, vol. 65, pp. 76–80, 2009. doi: 10.1016/j.petrol.2008.12.028

[49] S. Y. Misyura, I. G. Donskoy, "Dissociation of a powder layer of methane gas hydrate in a wide range of temperatures and heat fluxes," *Powder Technol.*, vol. 397, p. 117017, 2022. doi: 10.1016/j.powtec.2021.11.061

Igor G. Donskoy received the Ph.D. degree in 2014. Currently he is a Senior researcher in the Laboratory of Thermodynamics at Melentiev Energy Systems Institute SB RAS (Irkutsk). His main research interests include mathematical modelling in fuel processing and thermal engineering.

Applicability of Anomaly Detection Knowledge from Computer Science and Mathematics Publications to Oil and Gas Research

B.N. Chigarev [1,*]

[1] Oil and Gas Research Institute of the Russian Academy of Sciences (OGRI RAS), Moscow, Russia

***Abstract* — Anomaly detection in equipment processes is crucial for the oil and gas sector. Algorithms for detecting anomalies in measured data are best understood in Computer Science and Mathematics. Therefore, a possible transfer of knowledge from the latter area to the former can have a profound impact. This paper explores the potential for the knowledge transfer by analyzing bibliometric data of Computer Science and Mathematics papers published in MDPI journals, as well as publications available on SPE search platform. The research shows that the main algorithms extensively studied in MDPI publications and found in SPE publications, which address the anomaly detection problem, include Random Forest, Support Vector Machine, Long-term Memory Method and Recurrent Neural Network. The main advantages and disadvantages of these methods are briefly described. This paper provides examples of classical and highly cited publications that describe the work of these algorithms along with examples of articles that illustrate their application in the oil and gas industry. The sections of SPE disciplines with the largest number of publications using the algorithms that are frequently used for anomaly detection are presented.**

* Corresponding author.
E-mail: bchigarev@ipng.ru

http://dx.doi.org/10.25729/esr.2024.01.0002

Received January 7, 2024. Revised March 27, 2024. Accepted April 17, 2024. Available online April 30, 2024.

This is an open-access article under a Creative Commons Attribution-NonCommercial 4.0 International License.

© 2024 ESI SB RAS and authors. All rights reserved.

***Index Terms* — anomaly detection, MDPI, SPE, computer science and mathematics, bibliometric data, algorithm.**

I. Introduction

A. Relevance of the subject

Anomaly detection is a vital tool in the oil and gas sector, enhancing safety, security, environmental management, regulatory compliance, maintenance strategies, and operational efficiency. It identifies unusual patterns in sensor data, enabling early detection of anomalies, preventing accidents and equipment failure, monitoring environmental variables, reducing risks, and proactively responding to suspicious activities. Data integrity and anomaly detection are crucial for preventing errors and cybersecurity breaches [1–5].

B. The aim of this study

The objective of this study is to identify the most promising areas for transferring knowledge of "Anomaly Detection" from the fields of Computer Science and Mathematics to the field of oil and gas industry.

To achieve this objective, the following questions are proposed to be answered:

1. Which analytical approaches in the field of anomaly detection are the most developed in publications in the field of "Computer Science and Mathematics?"

2. Which analytical approaches in the field of anomaly detection are most in demand in the oil and gas industry?

Knowledge transfer is assumed to be most appropriate if this knowledge is developed in the field of "Computer Science and Mathematics" and is in demand in the oil and gas industry.

Publications on “Computer Science and Mathematics” are taken from MDPI journals. Publications in the field of oil and gas are taken from the SPE search platform.

The identification of promising issues for knowledge transfer was based on the use of bibliometric methods.

C. Literature review

A review of the literature shows that most publications are devoted to the use of anomaly detection to improve the safety and efficiency of oil and gas operations. The following are typical studies related to this topic.

The paper [6] presents an approach for fault detection and identification using a Self-Organizing Map algorithm, which is crucial for preserving industrial plant health and increasing reliability and efficiency in oil and gas operations. The intuitive and easy-to-understand results of this algorithm are presented.

Machine learning algorithms, including random forest, support vector machine, k-nearest neighbor, gradient boosting, and decision tree, are used to develop anomaly detection models for pipeline leaks in oil and gas operations. The support vector machine algorithm outperformed other algorithms in detecting pipeline leaks, proving its efficiency as an accurate model for pipeline leak detection [7].

A scheme for systematically analyzing flight data to detect anomalies in flight operations, applicable to both online and offline modes, is proposed in [8]. The authors analyze the fundamental aspects of the anomaly detection problem and consider it in the domain of flight operations. The framework relies on the steps of streaming or loading and storing data, creating and explaining the model, while relying on the analysis of domain experts. Logistic operations are important to any industry, so the transfer of the knowledge gained is appropriate for the oil and gas industry.

Random forest and Logistic regression methods used in articles [8, 9] are also used in the oil and gas industry, examples are shown in Table 1.

The paper [9] introduces a two-step methodology utilizing machine learning classification algorithms for anomaly detection in industrial processes. The authors analyze in detail the application of Random Forest Algorithm (RFA) and Decision Jungle Algorithm (DJA) methods to manufacturing processes with multiple phases. The proposed methodology involves first identifying the production phases and then applying an anomaly detection procedure to them. In the oil and gas industry, numerous production processes are multiphase as well. Therefore, the expertise of two-stage anomaly detection, as described in the publication in the field of Computer Science and Mathematics can be highly valuable for the research in the oil and gas sector.

Anomaly detection sensors can be used in oil and gas well-monitoring systems to detect network traffic anomalies, improving safety and efficiency. These sensors are designed to operate within existing well-monitoring infrastructure and compare against pre-set and moving averages to detect and report anomalies [10].

The paper [11] proposes an unsupervised method for anomaly detection in industrial machines, utilizing statistical features to calculate failure severity indicators and interrupt operation before breakdown. The unique feature of this method lies in the fact that it takes a set of time series data from multiple sensors as input. Time series analysis techniques are commonly used in well drilling, making it instrumental to have experience in analyzing recordings from multiple sensors.

Anomaly detection techniques are discussed in [12]. The article provides an overview of current research directions, including definitions, modes, outputs, and literature. It also aims to provide guidance on selecting the most appropriate approach for specific application domains.

In [13], the authors analyze 290 research articles (published in 2000–2020) on ML models for anomaly detection and identify 29 different models used in their application.

The publications [12, 13] are review-oriented in nature, but their value, especially that of [13], can be useful for oil and gas research when determining which method is best suited for a particular dataset.

No publications were found that explore the potential of transferring anomaly detection knowledge from computer science and mathematics for application in the oil and gas industry. Consequently, the topic proposed in the title of the paper is novel.

II. Materials and Methods

A. Data

This research used bibliometric data from the MDPI publisher website, up to September 11, 2023, for “anomaly detection” query. The query included filters for the years between 2019 and 2023, subjects such as Computer

Science and Mathematics, and article types such as articles and reviews. A total of 2 151 tsv outcomes were exported.

The employment of data from MDPI publisher offers several benefits. Firstly, it provides open access to all publications. Secondly, it encompasses a broad range of topics, as evidenced by the inclusion of the topic "anomaly detection" in 52 journals. Additionally, the exported bibliometric data comprises 16 fields, which include the essential fields required for our study, namely TITLE, JOURNAL, KEYWORDS, ABSTRACT, and DOI.

Journals with 20 or more publications at the time of export are:

Applied Sciences → 735, Electronics → 409, Mathematics → 127, Symmetry → 102, Entropy → 90, Information → 75, Future Internet → 72, Algorithms → 57, Processes → 55, ISPRS International Journal of Geo-Information → 41, Computers → 39, Buildings → 34, Journal of Imaging → 27, Big Data and Cognitive Computing → 25, Journal of Sensor and Actuator Networks → 25, Journal of Cybersecurity and Privacy → 20 articles.

B. Clustering of bibliometric records

The Carrot2 program [14, 15] with the Lingo3G algorithm was used for document clustering with the following parameters that differ from the defaulters: algorithm: minLabelWords: 2, maxWordDf: 0.8, phraseDfThresholdScalingFactor: 0.05. A detailed description of the Carrot2 program, the Lingo3G algorithm, and its parameters can be found at https://carrotsearch.com/lingo3g/.

Clustering was conducted utilizing the KEYWORDS and ABSTRACT fields. The texts of these fields underwent the following preprocessing steps:

1. Stemming texts by the Krovetz method, which allowed the terms to be normalized while preserving their readability.
2. Compiling a dictionary of normalized keywords.
3. Keeping only terms from the above dictionary in the ABSTRACT field.
4. Replacing the original KEYWORDS and ABSTRACT fields in the bibliometric records with the transformed ones.
5. Using the bibliometric data thus obtained further in the demo version of Carrot2.

C. Explanation of text preprocessing in progress

The Krovetz algorithm is characterized by its ability to make minimal alterations to the spelling of terms. In this sense, it can be considered as an intermediate approach that lies between lemmatization and stemming [16,17]. This feature is important not only in the context of record clustering but also when automatically assigning headers to clusters and subclusters. For example, using Porter stemming will render headers unreadable.

A good practice of text pre-processing is to remove stop words, but the choice of the list of stop words is subjective. Here, this procedure was replaced by leaving in the texts of abstracts only those terms that the authors themselves considered significant and included in the list of keywords. A dictionary of terms left in the texts of the abstracts was compiled from the list of all keywords. The common text utilities grep and sed were used for this purpose.

The test version of the Carrot2 program has a limit on the amount of data to be analyzed. Using the full texts of 2151 abstracts caused these limits to be exceeded.

The use of preprocessing not only made the records more consistent, but also allowed meeting the limitations imposed by the test version of the program.

D. Search for publications at SPE research portal (search.spe.org)

After identifying the main methods used for anomaly detection, obtained by analyzing the bibliometric data of MDPI publications, a search was conducted for publications related to oil and gas topics and the problem of anomaly detection. For this purpose, the SPE search engine was used, to which queries of the following form were set: "anomaly detection" AND "method," for example: "anomaly detection" AND "Random Forest."

Next, according to the results of each query, reading the abstracts of the found publications and additional information on the method, the following items were compiled: Advantages, Drawbacks, Highly cited publication, Table with Publications demonstrating the application of the method, and SPE Disciplines to which the found publications were referred.

In the absence of publications related to a particular method and anomaly detection problem, examples of publications close in meaning to the problem (Outlier Detection, Deviation Detection, Out-of-Distribution Detection, and Fault Detection) were searched for.

The number of publications found should be considered only as an estimate of the frequency of occurrence of articles on the topic being searched. This may be sufficient to select a specific anomaly detection method. The next stage of the research may require more complex queries, for example, to produce systematic reviews.

III. Results and Discussion

A. Clustering of bibliometric records

The methodology described in the previous section allowed identifying 29 clusters out of 2151 bibliometric records, with 61.0% of the documents falling into the main clusters. Figure 1 shows the clustering results for the six main clusters. In addition, a complete enumeration of all clusters is given in the form of a list to provide more detailed information.

The topics within the clusters and their corresponding subclusters reflect the methods used for anomaly detection, as well as the diverse range of domains in which they can be used.

The full range of clusters and their subclusters are presented in the list below.

The format of the list is as follows: cluster name, number of documents assigned to the cluster, number of subclusters in the cluster. It should be reminded that the algorithm used could assign each document to several categories.

- Anomaly Detection (339 Docs, 14 Subclusters)
- Neural Network (373 Docs, 14 Subclusters)
- Machine Learning (370 Docs, 14 Subclusters)
- Deep Learning (305 Docs, 14 Subclusters)
- Real Time (228 Docs, 14 Subclusters)
- Network Traffic (171 Docs, 14 Subclusters)
- Time Series (125 Docs, 14 Subclusters)
- Future Research (107 Docs, 14 Subclusters)
- Security Privacy (69 Docs, 14 Subclusters)
- Blockchain Technology (38 Docs, 14 Subclusters)
- High Resolution (24 Docs, 11 Subclusters)
- Quality Assessment (18 Docs, 14 Subclusters)

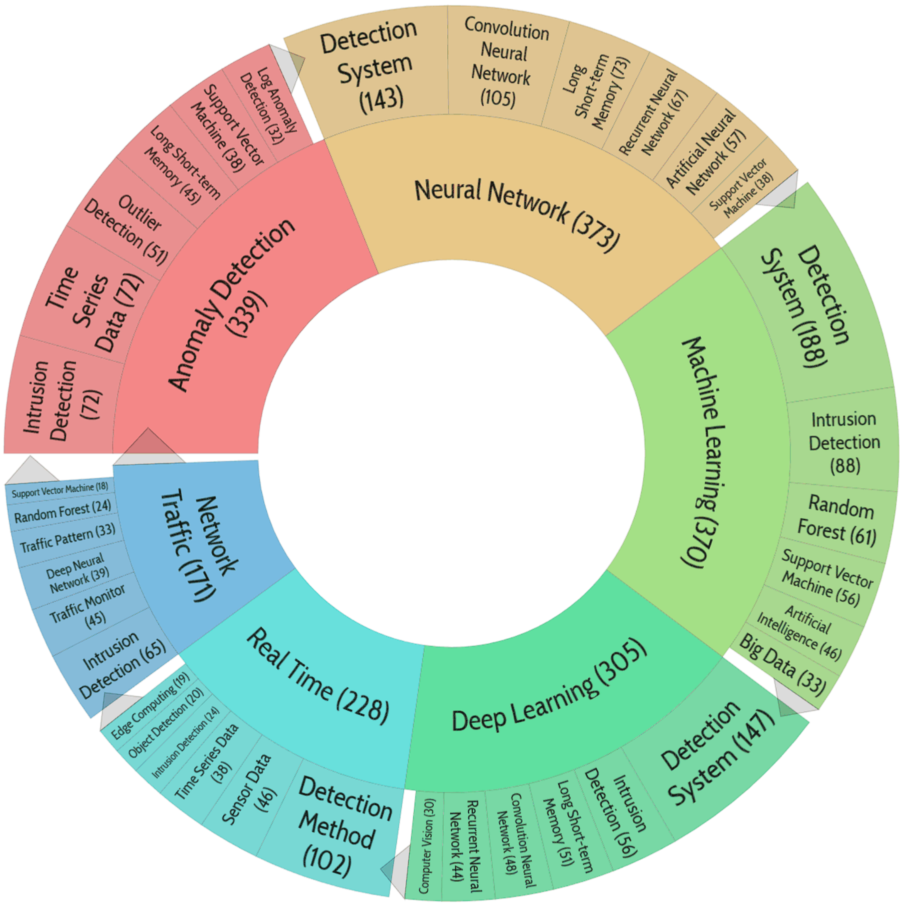

Fig. 1. Themes of the six main clusters and their subclusters of 2151 documents, using the Lingo3G algorithm.

- Wind Energy (19 Docs, 13 Subclusters)
- Signal Ratio (16 Docs, 13 Subclusters)
- Particle Swarm Optimization (15 Docs, 12 Subclusters)
- Knowledge Graph (13 Docs, 10 Subclusters)
- Fuzzy Sets (14 Docs, 12 Subclusters)
- Dimension Reduction (13 Docs, 12 Subclusters)
- Persistent Threat (13 Docs, 10 Subclusters)
- Texture Features (13 Docs, 13 Subclusters)
- Semantic Segmentation (11 Docs, 10 Subclusters)
- Energy Sector (12 Docs, 13 Subclusters)
- Electronic Control (13 Docs, 13 Subclusters)
- Hyperspectral Image (10 Docs)
- Maintenance Activity (9 Docs)
- Useful Life (8 Docs)
- Decision Boundary (8 Docs)
- Damage Severity (7 Docs)
- Other Topics (839 Docs)

The first four clusters show the greatest degree of overlap with the approaches used in anomaly detection. We therefore provide a complete list of their subclusters, emphasizing the methods used.

ANOMALY DETECTION (339 docs, 14 subclusters);

Intrusion Detection (72), Time Series Data (72), Outlier Detection (51), **Long Short-term Memory** (45), **Support Vector Machine** (38), Log Anomaly Detection (32), **Random Forest** (29), Anomalous Behavior (30), Data Mining (29), Cyber-physical System (23), Video Surveillance (18), Industry 4.0 (19), Attention Mechanism (17), Fraud Detection (16)

NEURAL NETWORK (373 docs, 14 subclusters);

Detection System (143), **Convolution Neural Network** (105), **Long Short-term Memory** (73), **Recurrent Neural Network** (67), Artificial Neural Network (57), **Support Vector Machine** (38), **Random Forest** (37), Attention Mechanism (23), Graph Neural Network (23), Computer Vision (21), Generative Adversarial Network (18), Adversarial Attack (10), Activity Recognition (10), Fraud Detection (5).

MACHINE LEARNING (370 docs, 14 subclusters);

Detection System (188), Intrusion Detection (88), **Random Forest** (61), **Support Vector Machine** (56), Artificial Intelligence (46), Big Data (33), **Convolution Neural Network** (27), Data Mining (26), Fraud Detection (15), **Generative Adversarial Network** (15), Edge Computing (13), Traffic Pattern (11), Activity Recognition (10), Social Media (9).

DEEP LEARNING (305 docs, 14 subclusters).

Detection System (147), Intrusion Detection (56), **Long Short-term Memory** (51), **Convolution Neural Network** (48), **Recurrent Neural Network** (44), Computer Vision (30), **Random Forest** (28), Artificial Intelligence (29), **Generative Adversarial Network** (21), Big Data (20), **Reinforcement Learning** (18), Video Surveillance (16), Defect Detection (15), Adversarial Attack (13).

For completeness, we present the total occurrence of the highlighted methods in the list of keywords and abstracts of all 2151 records.

Random Forest → 115 rows, 176 matches;
Support Vector Machine → 104 rows, 144 matches;
Long Short-term Memory → 107 rows, 142 matches;
Recurrent Neural Network → 51 lines, 64 matches;
Convolution Neural Network → 15 lines, 20 matches;
Generative Adversarial Network → 57 lines, 96 matches;
Reinforcement Learning → 27 lines, 60 matches.

The Random Forest and Support Vector Machine classification methods are widely studied and are considered classical approaches. Therefore, it is not surprising that they are widely used in the field of anomaly detection when normal and anomalous instances are separated into separate classes.

Long Short-Term Memory (LSTM) and Recurrent Neural Network (RNN) can be identified as a set of techniques effective for sequential data processing. Different types of sensors and logs serve as suitable data sources for these techniques, especially in the context of time series analysis.

B. *Results of a search of SPE publications and a description of the main features of the methods*

For this purpose, the SPE search engine was used, to which queries of the following form were set: “anomaly detection” AND “method,” for example: “anomaly detection” AND “Random Forest.”

The number of results returned for queries made from December 2018 to December 2023 is:

- ”Support Vector Machine” AND “anomaly detection” → 57
- ”Long Short-term Memory” AND “anomaly detection” → 53

- ”Random Forest” AND “anomaly detection” → 63
- ”Convolution Neural Network” AND “anomaly detection” → 3
- ”Recurrent Neural Network” AND “anomaly detection” → 35
- ”Generative Adversarial Network” AND “anomaly detection” → 6
- ”Reinforcement Learning” AND “anomaly detection” → 0
- ”Reinforcement Learning” → 0

The focus was on bibliometric data alone, not full text.

This simple search provides only a rough estimate of the occurrence of relevant publications on the topic.

For a more comprehensive study, it is necessary to select semantic equivalents of the phrase “anomaly detection” for each analytical technique, such as Outlier Detection, Deviation Detection, Out-of-Distribution Detection, and Fault Detection.

C. Summary characteristics of publications found for the query “Random Forest” AND “anomaly detection”

Advantages. The Random Forest technique is a popular machine-learning algorithm for classification and regression problems due to its high accuracy, robustness, emphasis on feature importance, versatility, and scalability. It combats overfitting by aggregating decision trees and reduces sensitivity to noise and outliers in the dataset.

Drawbacks. Random Forest is a computationally intensive algorithm with disadvantages, including difficulty in interpretation due to the ensemble nature, poor

TABLE 1. Publications Demonstrating the Application of the Random Forest Algorithm to Anomaly Detection Problems

Title and Reference	Short summary
Early Anomaly Detection Model Using Random Forest while Drilling Horizontal Wells with a Real Case Study [19]	This paper presents a machine-learning model to predict drilling surface torque for early detection of operational problems. The model uses real horizontal drilling data from the day before the stuck pipe incident. It predicts surface drilling torque based on typical patterns observed over the past 24 hours, using train and test a random forest model. The model is integrated with the Mahalanobis metric to assess the closeness of real observations to the predicted normal trend.
Explainable and Interpretable Anomaly Detection Models for Production Data [20]	This study compares machine-learning models on two datasets for anomaly detection. It aims to understand how these models make decisions. The models used include K-nearest neighbors, logistic regression, support vector machines, decision tree, random forest, and rule fit classifier. In one data set, the rule fit classifier outperformed the remaining models in both F1 and complexity. In the second data set, random forest outperformed the rest in prediction performance with F1, yet it had the lowest complexity metric.
Leak Detection in Natural Gas Pipelines Using Intelligent Models [21]	This study investigates the effectiveness of intelligent models in detecting small leaks in natural gas pipelines using operational parameters like pressure, temperature, and flowrate. Five models are used: Gradient Boosting, Decision Trees, Random Forest, Support Vector Machine, and Artificial Neural Network. Results indicate that Random Forest and Decision Tree models were most sensitive, with a 0.1% leak detection rate in 2 hours. All models have high reliability, but low accuracy, with Artificial Neural Network and Support Vector Machine performing best.
Assessment of Big Data Analytics Based Ensemble Estimator Module for the Real-Time Prediction of Reservoir Recovery Factor [22]	Estimating reservoir recovery factor is challenging due to high uncertainty, large inexactness, noise, and high dimensionality in reservoir measurements. The paper presents a big data-driven ensemble estimator module, which uses wavelet-associated ensemble models to estimate reservoir recovery factor. The module uses bagging and random forest ensembles to correlate reservoir properties with the recovery factor, and the Relief algorithm to understand their significance. The random forest exhibits the highest coefficient of correlation and minimal estimation errors.
Automating Dynamometer Charts Interpretation with Machine Learning [23]	The aim of the study is to create a mathematical model for the interpretation of Dynamometer Charts from Sucker Rod Pumps. The paper describes a data processing pipeline for obtaining, normalizing, transforming, and evaluating graphs. About 1000 models are trained and tested, including support vector machines, decision trees, K-nearest neighbors, and neural networks. The XGBoost algorithm performs best, although Random Forest algorithms are significantly more accurate in certain conditions.

performance in imbalanced datasets, and poor performance in noisy datasets with numerous irrelevant features, as well as in imbalanced datasets with high trees.

Highly cited publication. Random Forest [18].

Example of publication titles and their brief summary demonstrating the application of the Random Forests algorithm for solving anomaly detection problems found using the search.spe.org are presented in Table 1.

The most frequently referenced **SPE disciplines** in the publications found using the **"Random Forest"** query are:

Production and Well Operations (184): Artificial Lift Systems (28); Production Chemistry, Metallurgy and Biology (12); Well & Reservoir Surveillance and Monitoring (**112**).

Reservoir Description and Dynamics (694): Formation Evaluation & Management (276);

Improved and Enhanced Recovery (69); Reservoir Characterization (**285**); Reservoir Fluid Dynamics (72); Unconventional and Complex Reservoirs (154).

Well Drilling (200): Drilling Fluids and Materials (28); Drilling Measurement, Data Acquisition and Automation (12); Drilling Operations (**98**); Wellbore Design (20).

D. Summary characteristics of publications found for the query "Support Vector Machine" AND "anomaly detection"

Advantages. The Support Vector Machine (SVM) is a highly effective machine-learning algorithm known for its high-dimensional performance, resilience against outliers, adaptability to kernel functions, generalization, regularization parameter, efficient memory utilization, and non-linear classification efficacy.

Drawbacks. The Support Vector Machine (SVM) algorithm faces several drawbacks, including poor parameter selection, computational sensitivity to noise, lack of transparency, limited scalability, and binary classification limitations, making it challenging to interpret and handle large datasets.

Highly cited publication. LIBSVM: A library for support vector machines [24].

Examples of publication titles and their brief summary demonstrating the application of the SVM algorithm for solving anomaly detection problems found in the search engine of search.spe.org are presented in Table 2.

The most frequently referenced **SPE disciplines** in the publications found using the query **"Support Vector Machine"** are:

Production and Well Operations (147): Artificial Lift Systems (31); Production Chemistry, Metallurgy and Biology (16); Well & Reservoir Surveillance and Monitoring (**80**); Well Operations and Optimization (7).

Reservoir Description and Dynamics (688): Formation Evaluation & Management (219); Improved and Enhanced Recovery (70); Reservoir Characterization (**336**); Reservoir Fluid Dynamics (69); Unconventional and Complex Reservoirs (110).

Well Drilling (200): Drilling Fluids and Materials (28); Drilling Operations (**85**); Pressure Management (22); Wellbore Design (43).

E. Summary characteristics of publications found for the query "Convolution Neural Network" AND "anomaly detection"

Advantages. Convolution Neural Networks (CNNs) use convolutional layers to learn local patterns and features from input data, extracting meaningful features from raw data, and using parameter sharing for memory efficiency. They are robust to variations in input data and can handle large-scale datasets with modern GPUs' parallel processing capabilities.

TABLE 2. Publications Demonstrating the Application of the SVM Algorithm to Anomaly Detection Problems

Title and Reference	Short summary
An Unsupervised Stochastic Machine Learning Approach for Well Log Outlier Identification [25]	Outlier detection is crucial in Log Quality Control workflows, and machine learning implementations must address challenges. This paper presents a stochastic outlier detection algorithm using the One-Class Support Vector Machine (1CSVM) method. This method creates outlier flags for all data vectors, providing a proxy for uncertainty. It is robust, efficient, and more efficient than processing all wells set at once. The methodology's unique feature is weighting input data vectors based on petrophysics and measurement physics. This automated workflow is ideal for unconventional applications involving large volumes of legacy data.
Real-Time Drilling Models Monitoring Using Artificial Intelligence [26]	Drilling and Workover operations are evolving at a rapid pace, requiring more data to predict drilling problems. This paper presents a new approach using the Wellsite Information Transfer Specification Markup Language, applying an improved mechanism to monitor and evaluate anomaly detection models and demonstrating the benefits of iterative improvements. A regression classifier model using a support vector machine is developed to predict the expected number of alerts.

Drawbacks. CNNs are computationally intensive and time-consuming due to their large training data and resources. They are prone to overfitting, making them difficult to interpret. They require large memory for large input data sets or deep networks, which may limit their usability on devices with limited memory. Furthermore, they lack rotational and translational invariance.

Highly cited publication. Going deeper with convolutions [27].

Examples of publication titles and their brief summary demonstrating the application of the Convolution Neural Network for solving anomaly detection problems found in the search.spe.org search engine are presented in Table 3.

The most frequently referenced **SPE disciplines** in the publications found using the query **"Convolution Neural Network"** are:

Production and Well Operations (5): Artificial Lift Systems (2); Well & Reservoir Surveillance and Monitoring (**4**).

Reservoir Description and Dynamics (54): Formation Evaluation & Management (9);

Reservoir Characterization (**46**).

Well Drilling (10): Drilling Operations (**5**).

TABLE 3. Publications Demonstrating the Application of the Convolution Neural Network to Anomaly Detection Problems

Title and Reference	Short summary
Drilling and Completion Anomaly Detection in Daily Reports by Deep Learning and Natural Language Processing Techniques [28]	Unconventional oil & gas fields generate vast amounts of data, making data-driven methods challenging for analysis. Different activity coding systems and missing data make automatic anomaly detection difficult. An automatic text classification method was proposed using machine learning and natural language processing techniques for daily drilling and completion reports. Based on 460,000 operation records from 1,700 wells worldwide, Word2vec is used, and CNN is found to be the best method for text classification.
Virtual Multiphase Flowmeter Using Deep Convolutional Neural Networks [29]	This paper proposes a low-cost, instantaneous model for measuring oil, gas, and water volume in petroleum wells using artificial intelligence. The system uses pressure and temperature sensors from wells and opening control valve state to train a deep neural network with a convolutional layer to output fluid volume rate. The Schlumberger OLGA multiphase flow simulator software is used to provide data. Tests show the approximation achieves up to 99.6% accuracy, potentially replacing expensive multiphase meters or serving as a redundant digital sensor.
Prediction of Field Saturations Using a Fully Convolutional Network Surrogate [30]	The study focuses on developing surrogate models for predicting field saturations using a fully convolutional encoder/decoder network based on dense convolutional networks. The model extracts multiscale features from input data and uses these to recover input image resolution. It uses static and dynamic reservoir parameters as input features and outputs water-saturation distributions. This approach offers precision and cost-effectiveness, making it useful for production optimization and history matching.

TABLE 4. Publications Demonstrating the Application of the Recurrent Neural Network to Anomaly Detection Problems

Title and Reference	Short summary
Simulating the Behavior of Reservoirs with Convolutional and Recurrent Neural Networks [32]	Recurrent neural networks and convolutional neural networks are applied to model reservoir behavior from data. Recurrent neural networks have the ability to retain information from previous patterns, making them suitable for interpreting permanent downhole gauge records. Convolutional neural networks, with specific design modifications, are as capable as RNNs in modeling sequences of information and are equally reliable in making inferences for cases unseen during training. The study discusses the differences in processing information and memory handling between these two architectures.
Integration of Artificial Intelligence with Economical Analysis on the Development of Natural Gas in Nigeria; Focusing on Mitigating Gas Pipeline Leakages [33]	Artificial intelligence is used to develop models using gas flow data to detect potential gas leakages in Nigeria's natural gas pipelines. Machine learning algorithms such as Recurrent Neural Networks and K-nearest neighbors are trained and evaluated for accuracy and precision. The results indicate that recurrent neural networks outperform K-nearest neighbors in leak detection, but all models show high reliability.
Machine Learning for Deepwater Drilling: Gas-Kick-Alarm Classification Using Pilot-Scale Rig Data with Combined Surface-Riser-Downhole Monitoring [34]	Deepwater drilling often faces gas kicks due to the narrow mud-weight window. Traditional methods have time lag and can lead to severe gas influxes. A novel machine-learning model uses pilot-scale rig data and surface-riser-downhole monitoring for early detection and risk classification. Four ML algorithms are developed. The long short-term memory recurrent neural network algorithm shows the best performance, it is selected and deployed to early detect gas kicks and classify the corresponding kick alarms. The model achieves high recall, accuracy, precision, and detection time delay.

***F.* Summary characteristics of publications found for the query "Recurrent Neural Network" AND anomaly detection"**

Advantages. Recurrent Neural Networks (RNNs) are effective when sequential data are involved, for example, in natural language processing, speech recognition, and time series analysis. They can handle variable input lengths, maintain internal memory, and make context-based decisions. They can be pre-trained on large datasets and fine-tuned for specific problems.

Drawbacks. RNNs, due to their recurrent nature, are slow and computationally intensive, making training time challenging. They struggle to learn complex patterns, capture long-term dependencies, and can suffer from vanishing or exploding gradients.

Highly cited publication. Recurrent Neural Networks [31].

Examples of publication titles and their brief summary demonstrating the application of the Recurrent Neural Network for solving anomaly detection problems found in the search engine of search.spe.org are presented in Table 4.

The first publication can refer to both Convolutional and Recurrent Neural Networks.

The last work can also be attributed to long short-term memory algorithm as a special case of recurrent neural network.

The most frequently referenced **SPE disciplines** in the publications found using the query **"Recurrent Neural Network"** are:

Production and Well Operations (68): Artificial Lift Systems (8); Production Chemistry, Metallurgy and Biology (6); Well & Reservoir Surveillance and Monitoring (**43**).

Reservoir Description and Dynamics (288): Formation Evaluation & Management (80); Improved and Enhanced Recovery (29); Reservoir Characterization (**135**); Reservoir Simulation (43); Unconventional and Complex Reservoirs (35).

Well Drilling (49) → without subcategories.

***G.* Summary characteristics of publications related to those found for the query "Long Short-term Memory" AND "anomaly detection"**

The Long Short-Term Memory (LSTM) algorithm is a type of Recurrent Neural Network (RNN) known for its ability to process and analyze sequential data.

Advantages. LSTM overcomes the vanishing gradient problem, capturing long-term dependencies in sequential data. Its memory cell can retain information for long periods, making it suitable for speech recognition and natural language processing. LSTM also allows efficient transfer learning.

Drawbacks. The Long Short-term Memory (LSTM) algorithm has drawbacks such as higher computational cost, overfitting risk, and difficulty in implementing dropout. It also struggles with long-term information storage, making it difficult to refer to previously stored data.

Highly cited publication. Long Short-Term Memory [35].

Examples of publication titles and their brief summary demonstrating the application of the Long Short-term Memory algorithm for solving anomaly detection

TABLE 5. Publications Demonstrating the Application of the Long Short-term Memory Algorithm to Anomaly Detection Problems

Title and Reference	Short summary
A Machine Learning Workflow to Predict Anomalous Sanding Events in Deepwater Wells [36]	This study develops a predictive machine learning model using sensor and simulation data to inform Control Room Operators before significant damage occurs, using an anomaly detection architecture. The problem is addressed using Principal Component Analysis and Long Short-Term Memory Autoencoders, which reconstruct the original input. An alarm is triggered when the real-time anomaly score exceeds the training threshold.
Towards Real-Time Bad Hole Cleaning Problem Detection Through Adaptive Deep Learning Models [37]	The study presents an adaptive predictive deep-learning model that uses equivalent circulating density measurements, model results, and drilling data to predict potential bad hole cleaning conditions. The model has two components: an anomaly detector and a predictor. It uses Long Short-Term Memory cells to account for data correlations and generate future data conditioned to past observations. The approach is demonstrated on two real examples from offshore Norway.
Development of an Artificial Intelligence-Based Well Integrity Monitoring Solution [38]	The goal of an artificial intelligence-based well integrity monitoring solution is to build models to identify well annulus leakage events, given the well type and all relevant anomalies. Artificial intelligence models are created using Long Short-Term Memory Autoencoders and classifier to identify complex irregularities.

problems found in search engine of search.spe.org are presented in Table 5.

The most frequently referenced **SPE disciplines** in the publications found using the query **"Long Short-term Memory"** are:

Production and Well Operations (94): Artificial Lift Systems (9); Production Chemistry, Metallurgy and Biology (7); Well & Reservoir Surveillance and Monitoring (**62**).

Reservoir Description and Dynamics (314): Formation Evaluation & Management (95); Reservoir Characterization (**124**); Reservoir Fluid Dynamics (31); Reservoir Simulation (42); Unconventional and Complex Reservoirs (49).

Well Drilling (71): Drilling Operations (**31**); Pressure Management (8); Wellbore Design (8).

H. Summary characteristics of publications found for the query "Generative Adversarial Network" AND "anomaly detection"

Advantages. Generative Adversarial Networks (GANs) are an unsupervised learning method that can be trained using unlabeled data. They generate data similar to real data, including images, text, audio, and video. GANs have strong discrimination power, allowing them to distinguish between training data and generated data samples. They also generate realistic data instances that resemble the training-data distribution, making them a valuable tool for data analysis.

Drawbacks. GANs pose challenges in training due to instability, mode collapse, and hyperparameter sensitivity. They can cause a stalemate between generator and discriminator networks, resulting in limited or repetitive samples. Hyperparameter choices like learning rates, batch sizes, and network architectures are crucial. GANs can produce fake data. Additionally, they require significant computational resources.

Highly cited publication. Photo-Realistic Single Image Super-Resolution Using a Generative Adversarial Network [39].

Examples of publication titles and their brief summary demonstrating the application of the Generative Adversarial Network for solving anomaly detection problems, which are found in the search engine of search.spe.org are presented in Table 6.

TABLE 6. Publications Demonstrating the Application of the Generative Adversarial Network to Anomaly Detection Problems

Title and Reference	**Short summary**
Broadband reconstruction of seismic signal with generative recurrent adversarial network [40]	The resolution of seismic data depends on frequency and bandwidth, and complex exploration objects require higher resolution algorithms. Traditional methods can affect signal to noise ratio, reducing data reliability. A new method based on a generative recurrent adversarial network (GRAN) is proposed to generate pseudo sample sets constrained by geological layers and train the GRAN model for broadband seismic data reconstruction. The method's applicability is proven through blind well tests and is applied to actual work area seismic data processing, achieving excellent results.
Self-Supervised Subsea SLAM for Autonomous Operations [41]	The study proposes a deep learning-based Simultaneous Localization and Mapping (SLAM) method to estimate the 3D structure of a vehicle's surrounding environment from a single video. This method predicts a depth map of a given video frame while estimating the vehicle's movement between frames. The method is self-supervised and uses Generative Adversarial Networks to improve depth map prediction results. The study evaluates the method on the KITTI dataset and a private dataset of subsea inspection videos, showing it outperforms existing SLAM methods in depth prediction and pose estimation.

TABLE 7. Publications Demonstrating the Application of the Reinforcement Learning Algorithm to Anomaly Detection Problems

Title and Reference	Short summary
Novel Stuck Pipe Troubles Prediction Model Using Reinforcement Learning [43]	This paper defines the stuck pipe prediction problem as a multi-class problem considering the dynamic nature of drilling operations. A reinforcement learning-based algorithm is proposed to solve this problem, with performance and evaluation results shared. The algorithm's accuracy is demonstrated, and performance improvement through feedback channel retraining is demonstrated. The reinforcement logic connects solutions to operation reporting, enhancing accuracy through neural networks.
Deep Reinforcement Learning: Reservoir Optimization from Pixels [44]	This paper uses Deep Reinforcement Learning to optimize the Net Present Value of water flooding by altering the water injection rate. This is the first demonstration of AI's potential in understanding reservoir physics directly, without considering reservoir petrophysical properties or the number of wells in the reservoir.

The most frequency referenced **SPE disciplines** in the publications found using the query **“Generative Adversarial Network”** are:

Production and Well Operations (11): Artificial Lift Systems (2); Well & Reservoir Surveillance and Monitoring (**8**).

Reservoir Description and Dynamics (172): Formation Evaluation & Management (27); Reservoir Characterization (**143**); Reservoir Simulation (17).

Well Drilling (5): Drilling Measurement, Data Acquisition and Automation (2); Drilling Operations (2).

I. Summary characteristics of publications found for the query “Reinforcement Learning” AND “anomaly detection”

Since no documents were found upon direct request, this section presents an analysis of documents that can be only indirectly related to this topic.

Advantages. Reinforcement learning (RL) is an AI model that trains agents to learn sequences of actions, making it useful in complex environments. It is adaptive and intelligent, allowing agents to learn from their actions and rewards without explicit supervision. RL focuses on optimal behavior to maximize reward, making it suitable for decision-making problems and similar to human learning.

Drawbacks. RL is a time-consuming, expensive and complex learning method that involves interacting with the environment to find the optimal policy. It requires numerous interactions and may not be practical in real-world scenarios. The balance between exploration and exploitation, high dimensionality, deferred reward, security and hyperparameter sensitivity are also challenges.

Highly cited publication. Reinforcement Learning: An Introduction [42].

Examples of publication titles and their brief summary demonstrating the application of the Reinforcement Learning algorithm for solving anomaly detection problems found in the search engine of search.spe.org are presented in Table 7.

The first paper does not satisfy the search criterion “anomaly detection,” but it is related to the identification of an anomalous situation, i.e., it satisfies only the extended search for publications, revealing the topic at hand.

The most frequently referenced **SPE disciplines** in the publications found using the query **“Reinforcement Learning”** are:

Production and Well Operations (43): Artificial Lift Systems (7); Well & Reservoir Surveillance and Monitoring (**18**);

Reservoir Description and Dynamics (157): Formation Evaluation & Management (43); Improved and Enhanced Recovery (33); Reservoir Characterization (**55**); Reservoir Simulation (33); Unconventional and Complex Reservoirs (33).

Well Drilling (54): Drilling Equipment (7); Drilling Operations (29); Well Planning (5); Wellbore Design (6).

IV. CONCLUSION

Clustering Computer Science and Mathematics related documents according to their bibliometric entries on the topic of anomaly detection provides an easily interpretable list of publication topics, which can be further extended for an in-depth literature analysis. The dominant anomaly detection methods include Random Forest and Support Vector Machine for classifying normal and abnormal states, while Long-term Memory Method and Recurrent Neural Network are effective when sequential data such as time series from sensors or logs are involved.

The SPE search platform publications primarily use the same anomaly detection methods for engineering problems in the oil and gas sector, suggesting that the knowledge gained from Computer Science and Mathematics can be applied to these problems. The SPE search platform found no studies on methodology for addressing the limitations of anomaly detection methods. It seems more practical to search for solutions in articles related to Mathematics and Computer Science to mitigate the problems encountered when using these techniques in applied engineering problems.

In the oil and gas industry, anomaly detection problems are most often encountered in Production and Well Operations (Well & Reservoir Surveillance and Monitoring), Reservoir Description and Dynamics (Reservoir Characterization), and Well Drilling (Drilling Operations). The result is easily understandable, as the above applications form the foundation of engineering tasks in development.

V. Possible Applications of the Findings

This study could serve, for example, as a preliminary step towards preparing a systematic review on the suitability of the Long Short-term Memory method for anomaly detection in well integrity monitoring. When justifying the feasibility of the Long Short-term Memory method, the review should not only demonstrate its applicability but also consider ways to overcome possible shortcomings based on the relevant literature. This approach is analogous to a typical systematic review in medicine, looking at the side effects of a drug in the treatment of a particular disease.

Acknowledgment

This research was funded by the Ministry of Science and Higher Education of the Russian Federation, State Assignment No. 122022800270-0.

References

[1] A. Qassab et al., “Autonomous Inspection System for Anomaly Detection in Natural Gas Pipelines,” in *Abu Dhabi International Petroleum Exhibition & Conference*, Abu Dhabi, UAE, Nov. 2020, p. D041S105R002. DOI: 10.2118/202825-MS.

[2] J. Snyder, S. Scott, and R. Kassim, “Self-Adjusting Anomaly Detection Model for Well Operation and Production in Real-Time,” in *SPE Oklahoma City Oil and Gas Symposium*, Oklahoma City, Oklahoma, USA, Apr. 2019, p. D011S002R005. DOI: 10.2118/195234-MS.

[3] P. Santos et al., “AI Augmented Engineering Intelligence for Industrial Equipment,” in *SPE Offshore Europe Conference & Exhibition*, Aberdeen, Scotland, UK, Sep. 2023, p. D021S006R003. DOI: 10.2118/215491-MS.

[4] F. Beduschi et al., “Optimizing Rotating Equipment Maintenance Through Machine Learning Algorithm,” in *Abu Dhabi International Petroleum Exhibition & Conference*, Abu Dhabi, UAE, Nov. 2021., p. D031S088R001. DOI: 10.2118/207657-MS.

[5] Z. S. Irani, R. George, R. Dayal, “Technology for Continuous Cyber Monitoring of Offshore Assets,” in *ADIPEC*, Abu Dhabi, UAE, Oct. 2023, p. D031S101R003. DOI: 10.2118/217071-MS.

[6] L. Concetti, G. Mazzuto, F. E. Ciarapica, M. Bevilacqua, “An Unsupervised Anomaly Detection Based on Self-Organizing Map for the Oil and Gas Sector,” *Applied Sciences*, vol. 13, no. 6, p. 3725, 2023. DOI: 10.3390/app13063725.

[7] S. S. Aljameel et al., “An Anomaly Detection Model for Oil and Gas Pipelines Using Machine Learning,” *Computation*, vol. 10, no. 8, p. 138, 2022. DOI: 10.3390/computation10080138.

[8] L. Coelho E Silva, M. C. R. Murça, “A data analytics framework for anomaly detection in flight operations,” *Journal of Air Transport Management*, vol. 110, p. 102409, 2023. DOI: 10.1016/j.jairtraman.2023.102409.

[9] E. Quatrini, F. Costantino, G. Di Gravio, R. Patriarca, “Machine learning for anomaly detection and process phase classification to improve safety and maintenance activities,” *Journal of Manufacturing Systems*, vol. 56, pp. 117–132, 2020. DOI: 10.1016/j.jmsy.2020.05.013.

[10] X. He, E. Robards, R. Gamble, M. Papa, “Anomaly Detection Sensors for a Modbus-Based Oil and Gas Well-Monitoring System,” in *2019 2nd International Conference on Data Intelligence and Security (ICDIS)*, South Padre Island, TX, USA: IEEE, Jun. 2019, pp. 1–8. DOI: 10.1109/ICDIS.2019.00008.

[11] J. Da Silva Arantes, M. Da Silva Arantes, H. B. Fröhlich, L. Siret, R. Bonnard, “A novel unsupervised method for anomaly detection in time series based on statistical features for industrial predictive maintenance,” *Int. J. Data Sci. Anal.*, vol. 12, no. 4, pp. 383–404, 2021. DOI: 10.1007/s41060-021-00283-z.

[12] T. H. A. Musa, A. Bouras, “Anomaly Detection: A Survey,” in *Proceedings of Sixth International Congress on Information and Communication Technology*, vol. 217, X.-S. Yang, S. Sherratt, N. Dey, and A. Joshi, Eds. Singapore: Springer Singapore, 2022, pp. 391–401. DOI: 10.1007/978-981-16-2102-4_36.

[13] A. B. Nassif, M. A. Talib, Q. Nasir, F. M. Dakalbab, “Machine Learning for Anomaly Detection: A Systematic Review,” *IEEE Access*, vol. 9, pp. 78658–78700, 2021. DOI: 10.1109/ACCESS.2021.3083060.

[14] S. Osiński, D. Weiss, “Carrot2: Design of a Flexible and Efficient Web Information Retrieval Framework,” in *Advances in Web Intelligence*, vol. 3528, P. S. Szczepaniak, J. Kacprzyk, and A. Niewiadomski, Eds. Berlin, Heidelberg: Springer Berlin Heidelberg, 2005, pp. 439–444. DOI: 10.1007/11495772_68.

[15] C. Carpineto, S. Osiński, G. Romano, D. Weiss, “A survey of Web clustering engines,” *ACM Comput. Surv.*, vol. 41, no. 3, pp. 1–38, 2009. DOI: 10.1145/1541880.1541884.

[16] R. Krovetz, “Viewing morphology as an inference process,” *Artificial Intelligence*, vol. 118, no. 1–2, pp. 277–294, 2000. DOI: 10.1016/S0004-3702(99)00101-0.

[17] A. S. Nayak, A. P. Kanive, N. Chandavarkar, R. Balasubramani, “Survey on Pre-Processing Techniques for Text Mining,” *IJECS*, vol. 5, no. 6, pp. 16875–16879, 2016. DOI: 10.18535/ijecs/v5i6.25.

[18] L. Breiman, “Random Forests,” *Machine Learning*, vol. 45, no. 1, pp. 5–32, 2001. DOI: 10.1023/A:1010933404324.

[19] A. AlSaihati, S. Elkatatny, A. Mahmoud, A. Abdulraheem, “Early Anomaly Detection Model Using Random Forest while Drilling Horizontal Wells with a Real Case Study,” in *SPE/IADC Middle East Drilling Technology Conference and Exhibition*, Abu Dhabi, UAE, May 2021, p. D032S040R001. DOI: 10.2118/202144-MS.

[20] B. Alharbi, Z. Liang, J. M. Aljindan, A. K. Agnia, X. Zhang, "Explainable and Interpretable Anomaly Detection Models for Production Data," *SPE Journal*, vol. 27, no. 01, pp. 349–363, 2022. DOI: 10.2118/208586-PA.

[21] O. Akinsete, A. Oshingbesan, "Leak Detection in Natural Gas Pipelines Using Intelligent Models," in *SPE Nigeria Annual International Conference and Exhibition*, Lagos, Nigeria, Aug. 2019, p. D023S009R001. DOI: 10.2118/198738-MS.

[22] S. Tewari, U. D. Dwivedi, M. Shiblee, "Assessment of Big Data Analytics Based Ensemble Estimator Module for the Real-Time Prediction of Reservoir Recovery Factor," in *SPE Middle East Oil and Gas Show and Conference*, Manama, Bahrain, Mar. 2019, p. D041S038R003. DOI: 10.2118/194996-MS.

[23] M. A. Del Pino Fiorillo, "Automating Dynamometer Charts Interpretation with Machine Learning," in *SPE Latin American and Caribbean Petroleum Engineering Conference*, Port of Spain, Trinidad and Tobago, Jun. 2023, p. D021S010R003. DOI: 10.2118/213191-MS.

[24] C.-C. Chang, C.-J. Lin, "LIBSVM: A library for support vector machines," *ACM Trans. Intell. Syst. Technol.*, vol. 2, no. 3, pp. 1–27, 2011. DOI: 10.1145/1961189.1961199.

[25] R. Akkurt et al., "An Unsupervised Stochastic Machine Learning Approach for Well Log Outlier Identification," in *Proceedings of the 10th Unconventional Resources Technology Conference*, Houston, Texas, USA: American Association of Petroleum Geologists, 2022. DOI: 10.15530/urtec-2022-3721358.

[26] B. Alotaibi, B. Aman, M. Nefai, "Real-Time Drilling Models Monitoring Using Artificial Intelligence," *SPE Middle East Oil and Gas Show and Conference*, Manama, Bahrain, Mar. 2019, p. D021S001R004. DOI: 10.2118/194807-MS.

[27] C. Szegedy et al., "Going deeper with convolutions," in *2015 IEEE Conference on Computer Vision and Pattern Recognition (CVPR)*, Boston, MA, USA: IEEE, Jun. 2015, pp. 1–9. DOI: 10.1109/CVPR.2015.7298594.

[28] H. Zhang et al., "Drilling and Completion Anomaly Detection in Daily Reports by Deep Learning and Natural Language Processing Techniques," in *Proceedings of the 8th Unconventional Resources Technology Conference*, Online: American Association of Petroleum Geologists, 2020. DOI: 10.15530/urtec-2020-2885.

[29] R. Mercante, T. A. Netto, "Virtual Multiphase Flowmeter Using Deep Convolutional Neural Networks," *SPE Journal*, vol. 28, no. 05, pp. 2448–2461, 2023. DOI: 10.2118/214681-PA.

[30] K. Zhang et al., "Prediction of Field Saturations Using a Fully Convolutional Network Surrogate," *SPE Journal*, vol. 26, no. 04, pp. 1824–1836, 2021. DOI: 10.2118/205485-PA.

[31] S. A. Marhon, C. J. F. Cameron, S. C. Kremer, "Recurrent Neural Networks," in *Handbook on Neural Information Processing*, vol. 49, M. Bianchini, M. Maggini, and L. C. Jain, Eds. Berlin, Heidelberg: Springer Berlin Heidelberg, 2013, pp. 29–65. DOI: 10.1007/978-3-642-36657-4_2.

[32] A. Alakeely, R. N. Horne, "Simulating the Behavior of Reservoirs with Convolutional and Recurrent Neural Networks," *SPE Reservoir Evaluation & Engineering*, vol. 23, no. 03, pp. 0992–1005, 2020. DOI: 10.2118/201193-PA.

[33] C. G. Ezechi, E. R. Okoroafor, "Integration of Artificial Intelligence with Economical Analysis on the Development of Natural Gas in Nigeria; Focusing on Mitigating Gas Pipeline Leakages," in *SPE Nigeria Annual International Conference and Exhibition*, Lagos, Nigeria, Jul. 2023, p. D031S018R004. DOI: 10.2118/217163-MS.

[34] Q. Yin et al., "Machine Learning for Deepwater Drilling: Gas-Kick-Alarm Classification Using Pilot-Scale Rig Data with Combined Surface-Riser-Downhole Monitoring," *SPE Journal*, vol. 26, no. 04, pp. 1773–1799, 2021. DOI: 10.2118/205365-PA.

[35] S. Hochreiter, J. Schmidhuber, "Long Short-Term Memory," *Neural Computation*, vol. 9, no. 8, pp. 1735–1780, 1997. DOI: 10.1162/neco.1997.9.8.1735.

[36] M. C. Kara, M. Majeran, B. Peterson, T. Wimberly, G. Sinclair, "A Machine Learning Workflow to Predict Anomalous Sanding Events in Deepwater Wells," in *Offshore Technology Conference*, Virtual and Houston, Texas, Aug. 2021, p. D031S033R002. DOI: 10.4043/31234-MS.

[37] P. Nivlet et al., "Towards Real-Time Bad Hole Cleaning Problem Detection Through Adaptive Deep Learning Models," in *Middle East Oil, Gas and Geosciences Show*, Manama, Bahrain, Feb. 2023, p. D021S073R005. DOI: 10.2118/213643-MS.

[38] P. Aditama, T. Koziol, Dr. M. Dillen, "Development of an Artificial Intelligence-Based Well Integrity Monitoring Solution," in *ADIPEC*, Abu Dhabi, UAE, October 2022, p. D031S110R004. DOI: 10.2118/211093-MS.

[39] C. Ledig et al., "Photo-Realistic Single Image Super-Resolution Using a Generative Adversarial Network," in *2017 IEEE Conference on Computer Vision and Pattern Recognition (CVPR)*, Honolulu, HI: IEEE, Jul. 2017, pp. 105–114. DOI: 10.1109/CVPR.2017.19.

[40] Z. Zhang, W. Song, W. Wang, "Broadband reconstruction of seismic signal with generative recurrent adversarial network," in *Second International Meeting for Applied Geoscience & Energy*, Houston, Texas: Society of Exploration Geophysicists and American Association of Petroleum Geologists, Aug. 2022, pp. 2178–2182. DOI: 10.1190/image2022-3746443.1.

[41] F. Marques, P. Costa, F. Castro, M. Parente, "Self-Supervised Subsea SLAM for Autonomous Operations," in *Offshore Technology Conference*, Houston, Texas, May 2019, p. D011S002R006. DOI: 10.4043/29602-MS.

[42] R. S. Sutton, A. G. Barto, "Reinforcement Learning: An Introduction," *IEEE Trans. Neural Netw.*, vol. 9, no. 5, pp. 1054–1054, 1998. DOI: 10.1109/TNN.1998.712192.

[43] M. Alzahrani, B. Alotaibi, B. Aman, "Novel Stuck Pipe

Troubles Prediction Model Using Reinforcement Learning," in *International Petroleum Technology Conference*, Riyadh, Saudi Arabia, Feb. 2022, p. D021S042R003. DOI: 10.2523/IPTC-22151-MS.

[44] R. Miftakhov, A. Al-Qasim, I. Efremov, "Deep Reinforcement Learning: Reservoir Optimization from Pixels," in *International Petroleum Technology Conference*, Dhahran, Kingdom of Saudi Arabia, Jan. 2020., p. D021S052R002. DOI: 10.2523/IPTC-20151-MS.

Boris N. Chigarev is a leading engineer for scientific and technical information at Oil and Gas Research Institute of the Russian Academy of Sciences. He received the degree of Ph.D. in chemical physics, including combustion and explosion physics from V.I. Kurchatov Institute of Atomic Energy in 1989. His research interests are bibliometric analysis and research trends in the energy sector.

Additional Power Losses Under Non-Sinusoidal Conditions in a 22 kV Overhead Power Line

L.I. Kovernikova[1,]*, Bui Ngoc Hung[2]

[1] Melentiev Energy Systems Institute of Siberian Branch of the Russian Academy of Sciences, Irkutsk, Russia
[2] Ha Noi University of Mining and Geology, Ha Noi, Viet Nam

Abstract — **Non-sinusoidal conditions in the electrical networks cause active power losses at the fundamental frequency, corresponding to the first harmonic, and at harmonic frequencies, which are a multiple of the fundamental frequency. Non-sinusoidal currents flow through network components and create additional active power losses. One of the non-sinusoidal current sources is electronic equipment used in industrial plants to control process equipment. In Vietnam, coal mines use frequency-controlled induction motors when processing coal. The induction motors consume non-sinusoidal current, which creates additional active power losses in the supply network. The harmonic active power does not perform useful work. It causes economic damage to both the supply network and industrial enterprises. The power supply systems in industrial areas of Vietnam, where coal is mined, are characterized by low power quality. Companies engaged in coal mining and processing are forced to pay for additional losses of active power due to the low power quality under non-sinusoidal conditions, which reduces the economic efficiency of the companies' operations.**

The paper presents a review of the literature on the assessment of additional active power losses in overhead power lines at harmonic frequencies. An example of calculating additional losses of harmonic active power is given for a 22 kV overhead power line, through which electrical energy is supplied to the coal grading plant of the Kua Ong-Vinacomin company. Additional losses are calculated using the measurements of harmonic voltage and current at the point of the supply network connection to the 22 kV overhead power line, through which electrical energy is supplied to the coal mine and the coal grading plant. To assess the influence of the electrical equipment of the coal grading plant on the power quality in the supply network, measurements were carried out on 0.4 kV buses of electrical substation of the coal mine.

Index Terms — **power quality, harmonic, non-sinusoidal conditions, measurements, power system, frequency-controlled induction motors.**

I. Introduction

Non-sinusoidal conditions in electrical networks are one of the acute problems in the field of power quality. Apart from active power losses at the fundamental frequency (corresponding to the first harmonic), the electrical networks under non-sinusoidal conditions experience active power losses at other harmonics, the frequency of which is a multiple of the fundamental frequency. In [1], consideration is given to the economic damage to the supply network and consumers, which is associated with additional active power losses in electrical networks.

Overhead power lines are components of electrical networks. Non-sinusoidal currents flowing in them are not only of the 1st harmonic ($n = 1$), corresponding to the fundamental frequency $f_1 = 50$ Hz, but also of the harmonics that are multiples of the fundamental frequency, i.e., $n \geq 2$, for which $f_n = 50\,n$. Harmonic currents in power lines cause additional active power losses. Determining the magnitude of active power losses in power transmission

* Corresponding author.
E-mail: kovernikova@isem.irk.ru

http://dx.doi.org/10.25729/esr.2024.01.0003

Received February 1, 2024. Revised March 29, 2024. Accepted April 8, 2024. Available online April 30, 2024.

This is an open-access article under a Creative Commons Attribution-NonCommercial 4.0 International License.

© 2024 ESI SB RAS and authors. All rights reserved.

lines under non-sinusoidal conditions is the focus of many publications as this issue is highly relevant [2–6].

When a load with a nonlinear current-voltage characteristic is powered from a source with a sinusoidal voltage, the flow of active power of the 1st harmonic is directed into it [2]. Most of this power is consumed by the load to perform useful work, which is proposed to be called "working power" in [3]. Part of the active power of the 1st harmonic is converted by the nonlinear load into active power of harmonics with numbers $n \geq 2$ [2]. In [3], such active powers are proposed to be called "detrimental powers."

In [4], metering electrical energy under non-sinusoidal conditions is considered and misunderstandings that arise between energy supply entities and consumers when paying for electrical energy are pointed out. Electric energy meters measure active energy not only of the 1st harmonic but of other harmonics as well. For this reason, energy supply entities and consumers incur additional costs when paying for electrical energy.

Additional losses of harmonic active power in electrical networks can amount to several percent of losses under sinusoidal voltage [5]. Losses in the networks of industrial enterprises and in the networks of electrified railway transport can reach 10–15%. In [6], the values of active power losses at the fundamental frequency and additional losses at harmonic frequencies are given based on the values of harmonic currents measured during the day in a 110 kV power transmission line of Buryatenergo. At some points in time, additional losses amounted to 30% of the losses at the main frequency. The level of additional active power losses per day was 13.1% of power losses at the 1st harmonic. The influence of harmonic currents on the value of active resistance of power transmission line wires is considered in [7–13].

In Vietnam, in coal mining areas, low power quality is observed due to the use of frequency-controlled induction motors in coal mines during coal processing. These motors cause distortion in the shape of voltage and current waveforms, i.e., they are sources of harmonic currents in the supply electrical network. The power quality in the electrical networks of Vietnam must comply with two current regulatory documents [14–15]: "Circular No. 39/2015/ TT-BCT dated 11/18/2015 of the Ministry of Industry and Trade of Vietnam on the distribution of electrical energy" and "Circular of the Ministry of Industry and Trade of Vietnam 25/ 2016/ TT-BCT dated 30/11/2016 on the transmission of electrical energy."

This paper presents the results of measurements of harmonic voltages and currents at the connection point of the supply network and the 22 kV overhead power line, through which electrical energy is supplied to the coal mine and coal grading plant of the Kua Ong-Vinacomin company [16], and on the low-voltage side of the step-down 22/0.4 kV transformer supplying process equipment of the coal grading plant [17]. The article presents the results of calculation and analysis of additional harmonic active power losses in the 22 kV overhead power line feeding the coal mine. To assess the influence of frequency-controlled induction motors on the power quality in the supply network, measurements were carried out on 0.4 kV buses of an electrical substation of the coal mine.

II. Measurement Results for Harmonic Voltage and Current in the Power System of Coal Mine

The power supply diagram for the coal mine is shown in Fig. 1. Measurements were carried out at the beginning of the 22 kV overhead power transmission line at node 6001 and at the low-voltage side of the transformer feeding the coal mine and coal grading plant at node 4143. The PQ-Box150 device [18], manufactured in Germany, was used

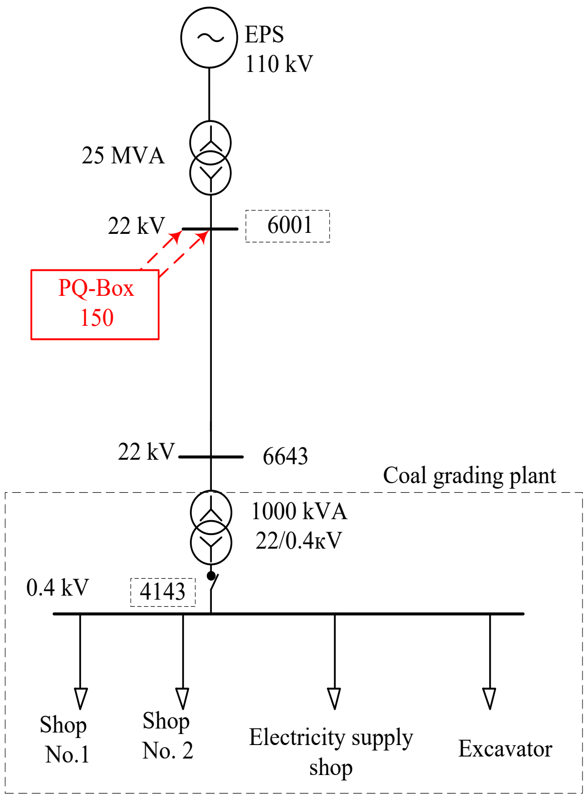

Fig. 1. Power supply system of the coal grading plant.

for the measurements. Measurements of power quality indices and operating parameters were carried out over 24 hours with an interval of 1 second.

A. Measurement results for power quality indices of the coal mine electrical network at node 4143.

There are two operational states at the coal grading plant: operating hours from 7 a.m. to 5 p.m., when all process equipment is in operation; and non-operating hours from 5 p.m. to 7 a.m. of the next day, when the main process equipment is not working.

Figures 2 and 3 show the curves for active and reactive power in three phases consumed by the load of coal mine in 24 hours. The maximum active power consumption during operating hours is 1035 kW, reactive power consumption is 419 kVAr. During the non-operating hours, the maximum active power consumption is 203 kW, reactive power consumption – 94 kVAr.

Figure 4 shows a diagram of the harmonic factors for the n-th harmonic components of voltage for operating hours and non-operating hours, when the load powers are minimum ($K_{U(n)min}$) and maximum ($K_{U(n)max}$).

The values of $K_{U(n)}$ during operating hours for most harmonics exceed the values of the factor during non-operating hours.

Figure 5 shows a graph of changes in the value of the total harmonic distortion of voltage K_U in phase A and its standard value K_{UN}. Most of the measured values of K_U exceed the standard value of 6.5% established in [14]. The highest value of K_U is 16.7%, the lowest – 3.8%.

The measurements of power quality indices on the 0.4 kV buses of electrical substation show that the values of the indices during operating hours and non-operating hours are different. This indicates the influence of the electrical equipment of the coal mine and coal grading plant on the operating parameters of the electrical network. The change in the values of power quality indices, which characterize the distortion of voltage and current

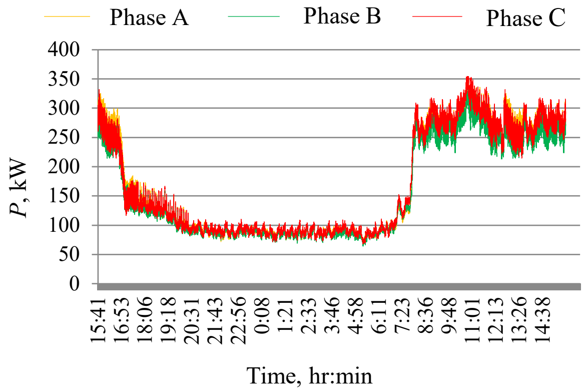

Fig. 2. Change in active power.

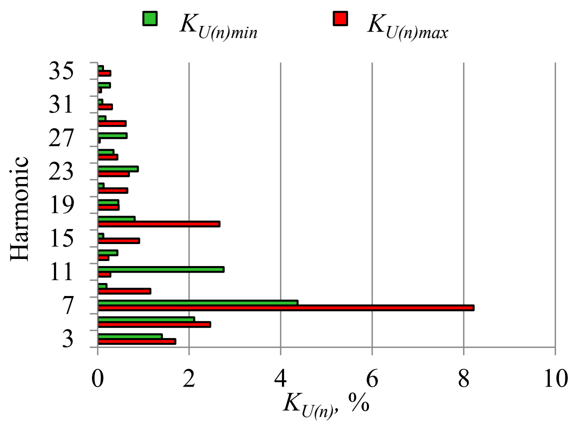

Fig. 4. Diagram of $K_{U(n)max}$ and $K_{U(n)min}$ in phase A.

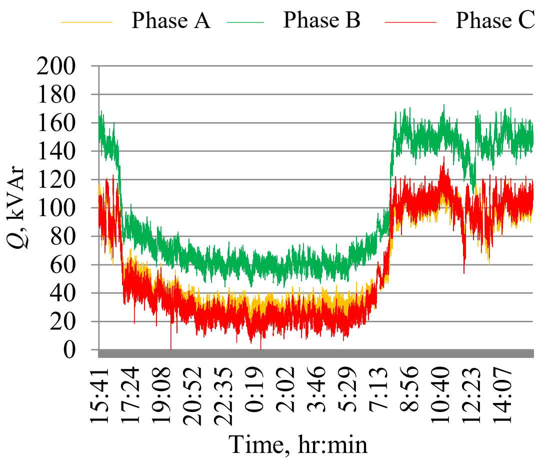

Fig. 3. Change in reactive power.

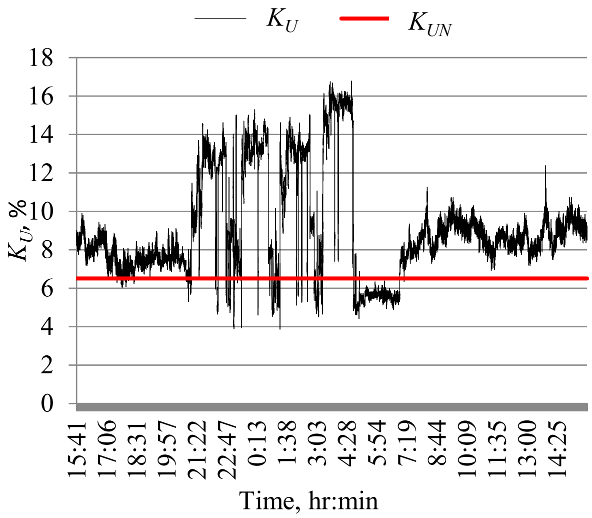

Fig. 5. Changes in K_U in phase A.

waveforms at node 4143, demonstrates the influence of the electrical equipment of the grading plant on the voltage and current of the 22 kV overhead power line supplying electrical energy to the coal mine and the coal grading plant.

When non-sinusoidal current flows through the power line, additional active power losses occur.

B. Power quality measurement results for node 6001 of the electrical network of the 110 kV power system.

The 22 kV overhead power line is connected to the 110 kV power system through a 25 MVA two-winding transformer at node 6001. Node 6001 is the beginning of the overhead power line that supplies electrical energy to the coal mine and coal grading plant. This three-phase power line is made with AS-185 wires [19] and has a length of 8 km. Measurements of operating parameters and power quality indices were carried out with PQ-Box 150 device for 24 hours with a measurement interval of 1 second. The results of calculations and analysis are presented for two operating conditions of the coal grading plant.

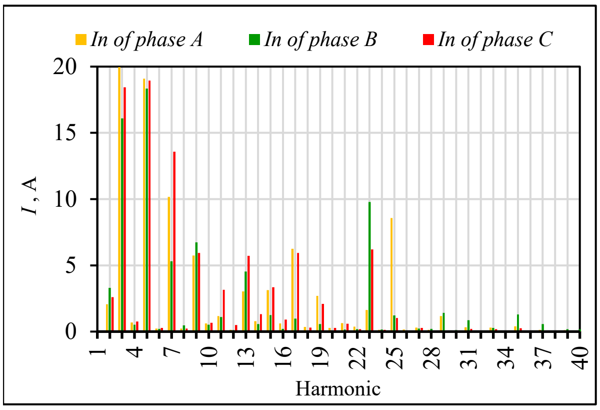

Fig. 6. Diagram of harmonic currents for operating hours.

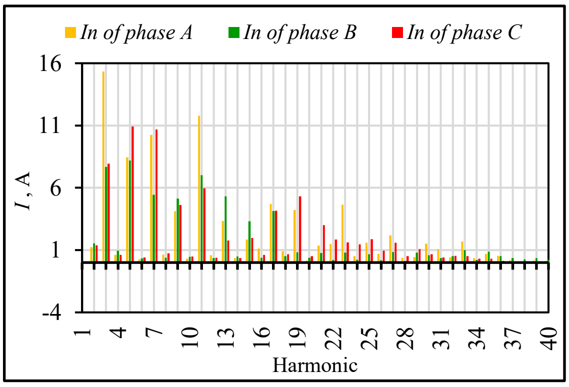

Fig. 7. Diagrams of harmonic currents for non-operating hours.

Figure 6 shows a diagram of the effective values of harmonic currents (I_n) based on one of the measurements performed during operating hours. The diagram illustrates that when all the process equipment is in operation, the currents of the 3rd, 5th, 7th, 23rd, and 25th harmonics have the highest values. The values of even harmonic currents are insignificant.

The parameters of harmonic conditions are probabilistic in nature [20]. Table 1 shows the maximum and minimum values of the measured harmonic currents in the phases, corresponding to the maximum (max) and minimum (min) values. The arrays of measured harmonic currents contain outlying observations [21], which significantly exceed the others in magnitude. Table 1 presents the values of the 23rd harmonic current in phases B and C and the value of the 25th harmonic current in phase A. They are highlighted in bold.

Figure 7 shows a diagram of the effective values of the harmonic currents of one of the measurements for the non-operating hours of the plant. As seen in the Figure, their magnitude is smaller than that of the harmonic currents during operating hours. The currents of the 3rd, 5th, 7th, and 11th harmonics have the highest values. The even harmonic currents are significantly less than the odd harmonic currents.

Table 2 presents the maximum and minimum values of odd harmonic currents for the non-operating hours. The Table contains outliers that have larger values. As in the operating hours, during the non-operating hours, these are the values of currents of the 23rd harmonic in phases B and C and the 25th harmonic in phase A. The harmonics of currents during the non-operating hours are smaller in magnitude than the those during the operating hours. The currents of the 3rd, 5th, 7th, and 11th harmonics have the

TABLE 1. Maximum and Minimum Values of Harmonic Currents for Operating Hours, A

Harmonic	I_n of phase A		I_n of phase B		I_n of phase C	
	max	min	max	min	max	min
1	478.75	5.99	473.64	2.80	478.46	3.08
3	53.92	0.36	46.11	0.28	40.43	0.26
5	59.3	0.30	52.40	0.12	54.68	0.32
7	24.78	0.11	15.63	0.04	32.31	0.14
9	15.88	0.09	18.78	0.10	19.11	0.13
11	8.24	0.00	7.60	0.00	13.37	0.01
13	12.44	0.02	12.13	0.04	16.95	0.04
17	16.60	0.03	4.77	0.01	17.35	0.01
19	8.70	0.01	3.91	0.00	9.27	0.01
21	7.57	0.00	1.70	0.00	4.51	0.00
23	9.52	0.01	**1 611.23**	0.50	**2 068.39**	0.81
25	**2 426.76**	0.34	4.32	0.01	8.21	0.01

highest values.

C. Additional active power losses

Alternating electric current is distributed unevenly across the cross-section of the wires [22]. The current density is greatest on the surface of the wire and decreases with distance from the surface into the depth of the wire. The phenomenon of surface effect occurs in the wire, which is characterized by an increase in the active resistance of the wire. Since the power transmission line supplying electrical energy to the coal grading plant is of insignificant length, the value of the active resistance of the line can be determined using expression (1) proposed in [12, 13]

$$R_n = R_1\sqrt{n}\ , \qquad (1)$$

TABLE 2. Maximum and Minimum Values of Harmonic Currents for Non-Operating Hours, A

Harmonic	I_n of phase A max	I_n of phase A min	I_n of phase B max	I_n of phase B min	I_n of phase C max	I_n of phase C min
1	441.91	5.63	437.8	2.64	442.04	2.89
3	38.37	0.21	29.99	0.12	26.11	0.05
5	42.21	0.01	35.78	0.01	38.57	0.07
7	35.96	0.08	16.90	0.03	31.70	0.08
9	15.00	0.07	13.45	0.06	15.08	0.03
11	20.59	0.03	16.02	0.03	19.60	0.02
13	9.76	0.02	11.14	0.04	14.05	0.01
17	11.86	0.04	6.10	0.01	12.33	0.02
19	9.77	0.01	5.72	0.00	12.12	0.01
21	10.51	0.00	3.20	0.00	9.74	0.00
23	11.79	0.01	**182.66**	0.09	**585.33**	0.31
25	**506.45**	0.18	2.53	0.00	6.77	0.00

TABLE 3. Total harmonic active power, W

Harmonic	Operating hours Phase A	Operating hours Phase B	Operating hours Phase C	Non-operating hours Phase A	Non-operating hours Phase B	Non-operating hours Phase C
2	3.7	27.0	23.8	1.3	1.4	1.1
3	1 246.9	1 149.9	816.3	463.9	324.9	138.0
4	2.8	1.5	3.5	0.6	1.2	0.6
5	2 255.6	1 803.3	1 809.4	193.9	138.5	275.7
7	368.4	109.7	757.8	329.2	107.0	354.7
9	175.4	299.6	304.8	122.4	140.8	106.7
11	16.9	10.6	49.1	79.3	44.9	84.7
13	88.0	119.0	165.2	33.7	65.0	34.3
22	1.0	0.1	0.7	5.1	0.3	3.4
23	46.8	3 667.2	7 824.3	73.5	125.6	705.3
24	0.7	0.2	0.7	3.6	0.2	4.1
25	11 136.2	18.7	20.5	325.2	1.2	18.9

TABLE 4. Total Harmonic Active Power

Active power	Operating hours	Non-operating hours
P_1, W	542 006.1	314 370.1
$(P_2 – P_{40})$, W	108.3	55.5
$(P_3 – P_{39})$, W	34 919.3	4 640.7
$P_{n\Sigma}$, W	35 027.6	4 696.2
$P_{n\Sigma} / P_1 \cdot 100$, %	6.5	1.5

where R_1 and R_n are the values of the active resistance of the wire at the fundamental frequency and at the harmonic frequency, n is the harmonic number. Additional active power losses at the n-th harmonic frequency are determined by the expression

$$P_n = I_n^2 R_1 \sqrt{n}\ . \qquad (2)$$

Table 3 shows the values of the calculated phase active powers for some even and odd harmonics. As seen in the Table, the operating conditions at each of the harmonics are unbalanced.

The results of calculations and analysis of the total active harmonic powers for three phases are given in Table 4. In the Table, P_1 is active power of the first harmonic, performing useful work; $(P_2 – P_{40})$ is total active power of even harmonics from 2 to 40, which do not perform useful work [3]; $(P_3 – P_{39})$ is total active power of odd harmonics from 3 to 39, which do not perform useful work [3]; $P_{n\Sigma}$ is total active power of even and odd harmonics. The value of harmonic active power for operating hours relative to the value of active power of the first harmonic is 6.5%, and for non-operating hours – 1.5%.

III. CONCLUSION

The results of calculation and analysis of additional active power losses in an overhead power line caused by harmonic currents that occur under non-sinusoidal conditions demonstrate that active power losses at harmonic frequencies can exceed 6% of active power losses at the fundamental frequency.

Loss of harmonic active power can be used as a metric to assess the efficiency of the use of electrical energy and its transmission through electrical networks. It is an assessment of the work performed by the network and supply companies, consumers, and government authorities to maintain power quality in accordance with the regulatory requirements.

ACKNOWLEDGMENT

The research was carried out under State Assignment Project (No. FWEU-2021-0001) of the Fundamental Research Program of the Russian Federation 2021-2030.

REFERENCES

[1] L. I. Kovernikova, V.V. Sudnova, R.G. Shamonov et al. *Power quality: current state, problems and proposals for solving them*, N. I. Voropai, Ed. Novosibirsk, Russia: Nauka Publ., 2017, 219 p. (In Russian)

[2] J. Arrillaga, D. Bradley, P. Bodger, *Power System Harmonics*. New York, USA: J. Wiley &Sons, 1985.

[3] L. S. Czarnecki, "Working, reflected and detrimental active powers," *IET Generation, Transmission & Distribution*, vol. 1, pp. 1–7, 2012.

[4] I. V. Zhezhelenko, *High harmonics in power supply systems of industrial enterprises*, 6th ed. Moscow, Russia: Energoatomizdat, 2010, 375 p. (In Russian)

[5] I. I. Kartashev, E. N. Zuev, *Power quality in electricity systems. Ways to control and ensure it*. Moscow, Russia: MPEI Publishing House, 2001, 120 p. (In Russian)

[6] N. N. Kharlov, V. S. Borovikov, V. V. Litvak, A. V. Pogonin, V. A. Melnikov, "Energy survey of non-sinusoidal conditions of multi-wire power transmission lines," *Electrichestvo*, no. 12, pp. 12–15, 2011. (In Russian)

[7] H. De Keulenaer, "Power quality self-assessment guide," *Energy Conservation*, no. 2, pp. 84–88, 2005. (In Russian)

[8] A. E. Emanuel, *Power definitions and the physical mechanism of power flow*. Hoboken, New Jersey, USA: John Wiley & Sons, Ltd, 2010, 264 p.

[9] A. K. Shidlovsky, V. G. Kuznetsov, *Improving the quality of energy in electrical networks*. Kyiv, Ukraina: Naukova Dumka Publ., 1985, 268 p. (In Russian)

[10] I. V. Zhezhelenko, *High harmonics in power supply systems of industrial enterprises*, 3rd ed. Moscow, Russia: Energoatomizdat, 1994, 272 p. (In Russian)

[11] A. Novitskiy, S. Schlegel, D. Westermann, "Estimation of Power Losses Caused by Supraharmonics," *Energy Systems Research*, vol. 3, no. 4, pp. 28–36, 2022.

[12] G. J. Wakileh, *Power Systems Harmonics*. Berlin Heidelberg, Germany: Springer, 2001, pp. 221.

[13] O. N. Voitov, E. V. Popova, L. V. Semenova, "Algorithm for calculation of power flow in electrical networks," *Elektrichestvo*, no. 12, pp. 19–26, 2013. (In Russian)

[14] Circular of the Ministry of Industry and Trade of Vietnam No. 39/2015/ TT - BCT dated 11/18/2015 on electricity distribution system.

[15] Circular of the Ministry of Industry and Trade of Vietnam No. 5/2016/ TT - BCT dated 30/11/2016 on electricity transmission system.

[16] L. I. Kovernikova, H. N. Bui, O. N. Voitov, L. V. Semenova, "Optimization approach to determining the parameters of active filters," in *Methodological Problems in Reliability Study of Large Energy Systems. Reliability of Energy Supply to Consumers in the Context of Their Digitalization*, issue 71, book 3. Irkutsk, Russia: ESI SB RAS, 2020, pp. 164-173. (In Russian)

[17] L. I. Kovernikova, N. H. Bui, "Problems of power quality in power supply system of a coal grading plant at one of the coal mines in Vietnam," *Smart Electric Power Engineering*, no. 2(10), pp. 4–16, 2020. DOI: 10.46960/2658-6754_2020_2_4. (In Russian)

[18] Operating Manual Network Analyzer PQ-Box 150. Power Quality Evaluation Software. Available at: http://www.a-elerle.de.

[19] *Handbook on the design of electrical power systems*, 2nd ed. rev., S. S. Rokotyan and I. M. Shapiro, Eds. Moscow, Russia: Energia Publ., 1977. (In Russian)

[20] L. I. Kovernikova, V. C. Luong, "Algorithm for modeling nonlinear loads of a high-voltage network using measured parameters," *Elektrichestvo*, no. 10, pp. 16–25, 2017. (In Russian)

[21] J. O. Irwin, "On a criterion for the rejection of outlying observations," *Biometrika*, vol. 17, no. 3–4, pp. 238–250, 1925.

[22] L. R. Neiman, K. S. Demirchyan, *Theoretical foundations of electrical engineering*, vol.2. Leningrad, Russia: Energia Publ., 1967. (In Russian)

Lidiia Kovernikova graduated from Novosibirsk Electrotechnical Institute in 1976. L.I. Kovernikova received the Ph.D. degree in engineering from the Siberian Energy Institute of Siberian Branch of the Russian Academy of Sciences (SB RAS) in 1995. Currently, L.I.Kovernikova is a Senior Researcher at the Melentiev Energy Systems Institute of SB RAS, Irkutsk, Russia. Her area of interests includes modeling non-sinusoidal conditions of electrical power systems, analyzing the power quality in electrical networks, and developing technologies to improve power quality.

Bui Ngoc Hung graduated from Hanoi University of Mining and Geology in 2006. He received the Ph.D. degree in electrical engineering from the Hanoi University of Mining and Geology. Currently, Nui Ngoc Hung is a lecturer at Hanoi University of Mining and Geology (the Department of Electrical and Electronics Engineering). His area of interests includes power quality in electrical networks and development of technologies to improve power quality.

Coal Industry Global Transformations: Analysis and Projections

L.S. Plakitkina*,[1]

[1] Energy Research Institute of the Russian Academy of Sciences, Moscow, Russia

***Abstract* — The paper explores the current global trends in coal production, exports, imports, and consumption with focus on China, India, and Russia up to the year 2050. Russia's coal production in 2022 is shown to rise to 443.6 million tons due to an increase in domestic coal consumption, which made it possible to compensate for a slight decrease in coal exports. At the same time, the growth in domestic coal consumption was 6.1% compared to the level of 2021. Of this, 23% was utilized by the electric power industry, 10.4% for coking, 6.9% for residential, industrial and agricultural consumers, and the remaining 6.8% of coal supplies were delivered to other consumers within the domestic market. In 2023–2024, Russia may see a slight decrease in coal production and export volumes, which is associated with sanctions, a decline in demand of European consumers, and a reduction in the use of this type of fuel or refusal from it in some Asian countries. The possibility of reorienting Russian coal supplies from West to East is limited by the plans of the Asia-Pacific countries along with commissioning new coal capacities in the near future to actively develop wind farms and solar power plants and adopt national hydrogen strategies. These factors, in turn, may lead to a decrease in Russian coal production and exports by 2050. However, it is too early to talk about the end of the "era of coal," at least until 2030.**

***Index Terms* — coal mining, coal exports, coal imports, coal consumption, coal market, China, India, Russia.**

I. Introduction

Currently, the situation with coal is ambiguous. On the one hand, the decarbonization of the economy, ensuring low-carbon development and carbon neutrality, contributes to the use of renewable energy in many countries of the world, which, in turn, displace gas and coal in the power industry structure.

The growth of climate requirements is a catalyst for current and future fundamental changes in the energy sector, including the coal industry. Discussions about the future of the coal industry are getting increasingly more intense in the world community. The plans of individual countries to reduce the use of this type of minerals and the emerging trend towards a decrease in investment in the coal industry suggest the inevitable end of the coal era.

However, on the other hand, there are good reasons to believe that we are witnessing a deep transformation rather than a "decline" in the coal industry.

Furthermore, the changes that occur in the coal industry under the influence of accelerated energy transition policies and the activation of the climate agenda are likely to both continue and intensify.

In this regard, let us consider current trends in the production, exports, imports and consumption of coal in the major countries of the world, including Russia.

II. Modern Global Trends in Coal Production

In 2021, according to the IEA [1, 2], the global coal production amounted to 7.7 billion tons with

* Corresponding author.
E-mail: luplak@rambler.ru

http://dx.doi.org/10.25729/esr.2024.01.0004

Received February 3, 2024. Revised March 11, 2024. Accepted April 2, 2024. Available online April 30, 2024.

This is an open-access article under a Creative Commons Attribution-NonCommercial 4.0 International License.

© 2024 ESI SB RAS and authors. All rights reserved.

approximately 60% being mined in China and India. It is worth noting that both countries are actively expanding the production of natural gas and renewable energy sources (RES) [3].

China accounts for 48.7% of the world's coal production, with India following at 10.7%, Indonesia at 7.4%, Australia at 6.0%, the USA at 6.8%, and Russia at 5.7%.

Currently, according to BP, 36% of the world's electricity is generated using coal as a fuel.

Coal-fired generation saw a remarkable surge between 2001 and 2021: in China by 4.7 times, in India by 3 times, in Indonesia by 5 times, and in Vietnam by 35 times. However, in Europe, it has reduced by half over the past 10 years. Newly commissioned generating capacities in Asian countries (Thailand, Malaysia, and others) are also mainly based on coal. In Russia, the share of coal in the structure of electricity generation is currently about 18% [4].

In 2022, according to preliminary data, coal production increased compared to the previous year: to 862 million tons in India, to 4.5 billion tons in China, and to 546 million tons in the EU countries. This surge marks the highest global coal production since 1982. Coal experienced a renaissance.

In Russia, coal production in 2022 increased to 443.6 million tons due to a rise in domestic coal consumption, which made it possible to compensate for a slight decrease in coal exports [5, 6]. About 5.0 million tons of coal in 2022 was mined in the Donbass (in 2021 – 7.5 million tons).

In recent years, a steady trend in the spatial development of the coal industry has emerged in Russia: the production of thermal coal has shifted away from the European and some eastern regions of the country, becoming increasingly more concentrated in the Kuznetsk basin. Coking coals are now moving towards the eastern borders of Russia, approaching the Asian markets.

In 2022, domestic coal consumption in Russia increased by 6.1% and reached 261.5 million tons, compared to 2021. At the same time, the electric power industry accounted for 23% of coal consumption, followed by coking with 10.4%. The remaining coal supply to the domestic market was allocated as follows: 6.9% for the needs of the population, utility and agro-industrial complex, and 6.8% for the other consumers in the domestic market.

Projections suggested that global coal production might surpass 8.3 billion tons, including about 4.9 billion tons in China, and about 950 million tons in India.

In 2023-2024, Russia may see some decrease in coal production, which is associated with the embargo and other factors.

The question arises: what is the situation with coal exports?

III. Coal Exports from the Major Countries of the World

In 2021, the total coal exports from the major countries of the world reached 1.3 billion tons. The shares of the main coal exporting countries at the end of 2021were as follows: Indonesia at 33.2%, Australia at 27.7%, Russia at 16.4% (3rd globally), the USA at 5.9%, South Africa at 4.8%, Colombia at 3.7%, Canada at 2.4%, Kazakhstan at 1.8%, and Mongolia at 0.9%. In 2021, according to coal companies, Russia exported 215 million tons of coal.

Indonesia maintained its leading position in 2022, shipping 494 million tons of coal for export.

On August 10, 2022, an embargo went into effect as part of the EU countries and the UK's 5th package of sanctions. This embargo restricts the purchase, import, or transit transportation of coal from Russia. Additionally, it prohibits the provision of services related to coal, including shipping insurance. As a result:

– Deliveries of Russian coal to the EU countries stopped (their volume amounted to more than 22% of all fuel exports), which, according to the Ember center, increased coal supplies from Kazakhstan (where, Russian coal is delivered according to parallel export schemes), as well as Indonesia, Colombia, and South Africa [7].

– Supplies of Russian coal to Japan, South Korea, Great Britain, and other countries reduced or completely halted.

Against this background, in 2022, the Russian coal exports, according to coal companies, decreased by 6.2%, i.e., to 201.7 million tons. Nevertheless, Russian coal exporters managed to maintain or increase their market share in areas where sanctions do not apply, in particular, in China, India, Turkey, and Malaysia.

Thus, in 2022, the volume of Russia's coal exports to China increased to 45.3 million tons (+65.7% by 2021), to Turkey to 24.5 million tons (+64.5% by 2021), and to India to 13.6 million tons (2.7 times higher than in 2021). At the same time, deliveries of Russian coal to Japan fell by 46.3%, to 13.9 million tons, and deliveries to Germany decreased by 66.3%, to 1.3 million tons.

Due to the sanctions, Russian companies became heavily dependent on their coal supplies to China, and had to sell their coal at a significant discount in 2022.

China offers Russia to build a cross-border railway corridor from Kuzbass Tashtagol to Urumqi (People's Republic of China (PRC)) on a concession basis, after which the export of Russian coal to China may increase.

However, it is important to take into account two points: firstly, the primary coal suppliers to the PRC are and, most likely, will continue to be: Indonesia, Mongolia, and Australia; and secondly, China is actively developing renewable energy sources and other alternative energy sources. Therefore, our projections suggest that China will increase the volume of coal exports until 2030 at the most.

In 2022, commercial production of coking coal began at the Syradasai coal deposit in Taimyr and its delivery to the PRC (100 thousand tons). In addition, it is possible to supply coal from the Syradasai deposit to Turkey and the countries of North Africa.

In general, in 2023, the Ministry of Energy of Russia predicted the stabilization of the Russian coal export [8] and the growth of Russian coal supply to the East.

However, it is worth noting that there may be a decrease in coal exports due to the Special Military Operation. At the same time, the delivery of coal from Siberia to Asia through the ports of the South and North-West is already reaching the threshold of profitability. The primary issue lies in the escalating costs of coal transportation to Asian markets, in particular, the expenses related to chartering ships and acquiring insurance services. There is a significant dependence on the imported foreign mining equipment and the depreciation of existing equipment.

In addition, the possibility of reorienting Russian coal supply from West to East is also limited by the fact that the Asia-Pacific countries, in addition to commissioning new coal capacities in the near future, are planning to actively develop wind and solar power plants, and are implementing national hydrogen strategies. Factors that may pose risks to suppliers of Russian coal for export include:

– the instability of world prices for primary energy resources and their dependence on both economic and political factors;

– the aggravation of competition among energy sources in the world market;

– the transition to a carbon-free economy and the prospect of introducing a "carbon" tax, leading to a decrease in the share of electricity generated from coal;

– the transition of the world economy to energy-saving technologies and the gradual displacement of coal from the energy balance, etc.

According to the IEA, the reduction in thermal coal exports from Russia will continue, and by 2025 the drop may be 4.3% compared to 2022 (up to 150 million tons).

IV. Current Trends and Structure of Coal Imports

The main coal importing countries in 2021 were: China – 332 million tons (24.2% of the global volume of imported coal), India – 199 million tons (14.5%), Japan – 173 million tons (12 .7%), South Korea – 89.7 million tons (5%), Taiwan – 69.8 million tons (5.1%), Vietnam – 43.9 million tons (3.2%), Germany – 38.4 million tons 2.8%), and Russia – 20.7 million tons (1.6%).

In 2022, the Russian Federation imported 19.7 million tons of coal, of which almost all (more than 99%) was supplied from Kazakhstan.

It is possible to substitute Kazakh thermal coal with Russian Kuznetsk coal through the modernization of the equipment of Russian power plants (primarily in the Urals).

In January-May 2023, coal supply from Kazakhstan to Russia decreased by 16%. In turn, Kazakhstan increased coal exports to Europe, Turkey, and the countries of Central Asia [9].

In 2022, China imported about 290 million tons of coal, of which the share of Russian coal delivered to China was only 15.6%.

India is another major coal importer, and Russia has high hopes for supplying its coal to the Indian market.

Although Russia managed to increase coal imports to India by 2.7 times in 2022 compared to the level of 2021 (up to 13.6 million tons), the share of Russian coal supplied to this country still remains insignificant. Furthermore, it is important to consider the following:

1) The main coal exporter to India is Australia;

2) In order to ensure India's energy security, the country's leadership intends to halt coal imports by the 2024-2025 financial year, commencing in April 2024, and increase domestic production;

3) Despite the projected increase in the demand for coal in the domestic market of India to 1.5 billion tons by 2030,

the country has adopted the program "Self-sufficient India," aiming to build new mines in the country and enhance coal production at existing domestic coal enterprises to meet the growing needs.

This situation will greatly complicate the supply of Russian coal to China and India, which are currently the primary importers of Russian coal.

V. Current Trends in Global Coal Consumption

Coal consumption worldwide reached approximately 8 billion tons in 2021.

China ranks first (53%), followed by India in a second place with 13.7%; the USA comes in third with 6.2%; Russia holds the fourth position (3.1%) and Japan ranks fifths with 2.2%. South Africa and Germany both have a share of 2.1% ranking sixths and sevenths respectively. Indonesia rounds off the rankings in the eighths place with a share of 1.8%.

China and India currently account for about 67% of all coal consumed globally. In subsequent years, this figure may exceed 70%.

Nevertheless, it is worth noting that China has recently announced their commitment to achieve carbon neutrality by 2060 [9], while India aims to achieve the same goal by 2050 [10, 11]. Russia has set a target of achieving carbon neutrality by 2060.

In 2021, there was a 6% increase in coal consumption in the world compared to the level of 2020, which is associated with the recovery of the world economy from the coronavirus pandemic and the collective determination to reduce reliance on gas imports from Russia.

In 2022, global coal demand witnessed a significant surge, according to the IEA, surpassing 8.3 billion tons. This growth was observed not only in the EU and India, with an 8% increase compared to 2021, but also in China, where the demand rose by 7%, in Indonesia by 36%, and in Finland by 10%.

In contrast, coal consumption in the US decreased by 7% reaching 457 million tons. In addition, coal consumption in Vietnam decreased by 4.2% [11].

In September 2022, China initiated the construction of an additional 165 GW coal-fired generating capacity, planning to increase this figure to 270 GW by 2025.

The increase in coal consumption in China was mainly due to a growth in demand for coal for non-energy purposes, i.e., the production of GTL, plastics, and fertilizers.

New generation capacities in other Asian countries (Thailand, Malaysia, and Vietnam) are also mainly based on coal.

Russia ranks 4th in terms of coal consumption (with a share of 3.1% in 2021). Compared to 2000, the volume of coal consumption in Russia remained practically unchanged, however, the share decreased from 5.3 to 3.1% [4].

The volume of coal consumption in Japan, which ranks 5th in the world, increased by approximately 20 million tons in 2021 against 2000, while its share compared to all countries decreased from 3.3 to 2.2%.

It is important to note that South Africa is going to completely abandon coal and switch to renewable energy sources [12].

In 2023, according to the IEA, coal consumption worldwide was expected to slightly surpass 8.3 billion tons, the level of 2022, although in the first half of 2023 there was a 1.5% increase compared to the same period in 2022.

An increase in coal consumption in 2023 was expected primarily in India (by 6.8%, to 1.1 billion tons) and in the EU countries (by 5.7%, to 685 million tons). This surge was a result of the temporary shift back to coal due to soaring natural gas prices, decreased hydropower generation, and the closure of nuclear power plants.

In 2024, the global coal consumption may reach approximately 8.4 billion tons, according to the IEA projections.

VI. Coal Consumption Projections

In the context of the emerging innovation and technological landscape, driven by the implementation of the Industry 4.0 program, we have developed a model enabling projections of coal consumption both on a global scale and in individual countries.

The coal consumption projections made using this model factor in changes in the coal consumption in the energy sector and metallurgy; world coal reserves; spatial development of coal mining in certain countries of the world; prices of coal, oil and gas; coal intensity of GDP; and other macroeconomic indicators [13–15].

The projections relied on three options for the development of the world economy:

Option I – low rates of decarbonization of the world

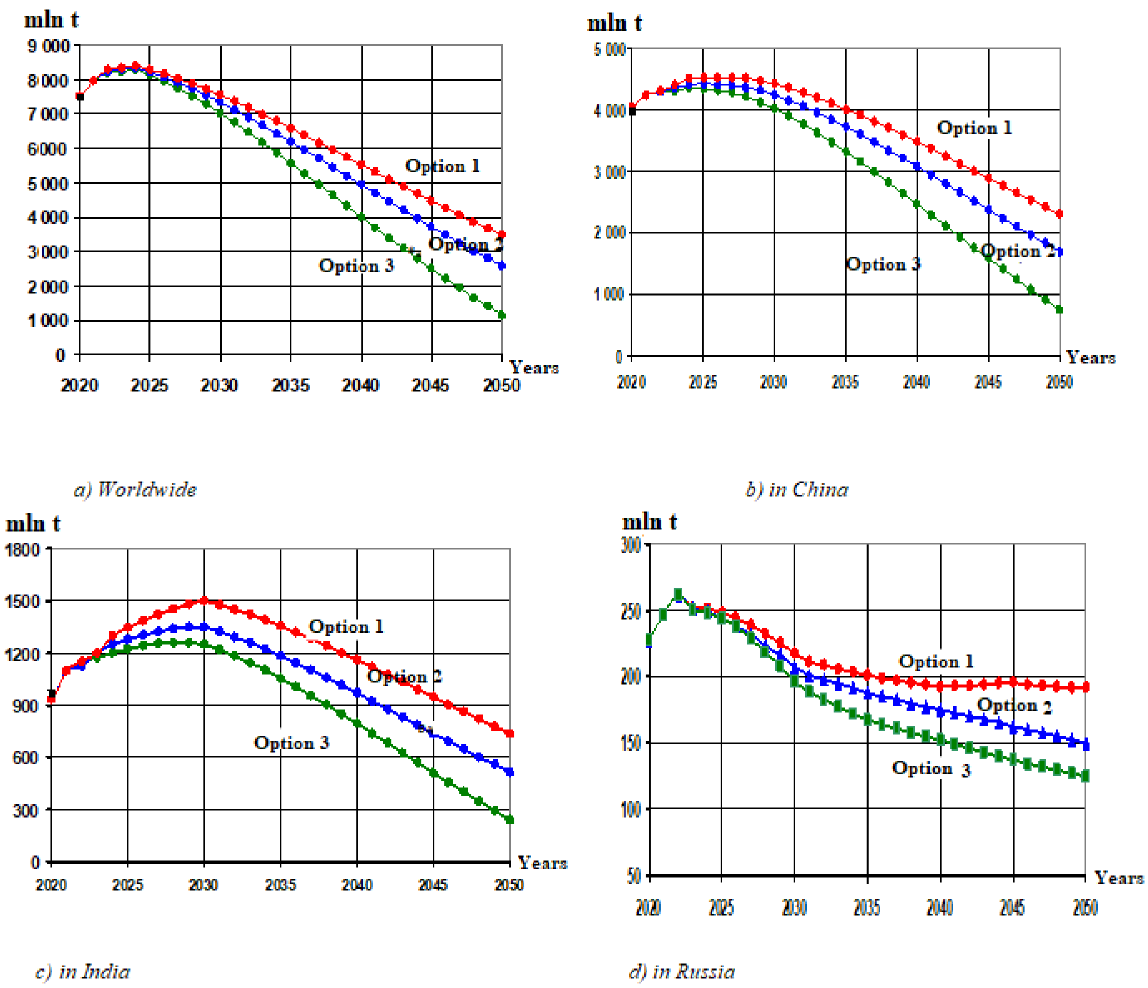

Fig. 1. Projections of coal consumption worldwide and in major countries until 2050.

economy, assuming decarbonization ends before the 1970s, and there is no embargo on Russian coal supply to the EU countries;

Option II – moderate rates of decarbonization of the world economy, assuming decarbonization ends before the 2060s and there is partial enforcement of the embargo on Russian coal supply to the EU countries;

Option III – high rates of decarbonization of the world economy, assuming decarbonization ends before the 2050s and there is strict enforcement of the embargo on Russian coal supply to the EU countries.

The projections of coal consumption in the major countries of the world and Russia, following the accepted options, are shown in Fig. 1.

Projections of the Russian coal production and exports according to the three scenarios are shown in Fig. 2.

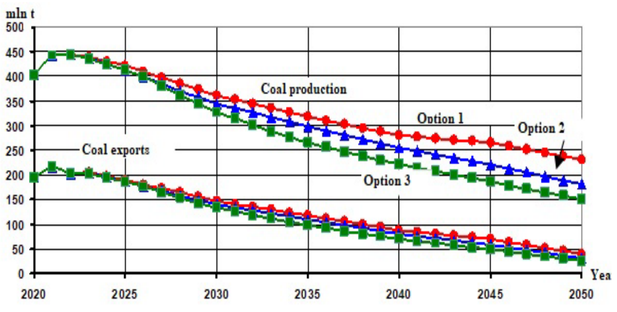

Fig. 2. Projections of Russian coal production and exports until 2050.

VII. Conclusion

The global coal industry has experienced rapid growth in recent years. However, with the global push for decarbonization of the economy and the pursuit of carbon neutrality by most countries of the world, a shift from the use of coal in energy and other industries has begun. This shift is expected to curb the growth rate of coal consumption in the future. The speed of this decline will depend on the scenarios for the development of the world economy: under favorable scenarios, the world anticipates a rapid abandonment of coal, whereas under unfavorable scenarios, the trend is expected to be the opposite. The reduction in global coal trade is likely to happen much faster, as it will be more economically profitable for importing countries to switch to the use of renewable energy sources and hydrogen.

The sanctions, restrictions, and embargo imposed on Russian coal will result in a decline in the production of Russian coal. This is due to the decreased demand from European consumers and reduced or discontinued imports by some Asian countries. Furthermore, some coal companies are currently facing the threat of bankruptcy.

A decrease in the volume of the Russian export coal market may result in the reduction in a large number of coal mining enterprises and personnel engaged in coal extraction and processing by the year 2050. Nevertheless, it is still too early to talk about the end of the "coal era," at least until 2030.

References

[1] "Coal Information 2021," International Energy Agency Statistics, Electronic database, OECD/IEA, 2022. [Online]. Available: https://www.iea.org/reports/coal-2021

[2] "Statistics report Key World Energy Statistics,' International Energy Agency Statistics, OECD/IEA, Sep. 2022, 80 p.

[3] BP Statistical Review of World Energy, Jun. 2023, 69th ed., 2023, 65 p.

[4] Yu. A. Plakitkin, L. S. Plakitkina, K. I. Dyachenko, "Forecast of the development of the global and domestic coal market under the influence of green energy trends and sanctions restrictions," *Coal*, no. 8, pp. 66–72, 2023. DOI: 10.18796/0041-5790-2023-8-66-72. (in Russian)

[5] "Novak says Russian coal production up 0.3% in 2022," *TASS.ru*, Jan. 11, 2023. [Online]. Available: https://tass.ru/ekonomika/16777769. (in Russian)

[6] I. E. Petrenko, "The results of the work of the Russian coal industry for 2022," *Coal*, no. 3, pp. 21–33, 2023. DOI: 10.18796/0041-5790-2023-3-21-33. (in Russian)

[7] H. Reid, N. Banya, "Europe imports more South African coal as Russian ban looms," *Reuters.com*, Jun.15, 2022. [Online]. Available: https://www.reuters.com/markets/commodities/europe-imports-more-south-african-coal-russian-ban-looms-2022-06-15

[8] "Ministry of Energy predicts stabilization of coal exports in 2023," *Vedomosti.ru, Jun. 07, 2023*. [Online]. Available: https://www.vedomosti.ru/business/articles/2023/06/07/979009-minenergo-prognoziruet-stabilizatsiyu-eksporta-uglya (in Russian)

[9] "Kazakh coal is too cheap in Russia. Deliveries for January-May decreased by 16%," *Forpost-sevastopol.ru.* [Online]. Available: https://forpost-sevastopol.ru/newsfull/941525/kazahskomu-uglyu-v-rossii-slishkom-deshevo-postavki-za-yanvarmaj-snizilis-na-16.html (in Russian)

[10] "China vows to end greenhouse gas emissions by 2060," *Kommersant.ru*, Sep. 23, 2020. [Online]. Available: https://www.kommersant.ru/doc/4502238?ysclid=lum1d4mqtw543885040 (in Russian)

[11] "Achieving carbon neutrality by 2050 will cost India six times more than China," *Plus One*, Mar. 22, 2021. [Online]. Available: https://plus-one.ru/news/2021/03/22/dostizhenie-uglerodnoy-neytralnost-k-2050-godu-oboydetsya-indii-v-shest-raz-dorozhe-chem-kitayu (in Russian)

[12] "Poverty and death: the power engineer spoke about the possible rejection of coal in South Africa," *Forpost-sz.ru*, Aug. 18, 2023. [Online]. Available: https://forpost-sz.ru/a/2023-08-18/nishcheta-i-smert-ehnergetik-rasskazal-o-vozmozhnom-otkaze-ot-uglya-v-yuar (in Russian)

[13] Yu. A. Plakitkin, L. S. Plakitkina, K. I. Dyachenko, "The coal industry of Russia in the conditions of low-carbon energy and sanctions restrictions," *Industry of Eurasia*, no. 1-2(2), pp. 56–62, 2022. (in Russian)

[14] Yu. A. Plakitkin, L. S. Plakitkina, K. I. Dyachenko, "The main trends in the development of the coal industry in the world and Russia in the conditions of low-carbon energy. Part I. Analysis of the pace and proportions of the development of the coal industry, formed under the influence of the leading countries of the coal market," *Mining Journal*, no. 7, pp. 10–16, 2022. (in Russian)

[15] Yu. A. Plakitkin, L. S. Plakitkina, K. I. Dyachenko, "The main trends in the development of the coal industry in the world and Russia in the conditions of low-carbon energy. Part II. Low-carbon development as a factor in reducing demand for coal and its impact on plans for the development of coal generation," *Mining Journal*, no. 8, pp.17–23, 2022. (in Russian).

Liudmila S. Plakitkina, Head of the Research Center for Coal Industry in Russia and in the World, Ph.D., Corresponding Member of the Russian Academy of Natural Sciences. The main interests are: systematic research to assess the development parameters of the Russian coal industry taking into account the development of its resource base and the achieved results of its work in domestic and global energy markets; analysis and forecasts of the development of the coal industry of the world, individual regions and countries of the world and Russia in the context of the implementation of low-carbon energy trends and strengthening of sanctions restrictions.

Competitiveness of Export-Oriented Systems of Long-Range Energy Supply

E.A. Tyurina[1,2], A.S. Mednikov[1,*], P.Yu. Elsukov[1], and S.N. Sushko[2]

[1] Melentiev Energy Systems Institute of Siberian Branch of Russian Academy of Sciences, Irkutsk, Russia
[2] Irkutsk National Research Technical University, Irkutsk, Russia

***Abstract* — The paper examines process chains including production, transport, and conversion of energy resources from Siberia and the Russian Far East to Asian countries. The study aims to find the most effective ways to supply energy to end consumers at various distances. The options considered include pipeline transport of natural gas from eastern regions of Russia to Asian countries; rail transport of coal from Russian export-oriented deposits to Asian countries; natural gas conversion into methanol, with methanol transport through pipelines of various diameters to Asian countries; and coal conversion into methanol, with methanol transport through pipelines of various diameters to Asian countries. Optimization is performed using previously developed mathematical models.**

***Index Terms* — methanol, natural gas, coal, export, Russia, Asia, mathematical modelling.**

I. Introduction

In light of the current global situation, Russia has to explore new avenues to export minerals, primarily coal, natural gas, and oil, while also enhancing its role in Asian countries [1–3].

When considering the options for transporting the energy of fossil fuels from export-oriented deposits in Russia's eastern regions to Asian countries, the problem arises of how to find the best ways to "deliver" the energy to the end users. This is due to the significant volume to be transported and long range [3–8].

Modern research focuses on modelling global trade [9], modelling energy systems [10], redistribution of natural gas flows [10], analysis of scenarios for the influence of external factors on the economies of countries [11–13] and on energy prices [14, 15], the influence of geopolitical events and mineral exports on the transition to renewable energy [16], and the impact of export activities on the environment [9, 17].

A computable general equilibrium model of world trade is used in [9] to quantify the possible impact of economic sanctions.

A detailed mathematical model is proposed in [10] to predict the movement of gas volumes through the pipeline of the European gas market.

The main components of a methodological approach are delivered in [11] to assess the level of significance of critical energy facilities on the example of individual shutdowns of the most important facilities of the Russian gas transmission network. The paper also presents approaches to modelling the energy sector of the country and its constituent energy (gas, electricity, and heat) systems.

Possible invariant measures aimed at reducing gas shortages for consumers in the case of emergencies at critical facilities of the gas industry are discussed in [12]. The study focuses on Russia's Unified gas system,

* Corresponding author.
E-mail: mednikov@isem.irk.ru

http://dx.doi.org/10.25729/esr.2024.01.0005

Received February 27, 2024. Revised March 28, 2024. Accepted April 11, 2024. Available online April 30, 2024.

This is an open-access article under a Creative Commons Attribution-NonCommercial 4.0 International License.

© 2024 ESI SB RAS and authors. All rights reserved.

providing a logical unfolding of the topic of searching for and identifying critical components of the system.

Shifting to gas in the Asian regions of Russia is presented in comparison with this process in the European part of the country. The level of gas infrastructure expansion in the Asian regions of Russia is far behind that in the European regions of the country [13].

The comprehensive approach proposed in [14] offers a deeper understanding of the interplay between energy trade dynamics, the updated NDCs, and carbon emissions. The study contributes to a more profound comprehension of the evolving fossil energy trade landscape and its implications for carbon emissions.

A global computable general equilibrium model [15] proves the impact of the Russian natural gas embargo on the economies of Russia and the EU.

Authors of [16] conclude that discontinuing imports of Russian energy resources would present a challenging scenario for the European Union. They propose using domestic supplies and reducing demand.

The paper [17] presents an investigation of whether financial development can reduce the export concentration in regional context, corroborating the role of the World Trade Organization membership, sanctions and investment potential. The Method of Moments Quantile Regression to analyse panel time-series data.

The time evolution of the amplitude of chaos for the Historical Prices of the Title Transfer Facility and the United States Natural Gas Fund commodities are analysed both before and during the special military operation [18]. Methods include Phase Space Reconstruction in Four-dimensional Euclidean Spaces from time series and Spearman Correlation between chaos intensities, elapsed time and prices.

In [19], the impact of geopolitical risk (GPR) on natural resources is evaluated by employing monthly (from January 1990 to January 2023) and daily (from 3rd January 2022 to 31st March 2022) data. The outcomes using wavelet QQ and novel Bayesian structural model reveal that GPR has a more profound impact on oil prices, natural gas prices, and gold prices (in a range of lower to upper quantiles) exhibiting that they are more sensitive to geopolitical uncertainties at all levels.

The study [20] examines the interplay between Russian mineral exports and renewable energy generation, taking into account geopolitical risks, within both the global and Chinese contexts. Utilizing the cross-quantilogram approach, this study reveals a positive spillover effect of Russian mineral exports on global and Chinese renewable electricity production, across various time frames, including monthly, quarterly, bi-annual, and annual memories.

The impacts of trading partners' environmental regulation on the export volumes of the Russian regions is analyzed using panel data covering about 140 000 observations in 84 Russian regions and 204 countries. The Gravity Model of international trade and Heckman Sample Selection methodology are employed [21].

There are various energy transmission and conversion options that require engineering and economic studies. These are pipeline transport of natural gas; rail transport of coal; conversion of natural gas and coal near export-oriented fields into synthetic liquid fuels (SLF), such as methanol, and its transport by methanol pipelines; and others [7, 8, 22, 23]. Options based on the conversion of gaseous and solid fuel into liquid fuel offer the advantage enabling pipeline transport of liquid fuel, which is much more economical for long distances and large scale compared to pipeline transport of natural gas or rail transport of coal [23].

Options for energy transport rely on both conventional well-established technologies (pipeline transport of natural gas or liquid fuel, rail transport of coal) and technologies that are novel in terms of the possibility of their large-scale adoption. This applies primarily to technologies for large-scale conversion of solid and gaseous fuels into synthetic liquid fuels. The conversion and subsequent SLF pipeline transport provides a lower price per unit of energy for the end user, while retaining the same profitability of the project (or an increase in the profitability while retaining the same competitive price). This process also offers enhanced performance of the energy carrier for the end user (the possibility of using it as a motor fuel, inexpensiveness of storage and transport in small batches, environmental friendliness, and others).

One promising synthetic liquid fuel is methanol. Methanol is a versatile intermediate for the production of a wide range of important chemical products. It is also an environmentally friendly liquid fuel that can be easily transported and stored. The main disadvantages of existing processes of converting fossil fuels into synthesis gas, followed by subsequent methanol production, are low thermal efficiency and large capital investment. This can be avoided by establishing systems for methanol and electricity co-production (MEC) based on the processes of coal gasification or conversion of natural gas and subsequent synthesis of methanol. In this case, the high-temperature heat of the gasification products as well as the heat and energy of the combustible purge gases of the synthesis process are utilized in the power generation plant. This is why fuel and electricity co-production systems are economically feasible and energy efficient.

It is important to emphasize that the above energy transport options can be considered as process chains that include series-connected links. Comparison of chains will be objective only if the parameters of the links in each process chain are optimized. Note that simultaneous optimization of the parameters of all links in the chain is a challenging task.

The Melentiev Energy Systems Institute SB RAS has developed an approach to optimize process chains. This approach involves a sequential optimization of each link in the chain. The criterion is the minimum price for the output product of each link. The optimization process takes into account a fixed level of internal rate of return on capital investment across all links and chains and the price of the output from the previous link, which is obtained during its optimization.

Our previous studies focused on power supply chains for remote consumers with various types of generation. Some models were borrowed from previous studies and then improved by increasing accuracy and updating the initial information [24].

II. Formulation of the Problem

As noted earlier, this work employs the approach to process chain optimization, which was developed at the Melentiev Energy Systems Institute SB RAS.

A mathematical problem statement of sequential optimization of links in the process chain can be represented as follows

$$\min_{x^i} c^i_{out} \tag{1}$$

subject to:

$$H^i(x^i, y^i, z^i) = 0, \tag{2}$$

$$G^i(x^i, y^i, z^i) \geq 0, \tag{3}$$

$$K^i = K^i(x^i, y^i, z^i, s^i), \tag{4}$$

$$U^i = U^i(x^i, y^i, z^i, c^i_{in}), \tag{5}$$

$$Q^i_{in} = Q^i_{in}(x^i, y^i, z^i), \tag{6}$$

$$Q^i_{out} = Q^i_{out}(x^i, y^i, z^i), \tag{7}$$

$$Q^i_{ac} = Q^i_{ac}(x^i, y^i, z^i), \tag{8}$$

$$c^i_{out} = Y^i(K^i, U^i, Q^i_{in}, c^i_{in}, Q^i_{out}, Q^i_{ac}, c^i_{ac}, IRR_z, \theta^i), \tag{9}$$

$$c^{j+1}_{in} = c^j_{out}, \tag{10}$$

$$Q^{j+1}_{in} = Q^j_{out}, \; j = 1, \dots, N-1, \tag{11}$$

$$\underline{x^i} \leq x^i \leq \overline{x^i}, i = 1, \dots, N, \tag{12}$$

where the subscript *i* stands for the number of a link in the process chain; c^i_{out} is energy carrier price at the output of the *i*-th link; H^i is system of equality constraints of the *i*-th link; x^i is vector of independent parameters of the *i*-th link to be optimized; y^i is vector of dependent calculated (from the system H^i) parameters of the *i*-th link; z^i is vector of input data (strength characteristics of materials and equipment characteristics that are not subject to optimization); G^i is system of inequality constraints of the *i*-th link, which sets boundaries within which its parameters can be changed; K^i is capital investment in equipment of the *i*-th link (in general case, a vector with the components that specify capital investment by year of the calculation period); s^i is specific cost characteristics of equipment; U^i is operating costs of the *i*-th link (in general case, a vector specifying costs by year of the calculation period); c^i_{in} is energy carrier price at the input of the *i*-th link; Q^i_{in}, Q^i_{out} are energy carrier consumption at the input and output of the *i*-th link respectively; Q^i_{ac} , c^i_{ac} are consumption and price of the energy carrier co-produced by the *i*-th link and consumed locally, i.e., without entering the (*i+1*)-th link; IRR_z is the given (for all links and all chains) value of the internal rate of return on investment; $\theta^i$is vector of economic parameters (rates of different taxes, etc.) used to calculate *IRR*; *N* is number of links; $\underline{x^i}$, $\overline{x^i}$ are vectors of minimum and maximum possible values of parameters to be optimized. The problem is solved by the method of mathematical modelling.

III. Results and Discussion

The considered potential options for energy supply to remote consumers in Asian countries are as follows:

- Pipeline transport of natural gas from eastern regions of

Russia to Asian countries.

- Rail transport of coal from export-oriented deposits to Asian countries.
- Conversion of natural gas into methanol, transport of methanol through pipelines of various diameters to Asian countries.
- Conversion of coal into methanol, transport of methanol through pipelines of various diameters to Asian countries.

Let us highlight the key distinctive features of the above energy transport options. Capital investment in gas pipelines is directly proportional to their length, while the methanol transport options have a significant part of capital expenditures independent of the transport distance, which are capital outlays on methanol production. At the same time, the specific cost of line pipes of methanol pipelines is significantly lower (per unit of equivalent amount of energy transmitted) than that of gas pipelines.

Conversion of natural gas and coal into methanol is assumed to be done using the systems for combined production of methanol and electricity [23]. Methanol pipelines with diameters of 1020 mm and 1220 mm are considered for long-distance methanol transport. The price of natural gas in Siberia and the Far East regions is assumed to be equal to 120–150 USD/1000 m^3, the price of coal - to 50–70 USD/tce based on [25, 26]. Specific costs

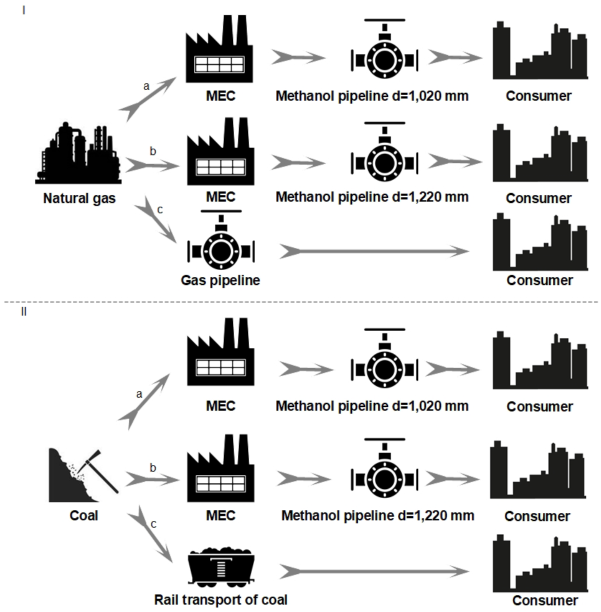

Fig. 1. Process chains of production and transport of energy resources from Siberia and the Russian Far East to Asian countries.

for rail transport of coal are 35–40 USD/tce-1000 km) [27]. The options in question differ significantly in the consumed amount of primary energy resource. The transport of natural gas through a 1420 mm pipeline can accommodate 36 billion m^3 (40 million tce) per year. The

TABLE 1. Prices of Energy Carriers at the End of Process Chains, Depending on the Options for Conversion and Transport of Energy Resources, USD/tce

Options for conversion and transport of energy carriers		Transport distance		
		3 000 (km)	4 500 (km)	6 000 (km)
Pipeline transport of natural gas from Russia's eastern regions to Asian countries through a 1420 mm diameter pipeline	1a – Gas price 120 USD/1000 m^3	171	211	257
	1b – Gas price: 150 USD/1000 m^3	197	238	284
Rail transport of coal from Siberian and Far East deposits to Asian countries	2a – Coal price: 50 USD/tce	170	230	290
	2b – Coal price: 70 USD/tce	190	250	310
Methanol production from natural gas fields in eastern regions of Russia, pipeline methanol transport to Asian countries through a 1020 mm diameter pipeline	3a – Gas price: 120 USD/1000 m^3	206	221	235
	3b – Gas price: 150 USD/1000 m^3	257	272	288
Methanol production from natural gas fields in eastern regions of Russia, pipeline methanol transport to Asian countries through a 1220 mm diameter pipeline	4a – Gas price: 120 USD/1000 m^3	199	210	222
	4b – Gas price: 150 USD/1000 m^3	251	262	274
Methanol production from coal deposits in eastern regions of Russia, pipeline methanol transport to Asian countries through a 1020 mm diameter pipeline	5a – Coal price 50 USD/tce	196	210	224
	5b – Coal price 70 USD/tce	234	249	264
Methanol production from coal deposits in eastern regions of Russia, pipeline methanol transport to Asian countries through a 1220 mm diameter pipeline	6a – Coal price 50 USD/tce	190	200	211
	6b – Coal price 70 USD/tce	227	238	250

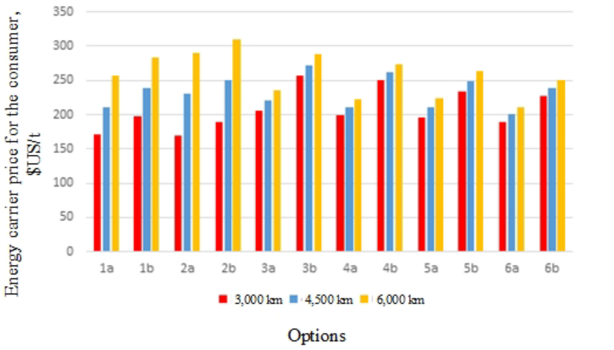

Fig. 2. Comparative performance of options for converting and transporting energy resources.

energy equivalent of methanol transmitted through a 1020 mm pipeline is 35 million tce per year, and through a 1220 mm pipeline – 70 million tce per year. Coal can be delivered by rail in amounts of up to 16–20 million tce per year.

Figure 1 shows the technologies considered in this study for energy production and transport. Table 1 shows the optimization results of the options for energy supply to consumers in Asian countries.

Figures 2 and 3 show the comparative economic feasibility of options for converting and transporting energy resources as a function of the transport distance.

The lowest unit price of final energy for an energy transport distance of 3 000 km is provided by the following: for options with coal as the initial energy carrier – its rail transport; for options with natural gas as the initial energy carrier – its pipeline transport. Options with the conversion of coal and natural gas into SLF when transported over 3 000 km prove inferior to direct transport of these energy carriers (without considering the higher methanol cost for the consumer). The lowest unit price of the final energy for the energy transport distance of 4 500 km is provided by the following: for options with coal as the initial energy carrier – coal conversion into methanol with its subsequent transport through a 1 220 mm diameter pipeline; for options with natural gas as an energy carrier – pipeline transport of gas and gas conversion into methanol with its subsequent transport through a 1 220 mm diameter pipeline. Note that with cheap coal, the unit price of final energy of methanol from coal is lower than the unit price of final energy from cheap gas.

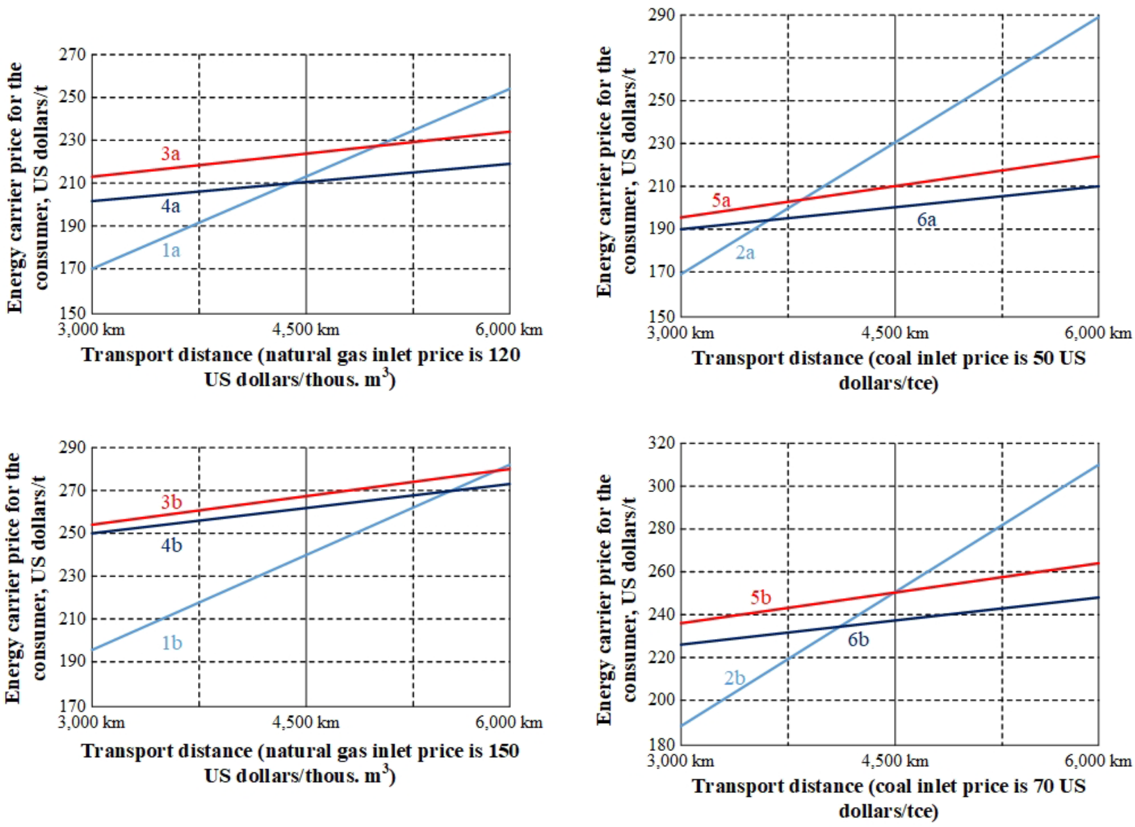

Fig. 3. Comparative performance of natural gas energy and coal energy transport options.

IV. Conclusion

The study examined the process chains of long-distance transport of energy carriers (natural gas, coal, and methanol from them) from Russia to Asian countries. Optimal options are obtained for various distances.

It is important to emphasize that in recent years, several large plants for the production of methanol from coal based on gasification technologies have been commissioned or are about to be commissioned in Asia. To this end, they use the technological solutions provided by world's leading companies: Shell, Siemens, and General Electric. In the current context, there are promising opportunities for the Russian Federation to enhance its existing technologies and collaborate with Asian organizations on combined fuel production projects.

V. Acknowledgement

The research was carried out under the State Assignment Project (no. FWEU-2021-0005) of the Fundamental Research Program of the Russian Federation 2021–2030; INRTU in Master's Training Program 13.04.01 "Heat power engineering and combustion engineering".

References

[1] S. Johnson, L. Rachel, C. Wolfram, "Design and implementation of the price cap on Russian oil exports," *Journal of Comparative Economics*, vol. 51, no 4, pp. 1244–1252, 2023. DOI: 10.1016/j.jce.2023.06.001.

[2] C. K. Chyong, J. Henderson, "Quantifying the economic value of Russian gas in Europe in the aftermath of the 2022 war in Ukraine," *Energy*, vol. 292, 130604, 2024. DOI: 10.1016/j.energy.2024.130604.

[3] S. Paltsev, "Scenarios for Russia's natural gas exports to 2050," *Energy Economics*, vol. 42, pp. 262–270, 2014. DOI: 10.1016/j.eneco.2014.01.005.

[4] S. Fortescue, "Russia's economic prospects in the Asia Pacific Region," *Journal of Eurasian Studies*, vol. 7, no 1, pp. 49–59, 2016. DOI: 10.1016/j.euras.2015.10.005

[5] I. Overland, J. Loginova, "The Russian coal industry in an uncertain world: Finally pivoting to Asia," *Energy Research & Social Science*, vol. 102, 103150, 2023. DOI: 10.1016/j.erss.2023.103150.

[6] P. A. Yanguas-Parra, N. Malz, P. Oei, A. Furnaro, Ch. Hauenstein, G. Quiceno et al, "Perspective: How a short-term relapse to coal could put exporting countries and just transition processes at risk," *Energy Research & Social Science*, vol. 97, 102989, 2023. DOI: 10.1016/j.erss.2023.102989.

[7] P. N. Kuznetsov, A. Ilyushetchkin, D. Chupin, M. Sukhorukova, "10 - Coal industry and the use of coal in the Russian Federation," in *Woodhead Publishing Series in Energy. The Coal Handbook (Second Edition)*, vol. 2, D. Osborne, Ed. Woodhead Publishing, 2023, pp.301–320. DOI: 10.1016/B978-0-12-824327-5.00003-X.

[8] V. Kutcherov, M. Morgunova, V. Bessel, A. Lopatin, "Russian natural gas exports: An analysis of challenges and opportunities," *Energy Strategy Reviews*, vol. 30, 100511, 2020. DOI: 10.1016/j.esr.2020.100511.

[9] N. Hosoe, "The cost of war: Impact of sanctions on Russia following the invasion of Ukraine," *Journal of Policy Modelling*, vol. 45, no 2, pp. 305-319, 2023. DOI: 10.1016/j.jpolmod.2023.04.001.

[10] Yu. M. Vasiliev, G. M. Fridman, "Mathematical modeling european gas market: advanced forecasting optimization model for natural gas flows through a pipeline network," *News of the St. Petersburg State Economic University*, vol. 3, pp. 15–24, 2019. (In Russian)

[11] S. M. Senderov, D. S. Krupenev, S. V. Vorobev, N. M. Beresneva, D. A. Boyarkin, "Methodological Approach to Assessing the Level of Significance of Critically Important Energy Facilities in the Interconnected Operation of Energy Systems," *Izvestiya RAN. Energetika*, no 2, pp. 31–45, 2023. (In Russian)

[12] S. V. Vorobev, S. M. Senderov, A. V. Edelev, "Search for Directions for Minimizing Gas Deficiency in Consumers in Emergency Situations at the Most Important Objects of the Gas Industry," *Izvestiya RAN. Energetika*, no 2, pp. 119–127, 2021. (In Russian)

[13] B. G. Saneev, G. G. Lachkov, "Features of gasification of the Asian regions of Russia," *Energy Policy*, no. 2, pp. 70–77, 2023. DOI: 10.46920/2409-5516_2023_2180_70.

[14] Q. Zhang, X. Mao, J. Lu, Zh. Guo, Z. Duman, Yo. Chen, P. Song, K. Tu, "EU-Russia energy decoupling in combination with the updated NDCs impacts on global fossil energy trade and carbon emissions," *Applied Energy*, vol. 356, 122415, 2024. DOI: 10.1016/j.apenergy.2023.122415.

[15] S. Perdana, M. Vielle, M. Schenckery, "European Economic impacts of cutting energy imports from Russia: A computable general equilibrium analysis," *Energy Strategy Reviews*, vol. 44, 101006, 2022. DOI: 10.1016/j.esr.2022.101006.

[16] B. McWilliams, G. Sgaravatti, S. Tagliapietra, G. Zachmann, "How would the European Union fare without Russian energy?," *Energy Policy*, vol. 174, 113413, 2023. DOI: 10.1016/j.enpol.2022.113413.

[17] M. Shakib, K. Sohag, M. K. Hassan, R. Vasilyeva, "Finance and export diversifications Nexus in Russian regions: Role of trade globalization and regional potential," *Emerging Markets Review*, vol. 57, 101059, 2023. DOI: 10.1016/j.ememar.2023.101059.

[18] P.R.L. Alves, "The Russia–Ukraine conflict and the amplitude of chaos in the prices of Natural Gas commodities," *Chaos, Solitons & Fractals*, vol. 179, 114452, 2024. DOI: 10.1016/j.chaos.2024.114452.

[19] A. Khurshid, Kh. Khan, A. Rauf, J. Cifuentes-Faura, "Effect of geopolitical risk on resources prices in the global and Russian-Ukrainian context: A novel Bayesian structural model," *Resources Policy*, vol. 88, 104536, 2024. DOI: 10.1016/j.resourpol.2023.104536.

[20] Md. M. Islam, K. Sohag, A. Berezin, B. S. Sergi, "Factor proportions model for Russian mineral supply-driven global energy transition: Does externality matter?," *Energy Economics*, vol. 129, 107242, 2024 DOI: 10.1016/j.eneco.2023.107242.

[21] Yu. Sokolova, N. Davidson, O. Mariev, "Global energy transition and foreign environmental regulations: Impacts on Russian regions' export volumes," *Journal of Environmental Management*, vol. 352, 120001, 2024. DOI: 10.1016/j.jenvman.2023.120001.

[22] M. R. Islam, *Pipelines. Emerging Technologies and Design Criteria. A volume in Sustainable Oil and Gas Development Series*. Gulf Professional Publishing, 2023.

[23] A. M. Kler, E. A. Tyurina, A. S. Mednikov, "A plant for methanol and electricity production: Technical-economic analysis," *Energy*, no. 165, 890–899, 2018. DOI: 10.1016/j.energy.2018.09.179.

[24] N. I. Voropai, S. V. Podkovalnikov, V. V. Trufanov et al., *Rationale for the development of electric power systems: Methodology, models, methods, their use*. Novosibirsk, Russia: Nauka, 2015. (In Russian)

[25] "Russian gas market," [Online]. Available: http://www.gazprom.ru/about/marketing/russia/

[26] "Government statistics," [Online]. Available: http://www.fedstat.ru/indicator/31448/

[27] "Freight transportation," [Online]. Available: http://cargo.rzd.ru

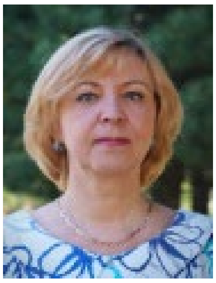

Elina Tyurina is a Dr. Eng., lead researcher at the Department of Thermal Power Systems of the Melentiev Energy Systems Institute SB RAS (ESI SB RAS), and the head of the Department of Thermal Power Systems at Irkutsk National Research Technical University (INRTU). Her scientific interests include mathematical modeling of mineral processing, co-production technologies, and others.

Aleksandr Mednikov is a Ph.D. in engineering, senior researcher at the Department of Thermal Power Systems of the ESI SB RAS. His research interests include hydrogen energy and fossil fuel recycling.

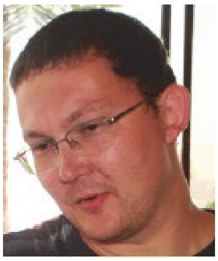

Pavel Elsukov is a Ph.D. in engineering, researcher at the Department of Thermal Power Systems of the ESI SB RAS. His research interests include mathematical modeling of power plants.

Svetlana Sushko is a candidate of technical sciences, associate professor of the Department of Heat and Power Engineering at INRTU. The main direction of scientific activity is increasing the thermal efficiency of thermal mechanical equipment of thermal power plants.

Active Filters for Standard-Compliant Power Quality in Electrical Networks

G.M. Mustafa, S.I. Gusev*

LLC NPP LM Invertor, Moscow, Russia

***Abstract* — The focus of this paper is on three circuits of Modular Multilevel Converters (MMC) with series connected single-phase full-bridge and half-bridge voltage source inverters, each of which operates in the pulse-width modulation (PWM) mode. The key defining feature of MMC-based active filters (AF) is their capability to perform selective fast filtering of voltage harmonics in real time. AFs suppress any given set of voltage harmonics, including the negative harmonic (fundamental frequency negative sequence voltage) with a given degree of suppression down to zero or a standardized value. This is achieved by enabling an appropriate setting in the control program. The study proposes a DSB-algorithm (D – damping, S – selective harmonic suppression, B – balancing) of MMC control to make power quality indices standard-compliant. The algorithm rests on the classical theory of automatic control and the theory of three-phase circuits. A comparative assessment of the use of various MMC circuits is made for voltage balancing adjustment and reactive power compensation. The findings suggest that the problem of voltage balancing adjustment by means of MMCs is unique because it requires the application of dedicated algorithms to ensure the reactive nature of the branches of MMC circuits in order to solve it.**

* Corresponding author.
E-mail: Gusev-si@lm-inverter.ru

http://dx.doi.org/10.25729/esr.2024.01.0006

Received February 28, 2024. Revised March 25, 2024. Accepted April 19, 2024. Available online April 30, 2024.

This is an open-access article under a Creative Commons Attribution-NonCommercial 4.0 International License.

© 2024 ESI SB RAS and authors. All rights reserved.

***Index Terms* — modular multilevel voltage source converter, fast harmonic filtering, balancing adjustment, DSB control algorithm.**

I. Introduction

The issue of power quality has become more acute in recent years due to the appearance of a large number of nonlinear loads that compromise the power quality in electrical networks. Conventional solutions based on static thyristor-controlled compensators (STC) with passive resonant filters or transistor-clamped three-level voltage source converters (STATCOM) fail to address the quality issues in a truly comprehensive way. The emergence of the MMC concept was instrumental in yielding robust technology for the design of active filtering, compensating, and balancing devices (AFCD), which could provide a comprehensive solution to the problems of making power quality parameters standard-compliant in power systems and electrical networks of industrial enterprises in accordance with State Standard (GOST) 32144-2013 [1]. The recent years have seen the development of theoretical, procedural, and regulatory frameworks of MMC-based AFCD design worldwide with the start of adoption of prototype AFCDs in AC networks [2–11]. There are several MMC circuits suitable for the design of AFCDs [12–14], and hence there is a need to make reasonable choices with respect to AFCD design schemes to solve specific problems [15].

Ensuring compliance of power quality parameters in electrical networks with the requirements, as stated in GOST 32144-2013 [1], requires addressing the following issues:

1) reactive power regulation (voltage stabilization);
2) balancing adjustment;
3) harmonic filtering;
4) transient response damping;

5) flicker reduction;
6) voltage dips elimination.

The advent of STATCOM devices based on MMC (modular multilevel voltage source converter) has provided a comprehensive and efficient solution to these issues. The appearance of such devices is a result of higher values of parameters of high-capacity power semiconductor devices such as fast-acting Insulated Gate Bipolar Transistors (IGBT) and Integrated Gate-Commutated Thyristors (IGCT) [18]. Another contributing factor is the advances in the development of digital signal microprocessors (higher speed, higher capacity), which enabled the implementation of the most complex control algorithms. MMC-based STATCOMs are capable of forming the output AC voltage of a given waveform in a wide range of frequencies and making use of the accomplishments of the theory of automatic regulation to create tracking regulation systems. PWM-controlled MMCs enabled the use of active power filter (APF), which is a versatile tool to make power quality standard-compliant. In terms of its integral action in an electrical network, MMC is a broadband controlled voltage source that amplifies the reference signal with high accuracy. Furthermore, the reference signal may vary at a high rate, in particular, it may contain significant harmonics. The output impedance of MMCs is negligible over a wide frequency range. Even highly distorted fast-changing currents do not cause malfunction of the MMC. Representing MMC as an ideal controlled voltage source allows us to claim that high-frequency tracking pulse-width modulation converters based on IGBT transistors form a new class of broadband power amplifiers whose action is not accompanied by power losses [7]. From the theoretical standpoint, the action of an active filter is treated as the algebraic transformation of sinusoidal variables into the sum of complex exponents of the positive and negative sequences, which yields

$$U(\theta)^k = \vec{A}_{pk} e^{jk\theta} + \vec{A}_{mk} e^{-jk\theta}, \qquad (1)$$

where $\vec{A}_{pk}$, $\vec{A}_{mk}$ is complex amplitudes of positive and negative sequence voltages; k is harmonic number; $\theta = \omega t$; $\omega = 2\pi f$; f is network frequency.

The negative sequence voltage at the fundamental frequency is considered to be one of the negative harmonics, which enables a unified approach to the design of the harmonic filtering and balancing adjustment algorithm.

II. APF Designs

Three MMC circuits with a series connected single-phase full-bridge (Fig. 1) and half-bridge (Fig. 2) voltage source converters (transistor and capacitor modules, or TCM) are most suitable for APF design. Each of such converters operates in the PWM mode, so that the average output voltage of the module is set equal to the input control variable, i.e., the voltage reference signal [3, 11]. Several TCMs are connected in series to form a phase branch (arm) of the MMC, and then three phase branches can be connected in a star (Y) or delta (D) topology, thus forming a tri-pole network, which is then connected to a three-phase network (Fig. 1), or into a bridge circuit, i.e., the Marquardt circuit (Fig. 2) [13, 14].

The basic component of the MMC is a single-phase transistor-clamped voltage source converter (VSC), which represents the basic state-of-the-art means for controlling the flow of electricity. A simple voltage source converter is made up of four or two transistors, each shunted by a backward diode (Fig. 3). The transistors are connected in a single-phase full-bridge (or half-bridge) circuit, forming a 4-pole network with two bipolar ports for connection to an external system (sources, loads, or intermediate nodes):

– a constant voltage (sign-constant voltage) port with two variables $u_1(t)$, $i_1(t)$;
– AC voltage port with two variables $u_2(t)$, $i_2(t)$.

Single-phase PWM converter (Fig. 3) is a controllable component that neither stores nor dissipates energy and whose AC port power is identically equal to the DC port power [16]:

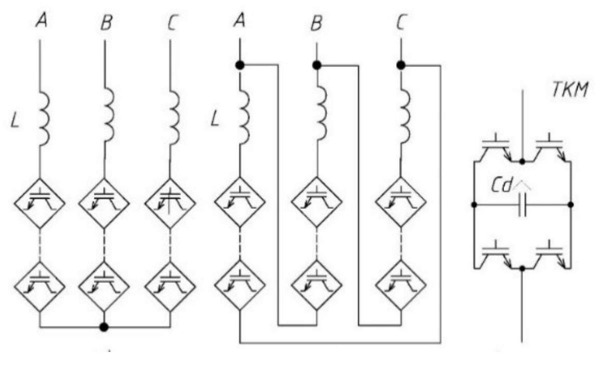

a) b) c)

Fig. 1. Modular multi-level circuit composed of series-connected TCMs (c) combined into a star (a) or delta (b) configuration.

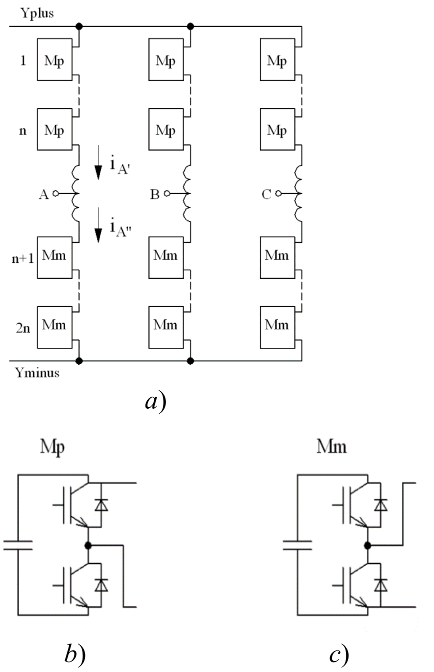

Fig. 2. Bridge-based modular multi-level circuit – Marquardt circuit (a), composed of half-bridge modules (b) and (c), the positive Y_{plus} and negative Y_{minus} poles of the circuit.

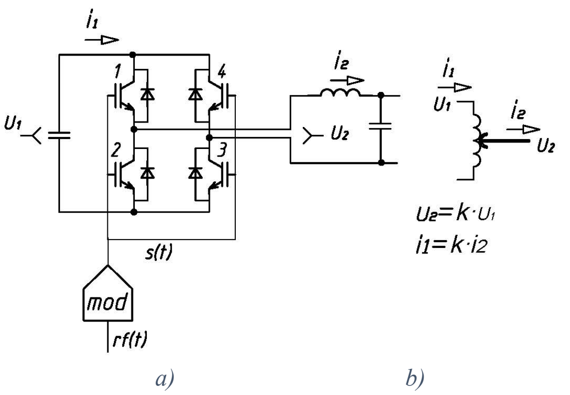

Fig. 3. The simplest single-phase PWM voltage converter (a) and its equivalent circuit (b).

$$p_2 = u_2 i_2 \equiv u_1 i_1, \tag{2}$$

with the voltage and current transfer ratio set by the control system that generates the switching PWM function of the transistors $s(t)$:

$$\begin{aligned} u_2 &= s(t)u_1, \\ i_1 &= s(t)i_2, \end{aligned} \tag{3}$$

linking the DC-side variables to the AC-side variables.

The switching function $s(t)$ is a step function with values [0, ±1] (three-step modulation) and the variables u_2, i_2 are step variables along with $s(t)$. After the local averaging operation [6] of the step function within the modulation period, which is obtained as:

$$\hat{x}(t) = \frac{1}{2h}\int_{t-h}^{t+h} x(\tau)d\tau\,, \tag{4}$$

each variable of the function $x(t)$ is divided into its basis $\hat{x}(t)$ and ripple $\tilde{x}(t)$:

$$x(t) = \hat{x}(t) + \tilde{x}(t).$$

The ripples $\tilde{x}(t)$ are suppressed by the output LC filter (inductor filter) and do not reach the load. Only the basic components of the variables are useful.

As a result, the average value of the switching function can be gradually changed in the range of [–1, 1], and accordingly, the PWM converter voltage can be gradually changed by the control system in the range of [$-u_2$, u_2]. If the modulator is properly designed, the switching function $s(t)$ generated by it has a locally averaged value

$$\hat{s}(t) = u_2/u_1. \tag{5}$$

In this case, the locally averaged voltage of the PWM converter coincides with the reference signal

$$\hat{u}_2 = u_z, \tag{6}$$

which is what is required to use it as an active element of the filter. Equalities (2), (3), (5), (6) describe the single-phase modules of the multilevel circuit and the entire modular multilevel circuit as a whole.

The PWM carrier frequency is usually high and well above the fundamental frequencies of the system. The power flows are controlled by the data signal of $rf(t)$, which is formed by the control system and acts through the modulator (*mod*) generating pulses to switch on transistors of the corresponding width. Equations (3) describe the PWM converter as a controlled electrical network 4-pole terminal that neither stores nor dissipates energy. The equations are exactly the same as the equations of the ideal transformer with variable controlled turns ratio as shown in Fig. 3b.

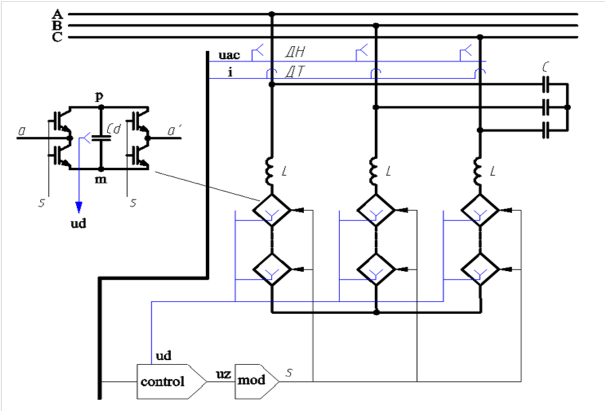

Fig. 4. Diagram of connection of the MMC Y-circuit to a three-phase network: TCM - left; electrical diagram - right.

Figure 4 shows the connection diagram for an active element based on the MMC Y-circuit connected to a 3-phase network.

The input of the control unit (*control*) receives feedback signals *i*, u_{ac} from the current (CS) and voltage (VS) sensors of the AC side and signals of constant voltages on the TCM capacitors – u_d, based on which the reference signal u_z of the PWM modulator (*mod*) is formed.

PWM pulses of the TCM of the phase branch are shifted between each other, creating a multilevel voltage with high equivalent frequency and a small modulation step (Fig. 5).

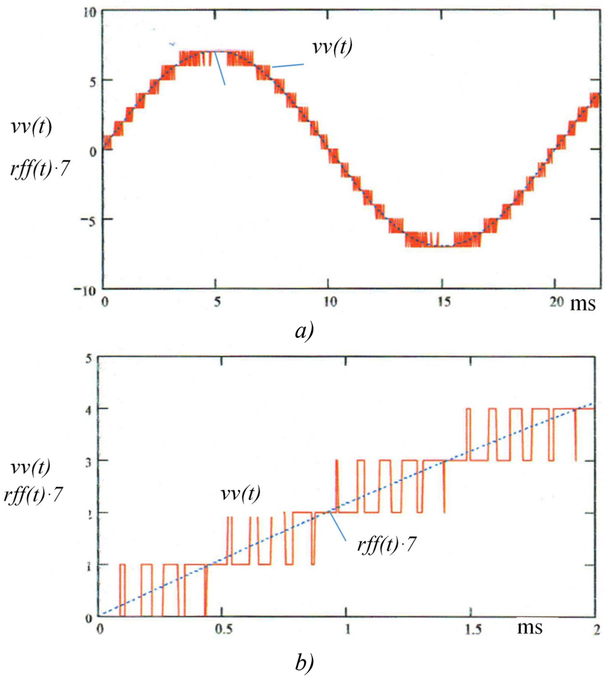

Fig. 5. Width modulation in a 7-module circuit (rff(t)-7 – reference voltage; vv(t) – output width-modulated voltage): (a) period of the output voltage; (b) enlarged detail.

The MMC output voltage averaged over a short interval repeats the output voltage reference data signal at the power output:

$$\hat{u}(t) = u_z(t). \tag{7}$$

The LC filter still need to filter the width modulation ripple but the energy impact of the filter in the multi-module circuit is negligible.

The shunt active filter can be represented integrally as an active element (*ae*) of an electrical network with frequency-dependent conductivity, just like any passive filter. The process of transformation into this form is shown in Fig. 6. Internal current i_{ae} and voltage u_{ae} feedback is used to transform the active element as an ideal voltage source (voltage follower) into a controllable current source (current follower):

$$i(t) = i_z(t). \tag{8}$$

The current reference signal i_z is generated by the main MMC regulator. If the voltage $u(p)$ at the point-of-coupling pole is used as the initial quantity for the current reference signal, the current reference signal is written as follows:

$$i_z(p) = G_{ae}(p)u(p), \tag{9}$$

where *p* is the Laplacian operator.

After feedback closing, the MMC acts as a circuit that shunts the point-of-coupling pole. This circuit has the

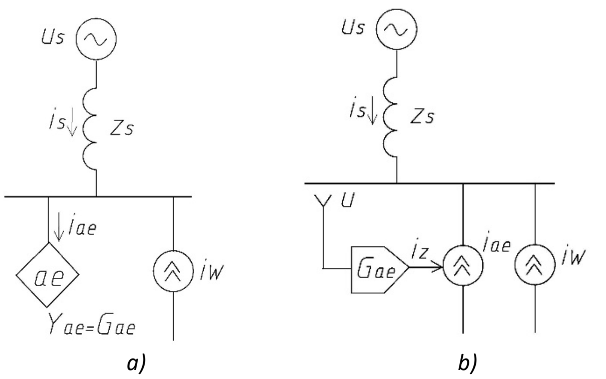

Fig. 6. Representation of the MMC as a network component with frequency-dependent conductivity: (a) a diagram of MMC connection to an electrical network; (b) an integral model of the MMC as an electrical network component with a conductivity function $Y_{ae}(p)$ equal to the transfer function $G_{ae}(p)$ of the main MMC controller.

frequency-dependent conductivity function equal to the controller transfer function $G_{ae}(p)$:

$$Y_{ae}(p) = G_{ae}(p). \tag{10}$$

It is physically possible to have a transfer function $G_{ae}(p)$ that is zero at both the positive line frequency

$$G_{ae}\,(j{\cdot}f_{nom}) = 0, \tag{11}$$

and at the negative line frequency

$$G_{ae}\,(-j{\cdot}f_{nom}) = 0. \tag{12}$$

In this way, it is possible to suppress the negative sequence voltage at the line frequency, i.e. to perform balancing adjustment of the three-phase voltage system.

III. DSB-Algorithm of MMC Control

The practical implementation of MMC-based STATCOM capabilities to ensure standard-compliant power quality parameters requires the synthesis of a branched multi-loop automatic control system capable of simultaneously controlling a set of a large number of parameters. In order to build such a system for solving practical problems, we have devised what we call the DSB algorithm of MMC control, which integrates classical automatic control theory and the theory of three-phase circuits. The DSB-algorithm is based on the sequential creation of three types of tracking automatic controllers [11, 17]: D (damp) – damping, S (select) – selective suppression, B (balance) – balancing, and the subsequent combination of their actions. The flow chart of the MMC control algorithm for the DSB algorithm is shown in Fig. 7.

The key MMC control variable, which is the voltage reference signal $u_z(t)$, is formed as a three-component sum of the voltages of regulators D, S, and B:

$$u_z = u_{damp} + u_{bal} + u_{sel}, \tag{13}$$

fed to the PWM modulator (mdl) input of the MMC circuit. The input signals that form the voltage reference signal are line current i_s, MMC output current i_{ae}, line voltage u_s, voltages of reservoir capacitors of MMC constant voltage links u_d. An LC filter (Y_{ae}, x_{ae}) is installed at the output of the MMC to provide PWM ripple smoothing.

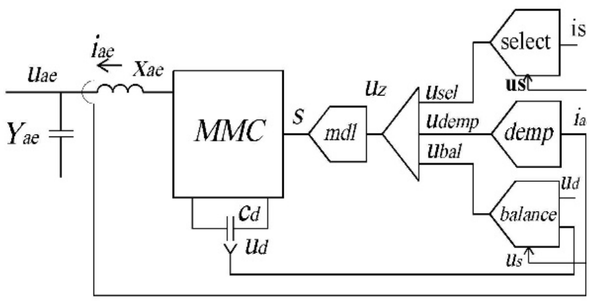

Fig. 7. Flow chart of the MMC control algorithm for the DSB algorithm.

Component D is formed by the output current feedback of the active element *iae* according to the equality:

$$u_{demp}(t) = R_{ae}{\cdot}i_{ae}(t). \tag{14}$$

This feedback acts like the resistor R_{ae} in (14) introduced into the output circuit of the active element. This "virtual resistor" dampens transient network fluctuations as efficiently as a real one. Figure 8 demonstrates the effect of the damping feedback. The Figure shows oscillograms of voltage on the 6 kV busbars of the Oktyabrsky mine

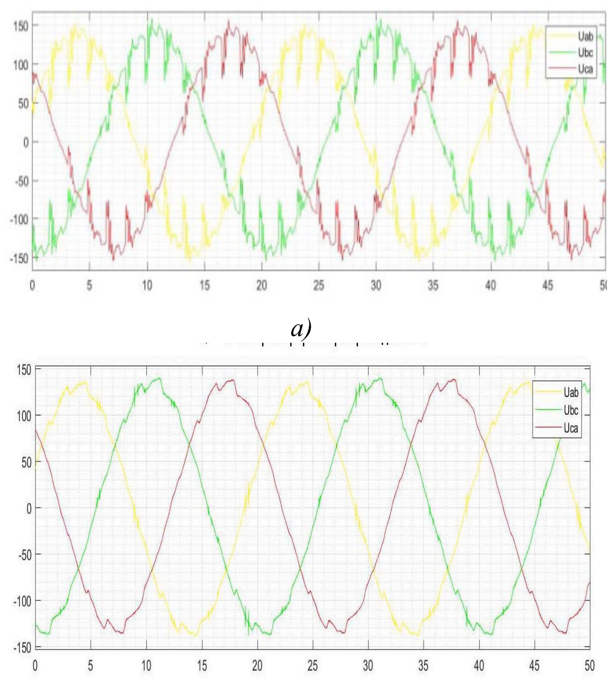

Fig. 8. Damping during operation of 2.4 MVA APF in the 6 kV network at the mine of PJSC Mining and Metallurgical Company "Norilsk Nickel": (a) voltage on the busbars before switching on the AF; (b) voltage on the busbars after switching on the AF.

network of PJSC Mining and Metallurgical Company "Norilsk Nickel" [6]. It reveals the significant impact of the active filter designed and manufactured by LLC "NPP LM Inverter" as depicted in Fig. 1b. This filter operates exclusively in the damping mode, demonstrating its efficiency. The busbar voltage is initially distorted by the thyristor rectifier of the skip hoist drive. The damping regulator effectively suppresses high-frequency voltage distortions that occur during switching of the rectifier thyristorsin the skip hoist drive.

The broadband damping feedback enables the design of a system for selective suppression of line current harmonics $is(\theta)$, which is based on the principle of quasi-stationarity. Damping causes the AC line current to be composed of the same harmonics that are generated by the distortion sources, which occurs after sufficiently short time intervals or with sufficiently slow changes in conditions. This enables a fast response to harmonic suppression by the selective filtering block *S (select)*.

The block *S (select)* is formed by means of the line current feedback *is* with the contribution from the line voltage u_s. The structure of the regulator of selective filtering of the *k*-th harmonic of the line current is shown in Fig. 9. The harmonic amplitude of the line current i_k, represented in the control system by the harmonic sum $I_k \cdot e^{j \cdot k \cdot \theta}$, is obtained from the current measured by the current sensor, multiplied by the *k*-th unit vector $e^{-j \cdot k \cdot \theta}$ of the negative sequence in Multiplier 1. To obtain the complex amplitude of the voltage harmonic $\vec{U}_k$, the output variable of the complex integrator block IN is multiplied by the assumed transfer resistance $Z_k = 1 / Y_k$, which is determined in Multiplier 2 by dividing the active element voltage by the line current at the frequency of the *k*-th harmonic (Y_k is the assumed line conductivity at the frequency of the *k*-th harmonic). Multiplier 3 restores the *k*-th harmonic reference voltage U_k of the active element by multiplying the value of the complex voltage amplitude $\vec{U}_k$ by the k-th unit vector $e^{j \cdot k \cdot \theta}$.

The structure of the regulator of selective suppression of the *k*-th harmonic of the line current is illustrated in Fig. 9. The amplitude of the harmonic current is obtained from the line current i_k (as measured by the line current sensor) multiplied by the negative sequence current in Multiplier 1. To obtain the complex amplitude of the voltage harmonic $\vec{U}_k$, the output variable of the complex integrator (IN) block is multiplied by the assumed transfer resistance $Z_k = 1 / Y_k$ from the active element voltage to the line current at the frequency of the *k*-th harmonic in Multiplier 2, where Y_k is the assumed network conductivity. Multiplier 3 uses the obtained value of the complex voltage amplitude to restore the reference voltage of the *k*-th harmonic U_k of the active element.

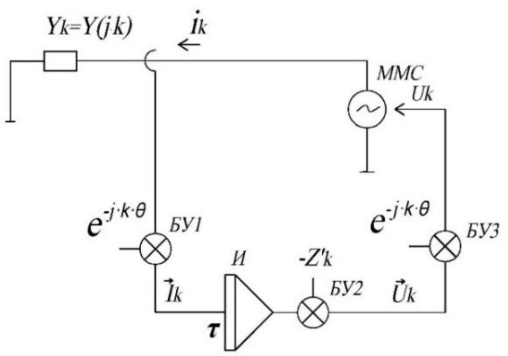

Fig. 9. Structure of the regulator of the selective filter of the k-th harmonic of the network current with feedback on the line current.

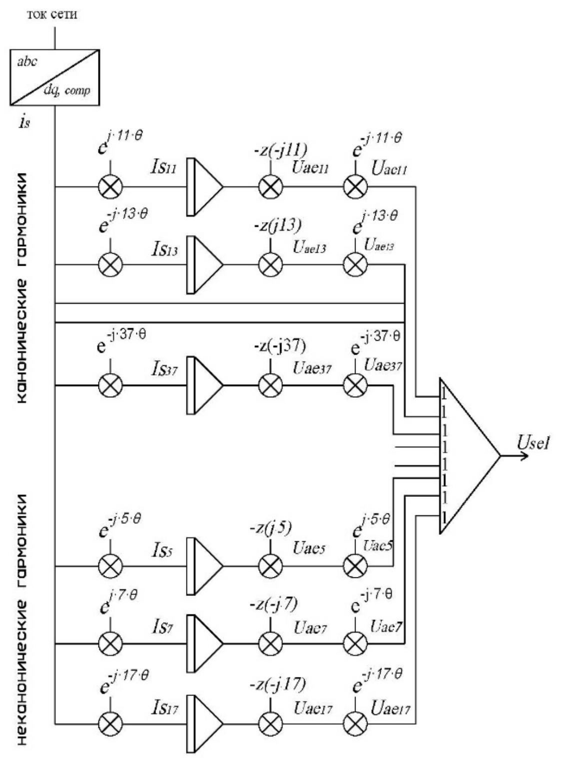

Fig. 10. The flow diagram of the calculator for selective harmonic suppression component U_{sel} that uses line current feedback.

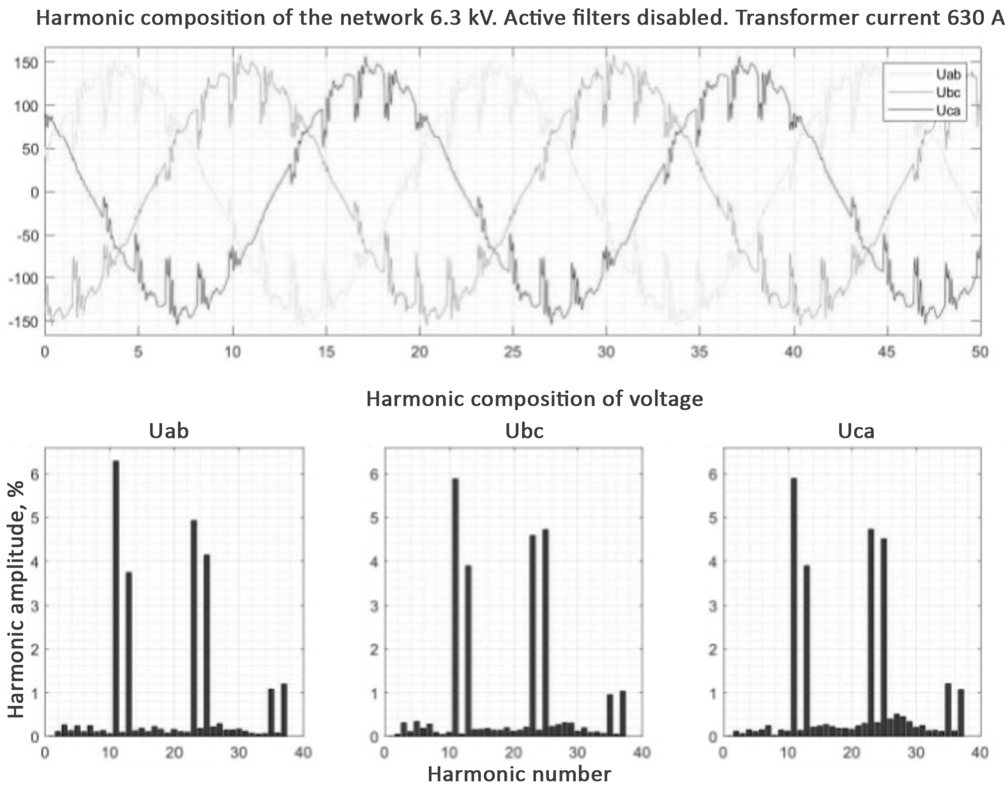

Fig. 11. Voltage oscillograms on 6 kV busbars before initiating the active filter for the modes of damping and selective filtering of the 11th and 13th harmonics at PJSC MMC "Norilsk Nickel."

The complete flow diagram of the calculator of each component of selective harmonic suppression is built by summing the regulators of the form presented in Fig. 9 for the entire set of selected harmonics (one regulator for each of the suppressed harmonics). This flow diagram is shown in Fig. 10.

The action of selective filtering can be exemplified by a case study of active filter operations at the facility of PJSC Mining and Metallurgical Company "Norilsk Nickel." Figures 11 and 12 show voltage oscillograms and histograms of the voltage harmonic content on the 6 kV busbars before and after initiating the active filter for the damping mode and the selective filtering mode targeting the 11th and 13th harmonics.The level of the 11th harmonic exceeded 6% before activating the active filter, but after enabling the filter, the maximum voltage harmonic level did not exceed 1%.

Component B is formed by the feedback on the voltages u_d of the reservoir capacitors of the constant voltage links of the MMC with the contribution from the line voltage u_s in this feedback. The component maintains the balance of energy, and hence the voltages of the reservoir capacitors in the vicinity of a specified level. The task of maintaining the energy balance of the reservoir capacitors arises as a consequence of the fact that the reservoir capacitors of the converter modules are not connected to the DC voltage energy source or sink.

A proportional-integral (PI) controller is used to regulate the balance power:

$$Pbal = \left(Kd + \frac{1}{p \cdot td} \right) \cdot \left(Ez - Ed \right), \qquad (15)$$

where p – the Laplacian; Ez – reference energy; Ed – energy of capacitors Cd; Kd, td – gain and time constant of the PI controller.

IV. Specific Features of Balancing Adjustment

The branches in the Y-circuit, D-circuit, and Marquardt circuit are reactive. Under all steady-state conditions, the average branch power must be zero. However, with balancing adjustment, the average phase powers can be non-zero. Balancing adjustment requires the exchange of

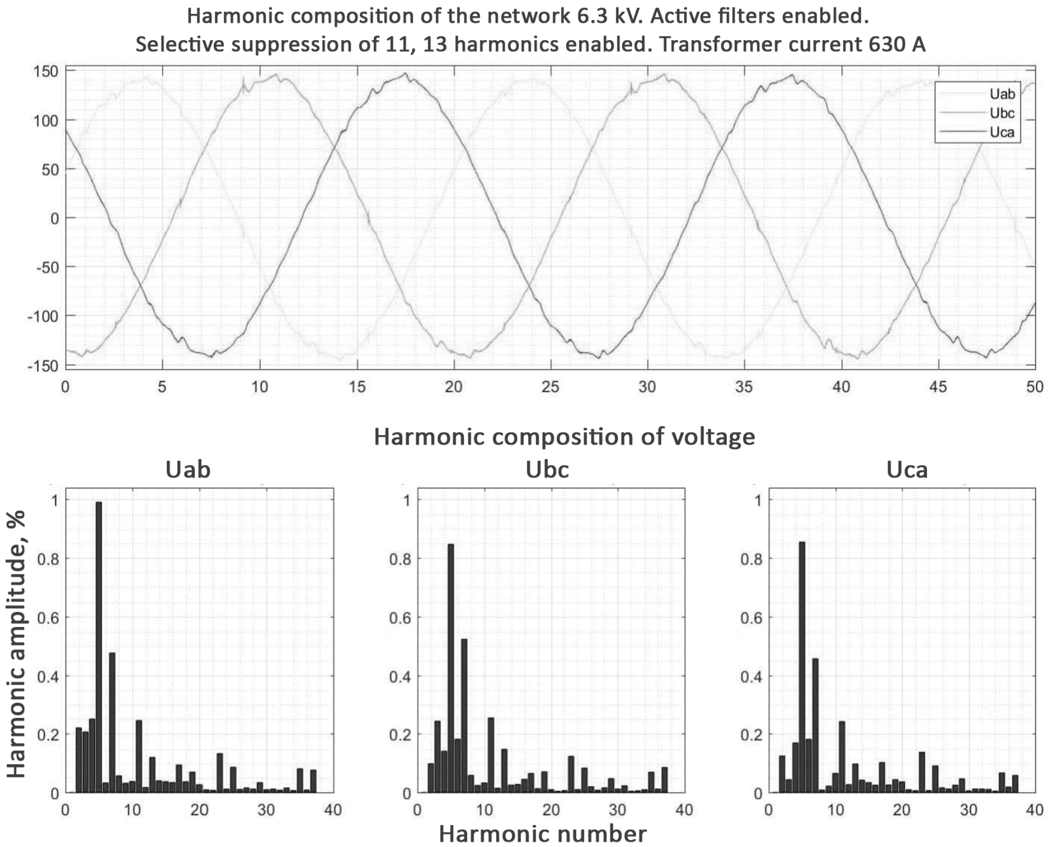

Fig. 12. Voltage oscillograms on 6 kV busbars after initiating the active filter for the modes of damping and selective filtering of the 11th and 13th harmonics at PJSC Mining and Metallurgical Company "Nornickel."

average powers between phases by introducing constant offset current in the Marquardt circuit, neutral offset in the Y-circuit, and circulating current in the D-circuit [10]. These currents affect significantly the technical and economic performance of the devices. In order to evaluate the technical and economic performance, we compared the three circuits with respect to the test conditions of compensation/balancing adjustment for a single-phase mixed resistive-inductive load with the conductivity Y_l, which is inserted between two phases.

$$\vec{Yl} = \begin{pmatrix} Y_0 \\ Y_1 \\ Y_2 \end{pmatrix} = \begin{pmatrix} \exp(j\varphi) \\ 0 \\ 0 \end{pmatrix}. \tag{16}$$

A STATCOM was connected in parallel to the load. Its design could be based either on the Marquardt circuit, the Y-circuit, or the D-circuit.

The STATCOM current $i_{sts}(t)$ must provide compensation for the reactive components of the load current:

$$i_{sts}(t) = -(i_{yma}(t) + i_{ymr}(t) + i_{ypr}(t)), \tag{17}$$

where i_{yma} and i_{ymr} are the negative sequence current components, i_{ypr} is the reactive component of the positive sequence current.

A. The Marquardt circuit

The test circuit is shown in Fig. 13. The balancing adjustment mode requires introducing a constant current offset ism_k common to these valves to balance the power in the branches of the Marquardt circuit:

$$\begin{aligned} iw_{2k} &= \frac{1}{2} istc_k - ism_k, \\ iw_{2k+1} &= -\frac{1}{2} istc_k - ism_k \end{aligned}. \tag{18}$$

The introduction of offsets guarantees that the conditions of zero average power of the valves are satisfied, i.e., it

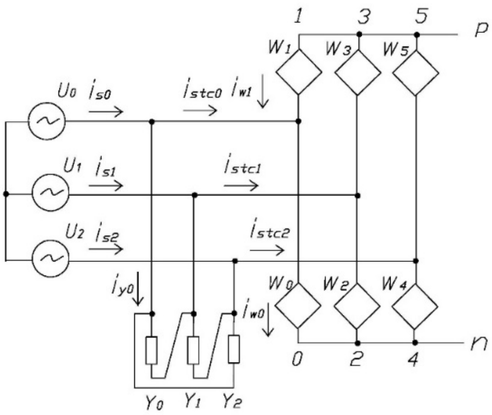

***Fig. 13**. A test circuit to analyze the operation of the Marquardt circuit.*

ensures that they stay reactive.

$$\int_T w(t)_k \, iw(t)_k \, dt = 0, \quad k = 0,1,\ldots,5, \tag{19}$$

where $w(t)_k$ is the voltage of the k-th valve.

The value of the offset current is defined by the equality

$$ism_k = \frac{1}{wsr} \cdot \int w(t)_{2k} \cdot \frac{1}{2} istc(t)_k , \tag{20}$$

where $wsr = \int_T w(t)_{2k} \, dt$.

Figure 14 shows the results of mathematical modeling for Marquardt circuit operation under balancing adjustment of a single-phase inductive load.

The network current $is(t)_k$ is a balanced clockwise-rotating current with zero phase shift with respect to the network voltage. Figure 14b shows one-by-one the loads of the controlled reactive valves for three phases during the operation in this mode: the voltage of the alternate valves w_{2k}, w_{2k+1} and their currents iw_{2k}, iw_{2k+1}. The phases are labeled as 0, 1, 2. The Figure also shows the phase currents of STATCOM $istc_k$. At a single-phase mixed resistive-inductive load at φ = π/6, with the load connected between phases 0, 1, offsets of currents in phases 0, 2 were needed: $ism_0 = -0.262$; $ism_2 = +0.262$. In this case, the active powers of the controlled reactive valves are zero for all three phases.

B. STATCOM Y-circuit

STATCOM Y- and D-circuits formed from three controlled reactive AC branches by connecting them in a star or delta topology are identical in terms of their functions, since they can be transformed into each other

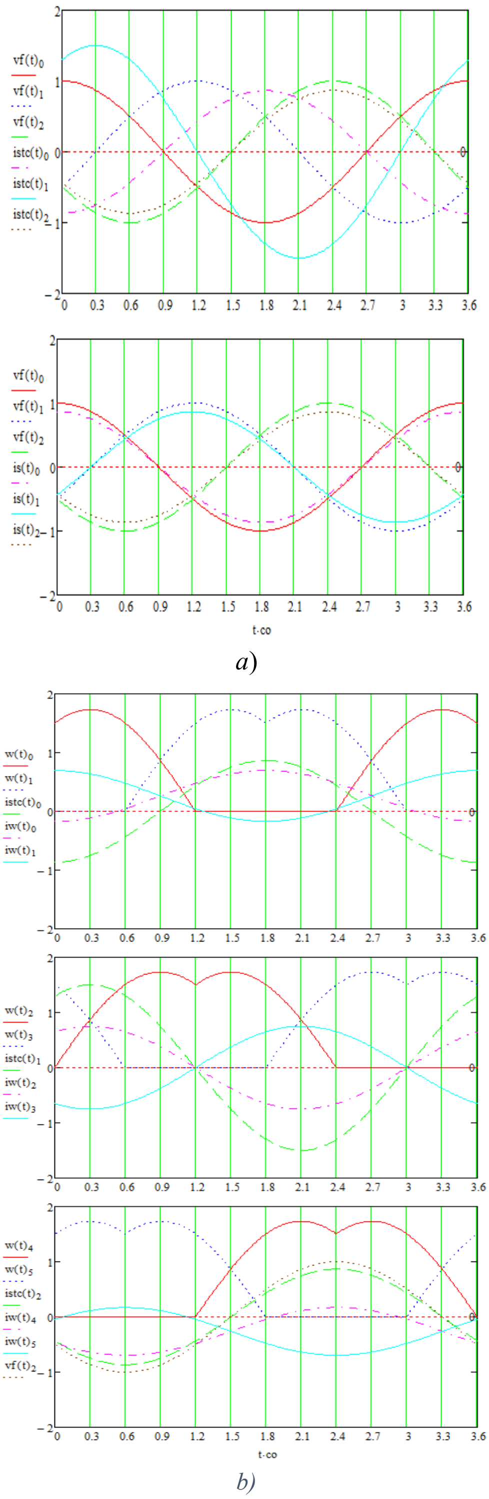

***Fig. 14**. Marquardt circuit operation in the balancing adjustment/compensation mode under reference conditions: (a) STATCOM currents $istc(t)_k$ and line currents $is(t)_k$ against phase voltages $vf(t)_k$ in the balancing adjustment mode; (b) STATCOM phase currents istc(t), voltages w(t) and currents iw(t) of valves.*

according to the known rules of electrical engineering. However, the use of Y-circuits in high- and medium-voltage electrical networks requires lower voltage applied to the controlled reactive branches, compared to the D-circuit, and fewer cells, which reduces the cost of MMC implementation. The Y-circuits need neutral offsets to be introduced to balance the power of the controlled reactive branches.

An analysis of the Y-circuit performance [10] shows that a Y-circuit composed of controlled reactive AC branches cannot act as a universal balancing and reactive power compensation device. There are no solutions to the equation that determines the neutral offset in this mode. The balancing mode requires a neutral offset equal to the phase voltage to absorb the negative sequence current no matter how small its value. The voltages on the controlled reactive branches and their powers increase as much as two-fold, making the application of the Y-circuit pointless. However, the Y-circuit can be used for reactive power compensation in conjunction with harmonic filtering and has an advantage over other circuits because of fewer cells required to achieve the result.

Figure 15 shows a Y-circuit made up of three reactive branches w_0, w_1, w_2 connected in a star configuration. The single-phase load is defined by expression (16).

Figure 16 shows the oscillograms of the Y-circuit operation when the balancing adjustment and mixed resistive-inductive load compensation are combined with the 30° phase. The neutral offset required for balancing is doubled, $||v_n|=2$, and the amplitude of the voltage applied to the valves reaches $ampw_1=3$. The residual power of the network is active. The required neutral offset of the Y-circuit in the hybrid mode reaches the value twice the phase voltage.

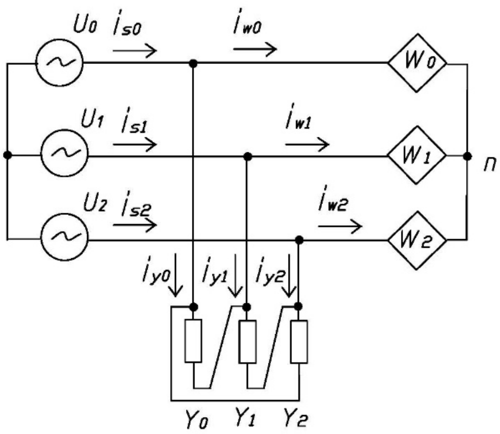

Fig. 15. Test Y-circuit.

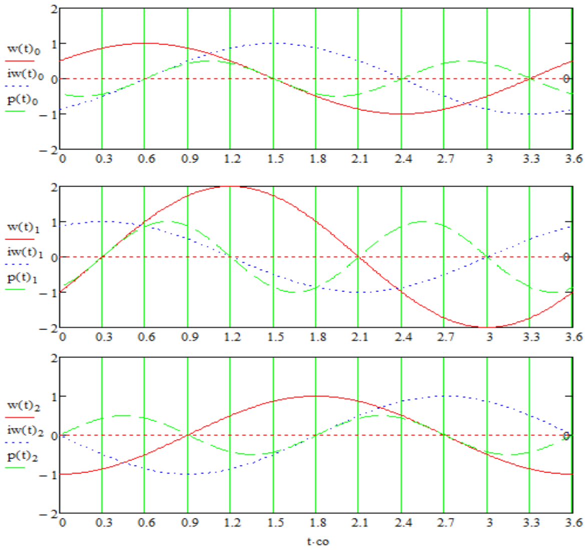

Fig. 16. Y-circuit operation with single-phase mixed resistive-inductive load in the balancing/compensation mode.

C. STATCOM D-circuit.

Figure 17 shows a test STATCOM D-circuit composed of three controlled reactive branches w_0, w_1, w_2 connected in a delta configuration. The load is the same as in the previous circuits.

The STATCOM current must provide compensation for reactive components (17):

$$istc(t) = -(iyma(t) + iymr(t) + iypr(t)).$$

The negative component, being reactive with respect to the sum of the three average phase powers, may have non-

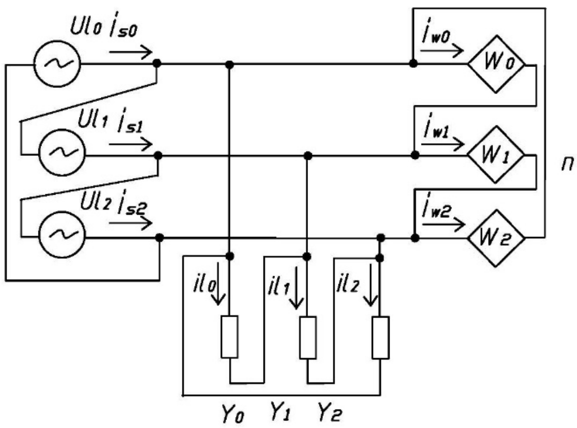

Fig. 17. STATCOM test D-circuit.

zero average powers of two or three phases. Balancing adjustment requires the exchange of average powers between phases. The D-circuit has one free variable to realize the inter-phase average power flow, i.e., the circulation current in the triangle *in*(·). It is easy to see that if *ma, mr* are amplitudes of two components of the negative sequence current, then the required harmonic of the circulation current is

$$in(t) = ma \cdot \cos t + mr \cdot \sin t. \qquad (21)$$

Valve currents including circulation currents are

$$iw_k(t) = istc_k(t) + in(t), \quad k = 0,1,2. \qquad (22)$$

When the circulation current is introduced in the mode of balancing/filtering of harmonics and complete suppression of unbalance, the current in one of the phase branches of the STATCOM doubles (Fig. 18), and, consequently, its rated power as a whole doubles as well. However, limiting the suppression of unbalance and harmonics to the standard-compliant level (K_{2U} = 4% for a 110 kV network) increases the phase current only by 20%. Figure 18 shows the waveforms of the STATCOM D-circuit operation in the mode of balancing and harmonic filtering with complete suppression of unbalance. The network voltage becomes balanced without waveform distortion. The STATCOM current in one of the phases has a double amplitude.

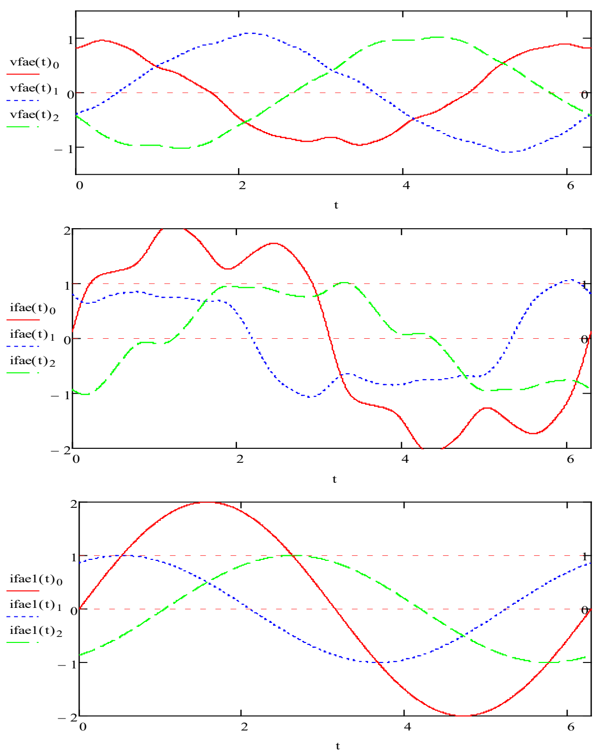

Fig. 18. STATCOM voltages and currents vfae(t), ifae(t) and the first harmonic of current ifae₁(t) under perfect filtering.

Figure 19 shows the D-circuit operation in the balancing/filtering mode with incomplete unbalance suppression (i.e., down to the standard-compliant value).

The STATCOM current increases from 8 to 20% depending on the ratio of unbalance and harmonic suppression factors. In all three phases, the power pulsates at twice the frequency, the average powers are zero, the line current *is*(–) is balanced and active.

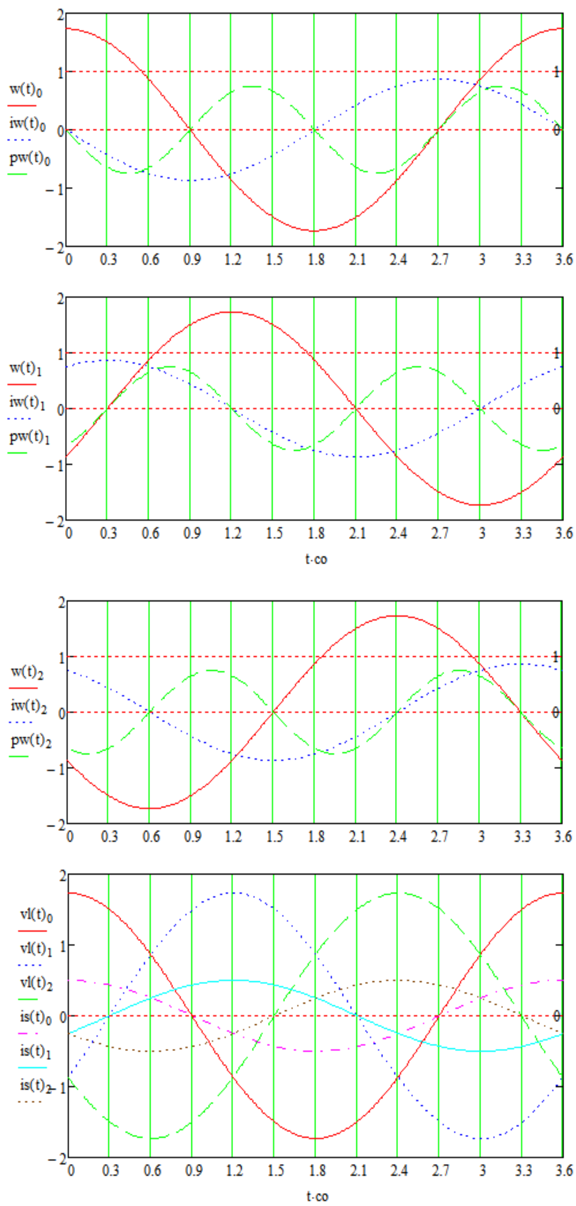

Fig. 19. Operation of the D-circuit in the balancing/filtering mode with incomplete suppression of unbalance under reference conditions.

V. Comparative Assessment of the Use of MMC Circuits for Balancing Adjustment and Reactive Power Compensation

When choosing a design of the STATCOM circuit for practical use, first of all, it is necessary to evaluate the costs of the basic power elements of the circuit, which are transistors and DC capacitors. The costs of STATCOM transistors are a function of two parameters: the highest voltage applied to the valves U_w and the highest current of the valves I_w. The capacitor costs are a function of the charge ripple dq. Table 1 lists the main parameters of the loads as per-unit quantities for the D-circuit and the two design options of using the Marquardt circuit (with isolated DC poles and with a capacitor shunting the DC poles) when operating in the balancing/compensation of a single-phase mixed resistive-inductive load under reference conditions.

All three options have the same applied voltages of the branches and cells, so that the voltage factor can be eliminated from the comparison.

The number of transistors is the same in all three options. Each symmetric cell with two pairs of D-circuit transistors corresponds to two Marquardt cells with one pair of transistors in each. The current loads I_w and the charge ripple dq are treated separately. The mrq0 option has the minimum current load of the transistors. However, it overestimates the charge ripple dq Option mrq1 has a low value of the dq parameter, but the current load I_w is overestimated and there is an additional cost incurred by the shunt capacitor.

A generalized comparison is made based on the current prices of IGBT power transistors and DC capacitor prices. There is also a number of somewhat artificial underlying assumptions:

- The sizing step of transistors and capacitors is not factored in;
- Transistor costs are assumed to be proportional to the nominal current, and capacitor bank costs are assumed to be proportional to their capacitance;
- The heuristic factor of 1.45 is used to take account of extra costs related to transistors (drivers, coolers, fans);
- Voltage ripple factor of capacitor banks during operation under steady-state conditions (the range) is assumed to be 8.3%.

The above assumptions were used to calculate the comparative costs of capacitor banks (Z_c), transistors (Z_t), and total costs (Z_s) for the three STATCOM design options as shown in Table 2.

The parameters shown in Table 2 are not stable. In any given case, the sizing step of transistors and capacitors can significantly affect the cost-effectiveness. Changes in capacitor and transistor technology can also involve significant cost changes.

Furthermore, the third function of STATCOM, that is filtering, was not considered in the study. Each of the STATCOM options under consideration can perform filtering in addition to balancing adjustment and compensation. The harmonics to be absorbed have almost no effect on the ripples dq, but can noticeably increase the required peak transistor currents, thus increasing the cost component Z_t in Table 2. Nevertheless, even under the above assumptions, the advantage of the D-circuit over the Marquardt circuit is much more compelling as evidenced by the findings of the study performed. The use of the Marquardt circuit as the STATCOM, compared to the D-circuit from controlled reactive AC branches, appears unfeasible.

Table 1. Load Parameters for the Basic D-circuit and Two Options of the Marquardt Circuit in the Balancing/Compensation of Single-Phase Mixed Resistive-Inductive Load under Reference Conditions

Circuit, algorithm	Paramer, per unit			
	U_w	I_w	dq	$dqpm^*$
D-circuit	1.732	0.866	0.433	-
mrq0 (with isolated DC poles)	1.732	0.75	0.717	-
mrq1 (with a capacitor between DC poles)	1.732	1.125	0.352	0.866

*$dqpm$ – charge ripple of the capacitor shunting the DC poles

Table 2. Comparative Costs of Capacitor Banks, Transistors, and Their Sum for Three STATCOM Design Options

Circuit, algorithm	Costs in notional units		
	Z_c	Z_t	Z_s
D-circuit	806	742	1 548
mrq0	2 671	642	3 313
mrq1	1 729	964	2 693

VI. Shunt or Series AF Connection

Both shunt and series connections of AF can be used for reactive power compensation, balancing adjustment, and filtering the voltage in outgoing lines. The modular multilevel converter can operate in either of the connection configurations.

In the case of a shunt connection, the AF operates with a sine-wave positive sequence voltage applied to it. Distortion components, i.e. negative sequence voltage and voltage harmonics are eliminated by the action of the AF. The AF current in this case consists of the negative sequence current and current harmonics. The shunt AF acts by creating an appropriate voltage drop across the total reactance at the connection point. The great bulk of the shunt-connected AF capacity is utilized to absorb the negative sequence current and the third harmonic of the current. The limiting resistance increases in proportion to the harmonic number. The contribution of harmonics to the AF load is negligible.

In the case of a series connection, the AF is activated via an isolating matching transformer in the break between the network and the outgoing lines. The series-connected AF operates by counteracting the distorting components of the network voltage with the same components of the AF voltage. The voltages of the outgoing lines are adjusted as part of this process. If the loads of the outgoing lines have no significant distorting factors, the current of the outgoing lines will be sinusoidal when supplied with sinusoidal voltage. The series AF voltage is formed from distortion components only:

- negative sequence voltage;
- voltage harmonics.

The network reactance does not affect the normal operation of the series circuit. However, operation with a series connection under emergency and abnormal conditions make it necessary for the AF to be equipped with a thyristor key that shunts the windings of the matching transformer and ensures unobstructed flow of currents in the event of a short circuit in the network.

In the series configuration, the main part of the AF power is consumed to suppress harmonics that determine the amplitude of the voltage applied to the phase valves; only a small fraction of power is consumed for balancing purposes. In contrast, in the shunt-connected circuit, due to the large network conductivity, the AF absorbs the negative sequence current for the fundamental frequency. As a result, the power of the shunt option significantly exceeds that of the series option.

Just as in the shunt-connected design, the negative sequence suppression mode is a unique feature of the series design, because of the need to ensure the balance the power in the active element branches. Furthermore, the series design has specific balancing features for the D- and Y-circuits, as is the case of the shunt-connected design. The series-connected D-circuit needs circulation current to be introduced to ensure balance and the current of the active branches is double the network current

$$I_{ae1} = 2 \cdot I_s \tag{23}$$

regardless of the unbalance level, similar to the voltage doubling on the active branches of the shunt Y-circuit. In a series Y-circuit, one has to introduce neutral offset to ensure balance. The balancing adjustment-only mode can make voltage amplitude of the phase branch of the AF reach twice this value. The Y-circuit requires twice the AF power to suppress unbalance.

In the hybrid balancing/filtering mode, the required voltage and currents of active phase branches $U_{ae,max}$, $I_{ae,max}$ of the D-circuit of the AF are determined by the following equations:

$$\begin{cases} U_{ae,\max} = U_{1m,\max} + U_{h,\max}, \\ I_{ae,\max} = 2I_{1p,\max}. \end{cases} \tag{24}$$

Regardless of the relationship between the components of the balancing voltage U1m and the harmonic distortion voltage U_h, it is essential to double the calculated current of the D-circuit AF branches. This means that the installed capacity of the active phase branches must also be doubled.

When the Y-circuit of the series-connected AF operates in the hybrid balancing/filtering mode, the corresponding equalities are as follows:

$$\begin{cases} U_{ae,\max} = 2U_{1m,\max} + U_{h,\max}, \\ I_{ae,\max} = I_{1p,\max}. \end{cases} \tag{25}$$

In this case, only one component of the negative sequence voltage U_{1m} is doubled. Thus, the Y-circuit becomes more preferable than the D-circuit when used in the hybrid balancing/filtering mode.

A comparison was made between the APF power required for unbalance suppression and harmonic filtering during distortions on 110 kV busbars of the 110 kV

Skovorodino substation. The results clearly showed that the required power of the series-connected design was more than two times lower than that of the shunt-connected option to achieve compliance with voltage quality standards. However, when the series-connected design was presented to the customer, it became evident that there were issues with the protective relaying system and emergency control facilities of the series-connected transformer. Due to these issues, the series-connected design was rejected despite its clear economic performance advantages.

Thus, to create active power filters providing harmonic filtering, balancing adjustment, and fast reactive power regulation, we can use STATCOMs based on three MMC circuits with a series connection of single-phase full-bridge and half-bridge voltage source converters, each of which operates in the PWM mode. The key defining feature of MMC-based active filters is that they are capable of selective fast real-time harmonic filtering. The AF allows suppressing any given set of harmonics, including the negative harmonic of the fundamental frequency (negative sequence), with a given degree of suppression (down to zero or standardized value) by appropriate setting in the control program.

For practical implementation of MMC-based STATCOM capabilities to make power quality parameters standard-compliant, we apply the so-called DSB control algorithm. This algorithm enables fast reactive power compensation, harmonic filtering and balancing adjustment of network voltage in real time.

The voltage balancing using MMCs is unique as to ensure the reactive nature of the valves during balancing adjustment it is necessary to introduce:

- the neutral voltage offset in the MMC Y-circuit;
- the constant current offset shared by these valves in the Marquardt circuit;
- the circulation current in the D-circuit.

At the same time, the shunt-connected Y-circuit requires the introduction of a neutral offset equal to the phase voltage, even when there is a small value of the negative sequence voltage. This leads to doubling the voltage on the phase branches and doubling the number of transistors, which renders the use of the shunt Y-circuit inefficient. When the circulation current is introduced into a shunt D-circuit, the design current (and power) of the D-circuit branches increases up to 1.08–1.2 with respect to the rated value, depending on the harmonic suppression factors specified.

The series-connected Y-circuit requires the introduction of the neutral offset equal to the value of the negative sequence voltage component. However, compensation of high-frequency distortions does not require the balancing neutral offset. Furthermore, provided that the harmonic voltage component is significant, the use of the Y-circuit proves quite effective to achieve compliance with voltage quality standards at individual coupling points and it also allows reducing the required power by 2–3 times compared to the case of shunt-connected AF.

The study of shunt-connected options for MMC circuits has demonstrated that the STATCOM D-circuit outperforms other alternatives in economic terms when used in the compensation/balancing mode. The use of the Y-circuit is inefficient due to the doubling of the required power even under minor unbalance. Preferring the Marquardt circuit over the D-circuit of MMC to ensure standard-compliant power quality parameters proves uneconomical. The shunt Y-circuit MMC is inefficient for balancing adjustment but can be successfully used for reactive power compensation and harmonic filtering.

VII. Conclusion

1. The advent of modular multilevel PWM converters provided the electric power industry with a versatile tool for achieving compliance with power quality standards in electrical networks. This technology allows simultaneously and effectively solving the problems of:

- reactive power management;
- harmonic suppression (filtering);
- negative sequence current suppression (balancing adjustment);
- transient damping.

2. We have devised a DSB algorithm based on classical automatic control theory and three-phase circuit theory to synthesize MMC control programs. The DSB algorithm suggests a sequential creation of three types of regulators (D – damping; S – selective suppression; B – balancing) followed by the combination of their actions.

The multi-loop regulation system based on the DSB algorithm creates fast active filters providing real-time reactive power compensation, voltage balancing adjustment, and harmonic filtering.

3. Our analysis of three MMC circuits for the design of

active filtering/compensating and balancing devices has shown that the most versatile and cost-effective option is the MMC circuit with a series connection of single-phase bridge PWM voltage source converters, whose phase branches are connected in a delta configuration.

References

[1] *Quality regulation of electric power in general-purpose electric power supply systems*, State Standard (GOST) 32144–2013. Moscow, Russia: Standardinform, 2014, 16 p. (In Russian)

[2] H. Akagi, E. H. Watanabe, M. Aredes, *Instantaneous Power Theory and Applications to Power Conditioning. Piscataway*. NJ: IEEE Press, 2007, 379 p.

[3] H. Akagi, "Classification, Terminology, and Application of the Modular Multilevel Cascade Converter (MMCC)," *IEEE Transactions on Power Electronics*, vol. 26, no. 11, pp. 3119–3130, 2011.

[4] E. Kontos, G. T. Tsolaridis, R. Teodorescu, P. Bauer, "High Order Voltage and Current Harmonic Mitigation Using the Modular Multilevel Converter STATCOM," *IEEE Access*, vol. 5, pp. 16684–16692, 2017.

[5] D. Braeckle, S. Mersche, M. Schnarrenberger, P. Himmelmann, M. Hiller, "Modular Multilevel Converters as active filters to mitigate low frequency current harmonics in converter fed grid applications," in *PCIM Europe 2018*, 5–7 June 2018, Nuremberg, Germany, pp. 218–225.

[6] I. L. Arkhipov, Yu. A. Goryushin, S. I. Gusev, G. M. Mustafa, Yu. M. Sennov, R. G. Shamonov, "Capacity rating of the active filtering and balance-adjusting device to achieve standard-compliant voltage on the busbars of 220 kv Skovorodino substation," *Elektricheskiestancii*, no. 3, pp. 46–53, 2016. (In Russian)

[7] G. M. Mustafa, S. I. Gusev, "Active series- and shunt-connected filtering and compensation devices," *Energetik*, no. 8, pp. 3–10, 2019. (In Russian)

[8] V. S. Chuprikov, "The use of fast-acting phase-regulated semiconductor reactive power compensation devices for standard-compliant power quality parameters in the UNPG," *Energy Expert*, no. 4, pp. 40–46, 2020. (In Russian)

[9] V. V. Aksenov, A. I. Demin, V. S. Chuprikov, "Ensuring power quality in power systems adjacent to the Trans-Siberian Railway and the Baikal-Amur Mainline. Hands-on experience gained in development and implementation of compensation devices," *Energetik*, no. 3, pp. 14–22, 2023. (In Russian)

[10] G. M. Mustafa, S. I. Gusev, "Filtering of higher harmonics in electrical networks under dynamically changing conditions," *Energiya Edinoy Seti*, no. 4 (33), pp. 44–52, 2017. (In Russian)

[11] G. M. Mustafa, S. I. Gusev, *Active filtering and balance adjustment devices for the power sector*, 2nd ed., revised and expanded. Moscow, Russia: MPEI Publishing House, 2022, 198 p. (In Russian)

[12] *Transmission of electric power by high voltage direct current. Active power filters. Requirements and guidelines for application*, GOST R 59031-2020. Moscow, Russia: Standardinform, 2020. (In Russian)

[13] R. Marquardt, "Current rectification circuit for voltage source inverters with separate energy stores replaces phase blocks with energy storing capacitors," Publication number DE10103031, 2002-07-25.

[14] R. Marquardt, A. Lesnicar, "New Concept for High Voltage – Modular Multilevel Converter," In *Proceedings of the 2004 IEEE 35th Annual Power Electronics Specialists Conference PESC'04*, Aachen, Germany, Jun. 20–25 2004.

[15] G. Tsolaridis, H. A. Pereira, A. F. Cupertino, R. Teodorescu, M. Bongiorno, "Losses and cost comparison of DS-HB and SD-FB MMC based large utility grade STATCOM," in *2016 IEEE 16th International Conference on Environment and Electrical Engineering (EEEIC)*, Florence, Italy, 2016, pp. 1-6

[16] G. M. Mustafa, "Technique for approximate analysis of pulse-modulated inverters with sine-wave output voltage." *Russian Electrical Engineering*, no. 10, pp. 2–8, 1987. (In Russian)

[17] G. M. Mustafa, "Filtering and compensation device for high-voltage DC power transmission," Patent 2521428C2. Russian Federation, MPK H02J 3/18/. Applied for on 05.07.2012, published on 27.06.2014. 35 p. (In Russian)

[18] *High Power Semiconductors for Industrial Applications*. www.infineon.com/power semiconductors.

Georgy M. Mustafa, Ph.D., Chief Research Officer, LLC NPP LM Inverter, Moscow, Russia, Gmm-mail@yandex.ru

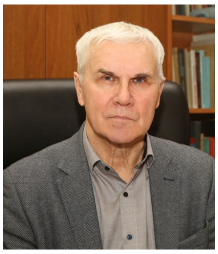

Stanislav I. Gusev, Ph.D., Chief Executive Officer, LLC NPP LM Inverter, Moscow, Russia, Gusev-si@lm-inverter.ru